NDOT Research Report

Report No: RDT05-051

Seismic Vulnerability Evaluation and Retrofit Design of Las Vegas Downtown Viaduct

January 2005

Prepared by Research Division
Nevada Department of Transportation
1263 South Stewart Street
Carson City, Nevada 89712

This work was sponsored by the Nevada Department of Transportation. The contents of this report reflect the views of the authors, who are responsible for the facts and the accuracy of the data presented herein. The contents do not necessarily reflect the official views or policies of the State of Nevada at the time of publication. This report does not constitute a standard, specification, or regulation.

TECHNICAL REPORT DOCUMENTATION PAGE

1. Report No. 05-051	2. Government Accession No.	3. Recipient's Catalog No.
4. Title and Subtitle Seismic Vulnerability Evaluation and Retrofit Design of Las Vegas Downtown Viaduct	5. Report Date January 2005	
	6. Performing Organization Code	
7. Author(s) M.S. Zadeh, M. Saiid Saiidi, A. Itani, S. Ladkany, Q. Yang, K. Mostafa, N. Johnson, S. Kandasamy, M. Hasan	8. Performing Organization Report No. CCEER-05-6	
9. Performing Organization Name and Address Center of Civil Engineering Earthquake Research Department of Civil Engineering/258 University of Nevada Reno Reno NV 89557	10. Work Unit No.	
	11. Contract or Grant No. **P364-00-803**	
12. Sponsoring Agency Name and Address Nevada Department of Transportation Structural Design Division Carson City Nevada	13. Type or Report and Period Covered	
	14. Sponsoring Agency Code	
15. Supplementary Notes		

16. Abstract

This study focused on the seismic vulnerability assessment and development of retrofit methods for Las Vegas Downtown Viaduct. The viaduct was built in the 1960's and similar to other bridges designed prior to 1970, lacks the necessary details to provide sufficient ductility capacity for dynamic loading caused by earthquakes. Several aspects of the behavior of the bridge were studied both at the system level and at component level. The studies at the system level included pushover analysis of the entire structure and an evaluation of the ductility demand. Another aspect of the system behavior was a study of the effects of incoherent ground motions on the forces and displacements of the bridge. Other segments of the study included the seismic evaluation of the ramp structures, the development of retrofit details for multi-column bents. Several research reports providing the details of the above aspects of the study have been prepared. This report presents a brief summary of the highlights of those studies. The study showed that the majority of the columns are in need of seismic retrofit but the as-built cap beams are adequate. For a thorough evaluation of the seismic demand the effect of incoherent ground motions has to be included. The column and pedestal retrofit methods developed and verified in this study proved to be effective and more economical than standard retrofit. Retrofit design methods are presented for both single-column and multi-column bents.

17. Key Words viaduct, columns, earthquakes, ductility.		18. Distribution Statement **Unrestricted. This document is available through the National Technical Information Service, Springfield, VA 21161**	
19. Security Classif. (of this report)	20. Security Classif. (of this page)	21. No. Of Pages 129	22. Price

Acknowledgements

The research presented in this report was funded by grants from the Nevada Department of Transportation and Federal Highway Administration. The opinions expressed in this article belong solely to the authors and do not necessarily represent the views of others. This report combines several reports on various tasks of the project. The NDOT program manager for this project was Troy Martin. Other participants in this project were Dr. Isakovic and graduate student, G. Dong. Tremendous assistance was received from Dr. P. Laplace and P. Lucas in the course of the shake table tests.

Abstract

This study focused on the seismic vulnerability assessment and development of retrofit methods for Las Vegas Downtown Viaduct. The viaduct was built in 1960's and similar to other bridges designed prior to 1970, lacks the necessary details to provide sufficient ductility capacity for dynamic loading caused by earthquakes. Several aspects of the behavior of the bridge were studied both at the system level and at component level. The studies at the system level included pushover analysis of the entire structure and an evaluation of the ductility demand. Another aspect of the system behavior was a general study of the effects of incoherent ground motions on the forces and displacements of the bridge. Other segments of the study included the seismic evaluation of the ramp structures, the development of retrofit strategies for single-column bents, and the development of retrofit details for multi-column bents. Several research reports providing the details of the above aspects of the study have been prepared. This report presents a brief summary of the highlights of those studies.

The study showed that the majority of the columns are in need of seismic retrofit but the as-built cap beams are adequate. For a thorough evaluation of the seismic demand the effect of incoherent ground motions has to be included. The column and pedestal retrofit methods developed and verified in this study proved to be effective and more economical than standard retrofit. Retrofit design methods are presented for both single-column and multi-column bents.

Table of Contents

List of Tables

Chapter 5

List of Figures

CHAPTER 1

Introduction

1-1 Background

Bridges designed prior to 1971 lack the necessary details to provide sufficient ductility capacity for the dynamic loading caused by earthquakes. These bridges were designed to resist static lateral force which is usually 2% to 4% of the dead load on the structure, depending on the foundation design, and some bridges were designed to withstand only gravity forces. The design guidelines did not include detailing of the reinforcement to provide sufficient displacement ductility under high lateral forces. The deficiencies for concrete bridges include insufficient shear strength, confinement, and structural detailing. These deficiencies usually cause non-ductile and unexpected modes of failure. Structural design codes have evolved to include the effect of seismic forces and are updated periodically to incorporate new information obtained from earthquakes and research. The current seismic design philosophy is based on large inelastic deformations and counts on energy dissipation during strong earthquakes.

The current seismic guidelines are applicable to new constructions. The bridges built prior to 1971 needed to be upgraded and retrofitted in order to resist strong seismic forces under dynamic loading. After the 1971 San Fernando earthquake, the California Department of Transportation began actively to retrofit bridges. Recent earthquakes such as the 1994 Northridge earthquake in California, 1995 Kobe earthquake in Japan and the 1999 Izmit earthquake in Turkey have shown retrofitted bridges to be successful in withstanding large lateral forces. Many bridges remain to be retrofitted to sustain high seismic forces.

The Nevada Department of Transportation (NDOT) has an ongoing program to evaluate and retrofit existing bridges in Nevada. Approximately 200 bridges through out the state have been identified that may be vulnerable to collapse due to a strong earthquake. Most of the bridges are located in Reno, Nevada area and some of them are in Las Vegas area. The Las Vegas downtown viaduct is one of the most important structures because of high average daily traffic. An extensive investigation has been conducted at the University of Nevada, Reno and Las Vegas involving detailed computer modeling and shake table testing of large scale models of the Las Vegas downtown viaduct. In this report the seismic vulnerability of the Las Vegas down town viaduct is evaluated. The report summarizes the studies and retrofit design development presented in several other reports[1-4].

1.2 Details of the Viaduct

The Las Vegas Downtown Viaduct is a reinforced concrete box girder system consisting of two parallel structures. In addition there are three ramp structures, two off-ramp and one on-ramp structure bridges (Fig. 1-1).

1.2.1 Main Structure

The main structure has 22 bents with integral bent caps. The viaduct provides for east-and west-bound traffic. The piers have two to four columns and the columns are of different heights. The column heights vary from 21 ft (6.4m) to 37 ft (11.3m). The details of the bridge in plan and elevations are given in Fig. 1-1. The heights of the columns shown in the elevation view of the bridge are the average heights of the columns in each pier. The column cross section shape is a parallelogram and is the same in all

columns. Column top is fixed to the bent cap but the base is pinned to the footing. Columns have different longitudinal reinforcement ratios ranging from 1.3 to 5.6%. The top of the column is densely reinforced compared to the base. Transverse reinforcements in all columns are #5 bars spaced at 12 in (305mm). The bent cap is integral with the deck and has a depth of 5 ft (1.53m). Most of the beams have different longitudinal reinforcement layout. The beam section adjoining the column is the most critical. These beam ends are only designed for gravity loads and not for load reversals due to earthquakes.

The push-over analysis of the main viaduct is presented in chapter 2. The effect of ground motion incoherency on the seismic response of the viaduct is studied in chapter 3. Finally the seismic evaluation of the main structure with its retrofit design is presented in chapter 6.

1.2.2 Viaduct Ramp Structures

Both the off-ramp bridges are box girders supported on single-column bents. The columns are octagonal shape. The off-ramps are named as 1RWD and 1RWL-2RWL as they appeared on the drawings of the bridges provided by NDOT (Fig. 1-1). The 1RWD off-ramp superstructure is supported by columns designated as 8WD and 9WD, while the 1RWL-2RWL off-ramp superstructure is supported by columns designated as 19WL, 22WL and 23 WL.

The on-ramp structure is reinforced concrete box girder consisting of three frames, six single-column bents, and two in-span hinges. Four of the six columns are supported on a pedestal with a one-way hinge at the pedestal base. The other two columns are directly connected to the footing with a one-way hinge at the column base.

The columns range from a height of 38.6 ft (11.8 m) to 18.5 ft (5.6 m) from top of footing to superstructure centerline. The seismic vulnerability of the on-ramp structure is discussed in chapter 5. Based on the results of the experimental studies and analysis, a step-by-step retrofit design method was developed.

1.3 Objectives and Scope

The overall objective of the research project was to determine the seismic vulnerability of the Las Vegas Downtown Viaduct, and to develop reliable and verified retrofit methods for all the elements of the bridge. Many aspect of the system and component response were evaluated. These included the push-over analysis of the entire bridge, differential ground motion effects on a reduced model of the bridge, shake table testing of single columns, shake table testing of multi-column bents, retrofit design development, and verification of the retrofit by testing and analysis. The retrofit approach did not follow the standard procedure because as-built model test data revealed unexpected failure modes in some parts, whereas better than expected performance elsewhere. The proposed retrofit method leads to substantial saving compared to standard retrofit techniques.

CHAPTER 2

Push-Over Analysis of Las Vegas Downtown Viaduct

2.1 Introduction

Push-over analysis is a nonlinear static analysis in which a structure is pushed incrementally in the lateral direction until it reaches collapse. For many structures, push-over analysis can be used to predict the seismic behavior of the structure. For the Las Vegas viaduct, push-over analysis was used to determine the lateral capacity of the viaduct in both the longitudinal and transverse directions. The change in the viaduct stiffness as lateral load increases and the point of yield displacement were determined. Since the viaduct is divided into eight frames, the push-over analysis can be used to determine the most critical frame in the viaduct. This chapter presents the results of push-over analysis of the entire bridge structure in the longitudinal (X) and transverse (Y) directions. Computer program DRAIN-3DX[5] was used in the analysis. Selected critical results are presented and the vulnerability of different piers is discussed.

2.2 Analytical Model Description

Figure 2.1 shows the outline of the viaduct structure. There are eight frames in the viaduct and are supported on 22 piers in addition to the abutment (pier A_0). The majority of the pier column sections are diamond shape. Piers P17W, P20W, P18E and P21E, consist of octagonal columns. To decrease the number of degrees of freedom and to enable analysis using the DRAIN-3DX program, the viaduct structure was modeled as a spine model[6]. The superstructure was modeled as elastic beam elements (element No. 17

in DRAIN-3DX) located at the center of gravity of the superstructure cross section. The columns; however, were modeled as fiber elements which are nonlinear beam elements (element No. 15 in DRAIN-3DX) since yielding is only expected to occur in columns. The fiber element can model the concrete and steel in the column cross-section assuming full bond between concrete and steel. Figure 2.2 shows a part of the model. The hidden lines in Figure 2.2 represent the boundary of the superstructure. Element 1-2 represents the superstructure model between piers P_X and P_Z. Since the superstructure beam is too rigid, the relative displacements between any two points on the superstructure beam were assumed to be negligible. To exploit this property, superstructure joints 3 and 4 were slaved to the master joint 1, and superstructure joints 5 and 6 were slaved to the master joint 2. In Figure 2.2, there are no elements connecting the top of the column section to the superstructure center. A complete slaving instead was used to connect joints 7, 8 and 9, 10 to the superstructure joints 3, 4 and 5, 6, respectively.

To model the connection between adjacent frames (Fig.2.3), compression and tensile elements were added at each hinge. The tensile element models the tensile action of the hinge restrainers as the two frames of the hinge moves away from each other. The compression element models the compression resistance upon gap closure. For the compression element, a slack of 0.125’ (38 mm) was specified to prevent the element from resisting force until the gap between the frames is closed (Fig.2.3). The same slack was also specified for the tension element.

2.3 Push-over Analysis and Results

The push-over analysis was performed by a load control where each master joint (Fig. 2.2) was loaded incrementally and the corresponding lateral displacement was calculated.

Figures 2.4 and 2.5 show the push-over analysis results for the viaduct in longitudinal and transverse directions, respectively. Since the viaduct is divided into east and west bounds, the push-over analysis was performed for each structure separately. In Figures 2.4 and 2.5, the push-over analysis results are depicted each of the eight frames. The y-axis represents the lateral horizontal force for the frame and the x-axis represents the corresponding lateral frame displacement.

2.4 Discussion of Results

As the viaduct is pushed laterally in its longitudinal axis (X-direction), each frame moves laterally depending on its stiffness. If the relative displacement between two consecutive frames exceeds the slack in the connecting elements (0.125' (38 mm)), a force in the connecting tensile elements is generated, which will increase the overall stiffness. It is apparent from Figure 2.4a for the east-bound viaduct that, starting from frame 2, the maximum relative displacement between any two consecutive frames does not exceed the slack in the tension elements. Between frame 1 and abutment (PA0), however, a relative displacement of 0.125 (38 mm) accompanied by an increase in frame stiffness is found (Fig. 2.4a, Frame 1). This is because the abutment is fixed. Once frame 1 displacement exceeded the slack in the connecting tensile elements, the restrainer

stiffness started to contribute to the frame stiffness. This is shown in the kink in the push-over diagram for frame 1 (Fig. 2.4a, Frame 1).

In the transverse direction (Y-axis), the push-over results (Figs.2.5a and 2.5b) show stronger and stiffer behavior than in the viaduct longitudinal direction (Figs. 2.4a and 2.4b). This is because the strong axis of all columns is in the transverse direction of the viaduct. Some of the columns are also fixed at their bases in Y-direction (columns with double curvature), which makes them much stiffer. This in turn increases the stiffness of the frames carrying these columns. As shown in Figs. 2.5a and 2.5b, frames 7 and 8 were stiffer than other frames pushed in Y-direction. This is because frames 7 and 8 include fixed-base columns in piers P17W, P18E, P20W and P21E.

The push-over analysis results can also show the level of displacement ductility at each pier. The displacement ductility for piers was calculated as the maximum displacement at top of the pier divided by the pier yield displacement. The maximum displacement for each pier was calculated directly from the push-over diagram while the yield displacement was determined from the geometrical and material properties of the pier. For the columns that are pinned at the bases, the yield displacement, Δ_y can be calculated from the conjugate beam method:

$$\Delta_y = \Phi_y H^2 / 3 \qquad (1)$$

Where Φ_y is the yield curvature of the pier cross section and H is the pier clear height. In the viaduct transverse direction, however, piers P17W, P20W, P18E and P21E are not pinned at the base. This requires that one-half of the clear column height be used in lieu

of H in Eq. 1. Table 2.1 shows the calculated yield displacement and displacement ductility demand for each pier. The yield displacement for each pier was calculated for both strong and weak pier axes. To calculate the displacement ductility, the maximum displacement component in each of the pier axes was calculated from the longitudinal or transverse component of the maximum displacement in the push-over analysis results by using the inclination angle of each pier.

In Table 2.1, the displacement ductility demands vary based on the location of the pier. For piers in frame 1, the attained displacement ductility is very low. This is because piers on frame 1 have the tallest columns in the viaduct. Tall piers have a relatively low stiffness and large yield displacement. The maximum displacement of these columns is limited because frame 1 is attached to the abutment. The column displacement ductility starts to increase as the distance from the abutment increases.

The displacement ductility demands on 1.5 or higher are shown in bold in Table 2.1. These are the columns that can be potentially critical and need to be retrofitted. Past research has shown that pre-1971 columns with minimal lateral steel have little ductility capacity. Uniaxial load tests of models of substandard reinforced concrete columns have shown that the displacement ductility capacity of even flexurally dominated columns is 1.5 to 2. Under bidirectional motion the capacity is expected to be lower. It can be seen in Table 2.1 that the ductility demand in nearly all the columns exceeds 1.5. Only three columns show a ductility demand of less than 1.5.

To determine if column shear is critical, the shear capacity of each column was investigated using Caltrans method. The shear demand and capacity as well as the shear demand-capacity ratio for the critical columns in each pier were calculated and shown in

Tables 2.2a and 2.2b for the east and west bounds bridges, respectively. In the column strong direction (direction 1), the maximum shear demand/capacity is at pier 16 (Table 2.2b). The maximum value is 0.73. Note that no strength reduction factors were used in calculating the shear capacities. Even though ratio is less than 1, considering the typical high scatter in shear capacity data, it is important to retrofit the columns to increase their shear capacity margins significantly.

2.5 Concluding Remarks

The pushover analysis results helped identify the most critical columns in the structure. It showed that the displacement ductility demands in nearly all the columns exceeded the ductility capacity of substandard columns at least in one orthogonal direction. The estimates of shear demands showed that the margin against shear failure is low. Both the lack of adequate ductility and the low shear capacity can be addressed by retrofit measures discussed in subsequent chapters.

CHAPTER 3

Influence of Ground Motion Incoherency on Seismic Response of Las Vegas Downtown Viaduct

3-1 Introduction

Traditionally in earthquake engineering analysis, the only ground motion parameter that is of interest is the acceleration. Acceleration histories and the corresponding design spectra are based on accelerograms recorded by strong motion instruments. Not being a part of an array, these instruments only give limited information on the ground motion at a certain site. As a consequence, it has to be assumed that all points of the ground surface beneath the foundation are excited synchronously and experience the same free-field ground motion. It is well known from actual earthquake records that the earthquake ground motions vary both temporally and spatially.

From a physical point of view, the spatial variation of seismic ground motion may be schematically thought to be the result of the combination of three different phenomena: (1) the incoherency effect, resulting from reflections and refractions of waves through the soil during their propagation (this effect is referred to as "geometric incoherency"); (2) the wave-passage effect, which is the difference in the arrival times of seismic waves at different locations; and (3) the local site effect due to differences in local soil conditions under various supports.

Because the Las Vegas Downtown Viaduct is a relatively long structure with some variation of soil stiffness from one end to the other, the effect of incoherent ground motions on the viaduct was explored. Because a detailed nonlinear response history analysis of the differential ground motion effect was beyond the scope of the current

study, the study was limited to linear systems. This chapter focuses on analyzing the influence of these three factors on the seismic response of multi-support structures. The coherency model of ground motions and the method of generating coherent ground motions based on phase difference spectra were utilized[7,8]. The materials presented in this chapter are the highlights of the study reported in Ref. 1.

3-2 Summary Background

Studies on the response of bridges and other structures subjected to different motions at supports were started more than 30 years ago[9] and continue today, from long bridges to short bridges, simply-supported beams to continuous beams, suspension bridges, cable-stayed bridges, building structures, dams, etc.. Some of the studies applied random vibration method[10-17]. Response-history analysis method was applied by Nazmy[18], Abdol-Ghaffar, et al[19], Price[20], Hao[21] and Behnamfar[22]. The influence of multiple support excitations on vibration control[23] and soil-structure interaction[24] was also studied.

Most of the studies show multiple-support seismic excitation has a significant effect on the structural response and should be considered in the earthquake-response analysis of bridges. It is uncertain whether the pseudo-static or dynamic response dominates the total response. The responses maybe underestimated or over-estimated by neglecting the ground motion spatial variations depending on the structure, ground motion properties, the location where the responses are evaluated, and the response parameter under consideration. Non-uniform ground motion excites antisymmetric modes of bridge vibration and introduces additional quasi-static deformations.

A breakthrough in understanding the coherency function has occurred with the installation of strong-motion arrays. Many empirical regression functions for coherency

were put forward[25-31]. These empirical studies are primarily based on the recording at the SMART-1 array in Taiwan, where soil conditions are more or less uniform throughout the array. Theoretical models of the coherency function for ground motions incorporating the incoherency, wave-passage, and site effect are developed[32-35].

3.3 Structural Responses

There are two general methods to account for the nonuniform seismic motion effects on structures: deterministic and stochastic. The basic approach in deterministic analysis is to estimate a set of compatible input records at the supports. The system is then analyzed using time-domain approach, called response-history analysis.

The stochastic methods for nonuniform seismic motion are also appealing, as they account for all the important parameters of the motion non-uniformity in an efficient and accurate manner. The difference among support motions is accounted for by the use of an incoherency function that is based on empirical, analytical, or field measurements. In most cases, the analysis is based on using the mode shapes of the structure. The apparent limitation for stochastic method is that it cannot handle nonlinear problems. For system with large nonlinearities, a step-by-step time integration approach is needed.

The analysis of the effects of incoherent ground motion on a seven-span reduced model of the Las Vegas Downtown Viaduct structure (G-947), is described in the following sections. The longitudinal response of two kinds of ground motions, one with narrow-banded spectrum and the other with wide-banded ground motion spectrum, is discussed.

3-4 Model of Downtown Viaduct

The Downtown Viaduct G-947, Las Vegas, is a 22-span, bridge (Figure 3.1). To simplify the analysis, the superstructure between adjacent hinges was modeled as a single lumped

mass and the associated columns were replaced by a single column. The viaduct was hence reduced to a seven-span bridge. Field test showed that the top soil is soft under the left three piers and medium firm under the right five piers in the reduced model of the bridge (Figure 3.2). These soils correspond to Type III and Type II of UBC 2000, respectively. The topsoil column under each support was modeled as a single-degree-of freedom system with equivalent frequency ω_{gs}=5.0rad/s, ω_{gm}=10.0rad/s and damping ratio ξ_{gs}=0.2, ξ_{gm}=0.4 for soft soil and medium soil columns[36]. The structural parameters are summarized in Table 3.1.

In the analysis, it was assumed that the damping ratio for all modes is the same and is equal to 0.05. The Rayleigh damping coefficients were determined from the natural frequencies, which are summarized in Table 3.2. Two types of ground motions were considered for the bedrock, narrow-banded ground motions and wide-band ground motions which are compatible with the Applied Technology Council ground motions for Type D (Stiff) soil.

3.5 Response under Earthquakes with Narrow-Band Spectrum

3.5.1 Generation of Coherent Ground motions

Eight acceleration histories of the bedrock at Points A to H (Figure 3.2) corresponding to the bridge supports (Points 1 to 8 in Figure 3.2), satisfying coherent function were generated. The ground motions at supports 3 and 5 are presented in Figure 3.3 as representative samples. The amplitude of the input acceleration histories are summarized in Table 3.3.

After the bedrock accelerations were generated, the motion of the topsoil was obtained from the filtered equation. It was assumed here that the bedrock motion is equivalent to Acc.5, and is uniform for points A to H. The acceleration histories relative to the bedrock, denoted as a_s for support 1 to 3 and a_m for support 4 to 8, are shown in Figure 3.4. Then the acceleration inputs to the structure are $a_{s5} = a_s + Acc.5$ at supports 1 to 3 and $a_{m5} = a_m + Acc.5$ at supports 4 to 8 (Figure 3.5). The total base displacements corresponding to acceleration a_{s5} and a_{m5} were obtained and presented in Figure 3.6.

3.5.2 Local Site Effects

To analyze the influence of local site, the earthquake history corresponding to that at support 5 (Figures 3.3b) was selected as the representative of the uniform input of the topsoil. The structural response for 3 input cases (Table 3.4) was analyzed, and the maximum values of the critical points were summarized in Tables 3.5 and 3.6. It is shown in Table 3.6 that inclusion of site characteristics reduces the relative displacement by up to 18% compared to the response for uniform excitation (i.e. $R_d/D^{5*}(\%)=81.9$) . It also shows that the maximum relative displacement is equal or smaller than the maximum dynamic displacement, which implies that at that time the dynamic displacement and relative pseudo-static displacement are out of phase.

3.5.3 Influence of Combination of Wave Passage and Local Site Effects

Even though, the topsoil is specified to be Type II and III, the values of SPT (Standard Penetration Test) in the right part and left part do not have great differences, as they are close to the border of Type II and III. It was assumed here that $v_{app} = 600m/s$ for the

whole bridge so the time delay ΔT between adjacent supports may be determined by $\Delta T_i = L/v_{app}$ as summarized in Table 3.7.

Here two cases are analyzed. It is assumed that the wave propagates from support 8 to support 1for the first case (Case 4) and from support 1 to support 8 for the second case (case 5)(Table 3.8). The analysis results are presented in Tables 3.9 and 3.10. It is shown in Table 3.9 that the ratio of dynamic displacement to relative displacement (D_d/R_d (%)) varies considerably from 46%-120%, which is the same for the ratio of relative pseudo-static displacement to relative displacement.

The ratio of dynamic response of incoherent ground motion to that of uniform is also smaller than 1.0, i.e., the wave passage decreases the dynamic response. Table 3.10 shows that the numerical results for case 5 are very similar to that for case 4 (Table 3.9). The results for internal forces lead to the same conclusions as those from displacements.

3.5.4 Effect of combination of Geometric Incoherency and Local Site

After the eight generated acceleration histories corresponding to the eight supports (Table 3.3) were modified by soft or medium soil columns, the structural input acceleration $a_{s1} \square a_{s2} \square a_{s3} \square a_{m4} \square a_{m5} \square a_{m6} \square a_{m7} \square a_{m8}$ and their corresponding displacements were obtained (Figures 3.8 and 3.9). It is shown in Table 3.11 (case 6) that the geometric effect results in the structural relative displacements that exceed those of uniform excitation, but the maximum dynamic displacement is much smaller than the pseudo static displacement.

3.5.5 Effect of Combination of Wave-Passage, Geometric Incoherency, and Site

Based on previous section, wave passage effect was added, and two cases (7, 8, summarized in Table 3.12) were analyzed. The results are presented in Tables 3.13 and 3.14.

The results when taking all three effects into account are very similar to those of taking geometric incoherency effect only. This indicates that the influence of geometric incoherency is dominant. The total internal forces and relative displacements in this case were 60% to 180% of those of uniform excitation, and broadly speaking the pseudo-static response constituted most of the response (approximately 60-80%).

3.6 Responses under Earthquakes with Wide-Band Spectrum

To investigate whether the conclusion drawn for narrow band spectrum is also fitted to wide-band excitations, the acceleration of the bedrock motion compatible to the response spectrum Type B in ATC-32,(Acc. B) was synthesized as presented in Figure 3.10. The response spectrum for wide-band excitation (Acc. B) and the narrow-band excitation (Acc.5) are shown in Figure 3.11. The wide band spectrum exhibits the same trend as that of narrow band spectrum (refer to Ref.1 for more details).

The absolute output accelerations of the soil columns are presented in Figures 3.12, and their corresponding displacements are shown in Figure 3.13.

3.7 Conclusions

Based on the numerical results presented in the previous sections, the following conclusions about the effects of incoherency of ground motion on the Las Vegas Viaduct structure can be made:

1. The incoherency of earthquake motions can have a dramatic influence on the structural response by modifying the dynamics response of uniform excitation and inducing pseudo-static response, which does not exist in structures subjected to uniform excitation.
2. The response to both narrow-band and wide-band excitation shows that pseudo-static

responses increase as number of the incoherency factors is increased.

3. For the structure studied in this report, the geometric incoherency and local site properties have a stronger influence than the wave passage effect.
4. Incoherent ground motion increased the nodal displacement. For the Las Vegas viaduct, the maximum top node displacements ranged from 0.056 to 0.068 m for uniform excitation (Table 3.5, Case 5*). The range changed to 0.038 to 0.10 m under incoherent motion (Table 3.13, Case 7). The difference is, in part, attributed to participation by higher modes during incoherent ground motion.
5. The total response when ground motion incoherency is considered may be larger or smaller than that of uniform excitation, depending on the structural member, soil properties, soil depth, and ground motion. . For the Las Vegas viaduct, it is shown that the response at 80% of the nodes is larger than that of uniform excitation and that in a detailed seismic demand analysis for this bridge the ground motion incoherency has to be accounted for using more detailed site investigation and analysis.

CHAPTER 4

Seismic Vulnerability Assessment of Off-ramp Structures of Las Vegas Downtown Viaduct

4-1 Introduction

Several bridge design codes have been modified to reflect the knowledge and experience gained from the disasters resulting from the major earthquakes of the last 10 years. Bridges constructed before 1970s, like the Las Vegas downtown viaduct, based on old seismic design guidelines, should be generally upgraded and retrofitted to withstand strong seismic forces. Retrofit systems consisting of concrete, steel and advanced composite jacket have been developed and used to retrofit many reinforced concrete bridge columns. The California Department of Transportation (Caltrans) has developed design recommendations for steel, glass and carbon fiber jackets[37].

In this chapter the seismic vulnerability of the off-ramp structures of the Las Vegas down town viaduct is evaluated using different codes. Based on the evaluation, a retrofit design of the reinforced concrete columns of two off-ramp structures is presented. The retrofit designs presented in this chapter follow standard methods and are not based on tests described in other subsequent chapters. The chapters that follow show that it is not necessary to use standard retrofit as it might be too expensive. Nonetheless, the results of standard retrofit are presented in this chapter for as information. The materials in this chapter are the important steps and findings of Ref. 2.

4.2 Description of the Off-Ramp Structures

There are two off-ramp and one on-ramp structures in the Las Vegas Downtown Viaduct. In this study presented in this chapter, the off-ramp structures were considered.

The columns of each off-ramp were named as they appeared on the drawings of the bridges provided by the Nevada Department of Transportation (NDOT). Figure 4.1 and Figure 4.2 show the elevation view of the 1RWD off-ramp and 1RWL-2RWL off-ramp respectively. The 1RWD off-ramp superstructure is supported by two columns designated as 8WD and 9WD, while the 1RWL-2RWL off-ramp superstructure is supported by three columns designated as 19WL, 22WL and 23 WL. Figure 4.3 and Figure 4.4 show the cross sections of the columns of 1RWD and 1RWL-2RWL off-ramps respectively. The bridge deck cross sections are shown in Figures 4.5 and 4.6.

The columns are connected to the footings by a series of dowels placed in a row. As a result the columns act as a one-way hinge in direction of the length of the bridge (Figures 4.7 and 4.8), (the weak direction of the column). The direction perpendicular to the length of the bridge is named transverse or strong direction of the column. All the columns were considered as fix connected at the bottom to the footing and pin connected at top to the superstructure in the strong direction, while in the weak direction the columns were considered pin connected at the bottom to the footing and fixed at the top. The foundation soil profiles are determined based on the subsoil investigation report provided by NDOT.

4.3 Evaluation of Existing Columns

The moment, shear and deformation capacities of the columns were determined to compare with the maximum moment, shear and deformation demands produced by the design ground motion. In order to determine the moment capacities of the columns, a computer program called RCMC[38] was used. RCMC is a computer program for moment-

curvature analysis of confined and unconfined reinforced concrete sections. The maximum plastic moment and displacement capacities of the columns in strong and weak directions, determined from the output of RCMC, are shown in Table 4-1.

The shear strength of the columns were calculated using Caltrans[39] , FHWA[40] and Wehbe[41] methods. The results are presented in Table 4.2. The Caltrans and Wehbe methods gave almost identical values for shear capacity. FHWA values were about 63% higher than the values obtained by other two methods. Confinement steel requirements were also calculated. The column design of both off-ramp bridge structures did not meet the minimum requirements for confinement steel and tie spacing according to ACI, AASHTO, ATC-32 and Caltrans. Therefore, all the columns of both off-ramps are considered to be substandard relative to current seismic code requirements.

4-4 Shear and Moment Demands of Columns Using UBC and AASHTO Methods

A full scale dynamic analysis was performed along with the complete response spectrum analysis [42]. For each off ramp, the total mass of the bridge deck and its mass moment of inertia were considered in the analysis. The lateral forces and natural periods of vibration of the bridge structure were calculated[42,43]. Two degrees of freedom, a lateral displacement vector [X] and a normal rotation [θ] vector were applied at the center of the bridge mass. A full eigenvalue and eigenvector analyses were performed to determine the natural modes and frequencies of the structure as shown by William[42].

The UBC code[44] procured were used as one evaluation tool even though the UBC provisions are developed for buildings. Figure 4.9 shows the design response spectra curve based on UBC for Zone 2B (Las Vegas area). From the dynamic analysis, resultant

base shear forces on the columns were calculated in the two orthogonal directions, the transverse (strong) and the longitudinal (weak). The values are shown in Table 4.3. For the transverse direction, the absolute maximum base shear was calculated by using the square root of the sum of the squares of the similar values (rotation and translation), (Clough)[45].

The force and displacement demands on the off-ramp bridge columns were also found using the seismic provisions of AASHTO. The response modification factor (R) was chosen as 3 for single columns from Table 3.7 of AASHTO. The uniform load method was used for both the transverse and longitudinal directions.

The maximum moment capacities of the columns were found to be higher than the moment demands calculated using the seismic provisions of UBC and AASHTO. However, the maximum shear demands in the strong directions of the columns, determined using UBC and AASHTO (before dividing by R), are higher than the capacities calculated using Caltrans[39] formula. Therefore, it was evident that the columns may experience brittle shear failure under a strong earthquake.

4-5 Finite Element Modeling and Evaluation of the Bridge

Three-dimensional non-linear computer program DRAIN- 3DX was used for modeling of the off-ramp structures. The maximum moment, shear, and displacement demands on the columns, determined from DRAIN-3DX analyses were compared with shear, moment and displacement capacities of the columns. Whenever the demand exceeded the capacity of the columns, two alternate retrofit designs using Carbon Fiber Polymer Jacket (CFRP) and Glass Fiber Polymer Jacket (GFRP) are presented.

The distributions of nodes on both off-ramp structures are shown in Figures 4.10 and 4.11.

In general, a rigid footing has six degrees of freedom, three translations and three rotations as shown in Figure 4.12. Ground acceleration and twisting rotations in the Z-axis were not considered in the modeling of structures. Therefore, only four degrees of freedom Fx, Mx, Fy, and My were considered while calculating the footing stiffness using a method by Darwish et al.[46]. This is basically a combination of FHWA[47] method and Dorby et al[48,49] method.

According to Darwish[46], the depth of influence underneath the footing is taken as the shortest dimension of the footing. Based on the NDOT provided sub soil report, the shear modulus G was calculated for each soil layer. The stiffness of footing for translation and rocking was then determined (Table 4.4).

DRAIN-3DX input files for each off-ramp structures were run for two different acceleration records, Sylmar and ATC, at three different intensity levels. Tables 4.5, 4.6 and 4.7 show the summary of Drain analysis with Sylmar earthquake at 0.5 ,1.0 and 2.0 intensities respectively. The summary of Drain analysis for ATC earthquake with similar intensities is shown in Tables 4.8, 4.9 and 4.10. The results show that the shear demand on the columns due to all types of applied earthquake is higher than the shear capacity of the columns. Therefore, all the columns have to be retrofitted.

4-6 Column Retrofit Design

The retrofit of the columns was designed with carbon fiber reinforced polymer (CFRP) and glass fiber reinforced polymer (GFRP) based on the design guidelines

provided by Caltrans[39]. The material properties supplied by Master Builders Technologies, which is approved by Caltrans, were used for retrofit design. A summary of the material properties is given in Table 4.11. Note that the results presented in this section are only to show the needed retrofit using standard retrofit procedures. Subsequent chapters demonstrate that the amount of retrofit can be substantially reduced based on the shake table test data in those chapters. The final retrofit design should be based on the procedures and examples presented in subsequent chapters.

According to Caltrans, the minimum confinement stress is 300 psi in the lap-splice and/or plastic hinge zone with a maximum material elongation of 0.001 in/in in the lap-splice zone and 0.004 in/in in the plastic hinge zone. A minimum confinement stress of 150 psi and material strain of 0.004 must be maintained elsewhere in the column, with appropriate transition. Based on minimum confinement requirement, the number of layers required in the plastic hinge zone and elsewhere in the columns is determined as shown in Table 4.12 and Table 4.13 for 1RWD off-ramp and 1RWL-2RWL off-ramp respectively.

According to Caltrans the retrofitted columns should achieve an actual displacement ductility in the range of 8 to 12. For the retrofit design, a minimum displacement ductility of 8 was selected for the columns. Table 4.14 and Table 4.15 show the minimum jacket thickness required for minimum ductility requirements for 1RWD and 1RWL-2RWL columns respectively.

The jacket thickness must also provide shear strength to meet the shear demands produced by different level of earthquakes. Typically the design of the jacket is not controlled by shear strength. Table 4.16 shows a summary of the results. In all cases, the

number of required layers is governed by the minimum confinement requirements of Caltrans[39]. The number of layers of CFRP jacket inside the plastic hinge region for 1RWD and 1RWL-2RWL columns are 17 and 19 respectively, while outside the plastic hinge region the numbers of layers are 9 and 10. Similarly, the number of layers of GFRP jacket inside the plastic hinge region for 1RWD and 1RWL-2RWL columns are 22 and 24 respectively, while outside the plastic hinge region the numbers of layers are 11 and 12. The length of plastic hinge region at the top and bottom of the columns is shown in Table 4.17.

All the columns with CFRP and GFRP jackets were modeled using RCMC program to determine their moment capacity. Table 4.18 shows the moment capacity of the columns with jackets. The shear strength provided by jacket and required shear strength of jacket are shown in Table 4.19. It is evident that the moment and shear capacity of the retrofitted columns with FRP jacket is higher than the maximum moment and shear demand resulting from ATC x 2.0 intensity earthquake.

4-7 Conclusions

1. The moment and shear demands calculated by the response spectral analysis, UBC 97, correspond to the DRAIN output for ATC x 0.5 and Sylmar x1.0. It is also evident that by dividing the maximum moments and shear obtained from the AASHTO analysis by a response modification factor of three, the recommended design moment values are below the values obtained from a response spectral analysis.
2. The analytical study of the bridge columns showed that they are unable to withstand shear from strong earthquakes.

3. Retrofit design of the columns was governed by minimum confinement requirements. However, as shown in subsequent chapters, it is not necessary to design the jackets based on this criterion and that the number of layers can be reduced significantly while still providing satisfactory performance.

CHAPTER 5

Seismic Retrofit of Octagonal Columns with Pedestals

5-1 Introduction

The primary objective of the part of the study presented in this chapter was to identify seismic vulnerability and develop retrofit methods for the piers in a seven-span on-ramp structure that is part of the Las Vegas Downtown Viaduct. Unlike the work in Chapter 4 in which standard analysis and retrofit design were used, in the study in this chapter included shake table testing of several as-built and retrofitted models. The performance of the models and related analyses formed the basis for retrofit recommendations for all single column piers in the Las Vegas Viaduct. This chapter presents the highlights of the study presented in Ref. 3.

5.2 Prototype Selection and Preliminary Analysis

Ramp DW is a seven-span reinforced concrete box girder structure consisting of three frames, six single-column bents, and two in-span hinges. A plan view of the ramp is shown in Fig. 5-1. The selection of a prototype column for testing was made based on susceptibility to shear failure in the strong direction of the columns. Properties used in the selection of the prototype are shown in Table 5-1. The ramp consists of two types of columns. One type is with a pedestal and a larger vertical steel ratio, the other without a pedestal and a smaller vertical steel ratio. Of these two types, the shortest from each group, columns 8DW and 10DW, were determined to be the ideal candidates for a prototype. In each of the column groups the lateral and vertical steel ratios are identical,

and the axial load indices are very close. Column 8DW was chosen over 10DW because while they have a similar column height and the same lateral steel ratio, column 8DW has a vertical steel ratio of approximately 50 percent greater than column 10DW. The higher steel ratio leads to a greater shear demand in column 8DW.

Three identical quarter-scale as-built specimens of column 8DW were constructed for shake table testing. The dimensions of the specimen are shown in Fig. 5-2. A scale factor of 0.25 was governed by the capacities of the shake table.

To predict the seismic performance of the specimen, preliminary static and dynamic analyses were performed. Load capacity, stiffness, and maximum displacements were calculated by the use of moment curvature, pushover, and dynamic response history analyses.

Program RCMC was used for cross sectional property analysis. Because of the low amount of lateral steel in the column, the concrete properties were assumed to be unconfined. RC-Shake was used for preliminary dynamic analysis of the specimen to select the acceleration record to be used as the input motion for shake table testing. The ATC-32, Sylmar, and El Centro records were used in the analysis and scaled by a time scale of 0.476 seconds. The timescale accounted for the quarter scale length and a slight difference of simulated inertia and axial loads applied during the test. The Sylmar record was selected as the input motion for testing because it was determined to cause the largest ductility demand in the column without exceeding the shake table capacity.

5.2.1 Material Properties

The material properties for the scaled specimen were very similar to that of the prototype. The concrete had a 3/8-in (9.5 mm) maximum aggregate size and was rated

for a compressive strength of 5000 psi (34.5 MPa). The small aggregate size was needed because of the quarter scale concrete cover and bar spacing. The concrete was ordered with a specified strength of 5000 psi (34.5 MPa) expecting a cured strength of approximately 6000 psi (41.4 Mpa) to match the prototype. The columns were poured in three stages, first the footing, followed by the pedestal and column, and last the stub head. The 28-day strength for the column and pedestal was approximately 5700 psi (39.3 MPa).

Due to the unavailability of Grade 40 steel in #3 bar, Grade 60 steel was used and subjected to heat ramps to obtain the target yield stress of 44 Ksi (303 MPa). Stress-Strain curves for #3 rebar are shown in Fig. 5-3. The measured yield stress of the treated steel was 41.7 Ksi (288 MPa). Wire used as reinforcement in the specimens also had a target yield stress of 44 ksi (303 MPa). The measured properties for each wire type are listed in Table 5-2. The average yield stress for the wires was 40.5 Ksi (279 MPa).

5.3 As-Built Specimen Test Procedure and Results

The specimen was extensively instrumented with strain gauges, displacement transducers, load cells, and accelerometers. The data were recorded at a rate of 160 samples per second by the use of a Pacific Instruments data acquisition system.

The quarter scale as-built specimen, OLVA (Octagonal Las Vegas column, As-built) was tested rigidly attached to the shake table and to the mass link. The mass link connected the top of the column to the inertial mass system simulated by the mass rig. A drawing of the shake table setup is shown in Fig. 5-4. The schedule of testing for OLVA is shown in Table 5-3. The column was subjected to amplitudes of Sylmar in intervals of 0.25x

from 0.25x to 2.0x. A summary of displacements at peak forces and forces at peak displacements in the direction of testing is shown in Table 5-4.

The testing was stopped at 2.0x Sylmar because of severe cracking of the pedestal and significant out-of-plane displacement. The displacement histories for all runs of OLVA in the primary test direction are shown in Fig. 5-5. The cracking of pedestal began at displacement ductility of 0.6, which was a cause for concern. The ultimate deflection was 1.65 in (41.9 mm) providing a displacement ductility of 6.9. The curvature profile for all test runs of OLVA is shown in Fig. 5-6.

Testing of OLVA showed that shear and confinement in the column (above the pedestal) were not problematic for the as built columns. Pedestal cracking proved to be the largest issue of concern because it occurred under relatively small earthquakes and because the damage in pedestal is hidden under the grade level. This leads to a possibility of damage not being detected during inspection. Undetected cracking of the pedestal and exposure of steel to moisture even under a small earthquake would lead to corrosion and further pedestal deterioration.

5.4 Retrofit Specimens and Test Results

Based on shake table testing of OLVA, it was determined that the primary deficiency of the as-built column is in horizontal pedestal reinforcement. Two retrofit methods were attempted on two additional specimens, OLVR-1 and OLVR-2. In OLVR-1, only the pedestal was retrofitted, whereas in OLVR-2 both the pedestal and the column base were retrofitted.

5.4.1 OLVR-1

The pedestal retrofit design consisted of two stages. The first stage was to extend the pedestal, increasing the moment capacity of the pedestal base to assure a diversion of plastic hinging into the column. The second stage was to reinforce the pedestal to provide sufficient pedestal strength to prevent pedestal separation from the column. Three options were considered for providing pedestal connection to the column; A steel jacket, carbon fiber reinforced plastic (CFRP), and glass fiber reinforced plastic (GFRP).

Of the three jacket types, GFRP was selected because of ease of construction and lower total cost. Prior to the application of the GFRP, the surface of the pedestal was smoothed with a lightweight chipping-hammer and cleaned with a wire brush. Uneven portions of the pedestal including the seam of the pedestal extension and the existing pedestal were filled with grout.

The test setup and procedure for OLVR-1 and OLVR-2 were identical to those of OLVA except for the addition of a frame for transverse lateral support. The input earthquake record was the same for all models and was applied in the strong direction of all models. Testing was stopped at 2.75xSylmar because of column shear failure. The shear failure was combined with extensive spalling and bar exposure at the base of the column due to plastic hinging (Fig. 5-7). A summary of displacements at peak forces and forces at peak displacements in the direction of testing is shown in Table 5-5.

An elasto-plastic load deflection relationship using the load and deflection envelopes for all the runs is shown in Fig. 5-8. This plot shows the maximum displacement ductility the column achieved during each run. The idealized plastic yield force was 60.4 kips (269 kN) at a deflection of 0.28 in (7 mm). Shear cracking began at a ductility of

1.7. The ultimate deflection was 1.23 in (31.2 mm) providing a displacement ductility capacity of 4.6.

The pedestal retrofit was a success because it shifted plastic hinging into the column. A ductile plastic hinge was indeed formed in the column. However, the low ductility capacity and increase of shear demand indicated that the retrofit needed improvement. This was the consideration for the retrofit of OLVR-2.

5.4.2 OLVR-2

The retrofit of OLVR-1 was successful in moving the failure mechanism out of the pedestal and into the column. OLVR-1 showed substantial flexural yielding of the base of the column, but ultimately failed in shear. Failure in the column instead of the pedestal caused the displacement ductility to drop from 6.9 to a moderate value of 4.4.

Priorities for the retrofit of OLVR-2 included increasing column ductility and bringing the column plastic shear demand down to that of the as-built. Given that no pedestal damage was seen in the retrofit of OLVR-1, the pedestal retrofit in OLVR-2 was the same as that of OLVR-1 but the column was retrofitted. Two options and a combination of the two options were considered. The first was to sever some of the bars at the base of the column to lower the shear demand and to increase ductility. The second was to apply a jacket to the column for an increase in shear capacity. Both of these options were to include the retrofit of the pedestal as it was applied to OLVR-1. For OLVR-2, it was decided to reduce the cross section of the column immediately above the pedestal. This was accomplished by severing some of the extreme bars and removing the associated concrete. To determine how many bars to cut at the base of the column, plastic moment capacities of different bar configurations were calculated using RCMC.

A summary of displacements at peak forces and forces at peak displacements in the direction of testing is shown in Table 5-6. An elasto-plastic load deflection relationship using the load and deflection envelopes for each run is shown in Fig. 5-9. This plot shows the maximum displacement ductility that the column achieved during each run. The idealized plastic yield force was 48.6 kips (216 kN) at a deflection of 0.32 in (8.1 mm). Shear cracking began at a ductility of 2.2. The ultimate deflection was 1.87 in (48 mm) providing a displacement ductility of 5.9.

5.5 Retrofit Evaluation and Design Recommendations

Similar to the retrofitted pedestal in OLVR-1, the pedestal of OLVR-2 remained intact and undamaged throughout testing. Because of the cut section at the base of the column, the demand on the OLVR-2 pedestal was approximately 20 percent less than that of OLVR-1. OLVR-2 testing reassured that the pedestal retrofit of OLVR-1 was successful, and showed that the cut at the base of the column of OLVR-2 was effective in moving the plastic shear of the column closer to the capacity of the as-built. Though OLVR-2 reached larger displacement ductility than OLVR-1, and the base of the column underwent more extensive plastic hinging, OLVR-2 still failed in shear, proving that in addition to the OLVR-2 retrofit, the column requires further modification by the addition of an FRP jacket with a minimal number of layers.

5.5.1 Design Recommendations

Based on the data from shake table tests, design recommendations were developed for the retrofit design of the octagonal columns in Ramp DW of structure G-947. The

specimen testing applied directly to the columns with pedestals. These are columns 5DW through 8DW. Design recommendations for these columns as well as for the columns without a pedestal, columns 9DW and 10DW are included. The same procedure may be applied to other single columns in the off-ramp structures (discussed in Chapter 4). Retrofit design guidelines for on-ramp bridge columns are presented in Appendix A.

5.6 Nonlinear Dynamic Analysis of Ramp Structure

In addition to the experimental study of the most critical column, a computer model of Ramp DW was created to determine how the as-built ramp columns will respond under earthquake loading and what demands the columns were subjected to for various earthquake intensities. The software used for the nonlinear analysis was the finite element package DRAIN-3DX[5]. Drain models structures as a 3-dimensional assemblage of linear or nonlinear elements connected at the nodes. The program contains several different element types. Drain is capable of many different types of analysis including modal analysis, static analysis, and dynamic analysis. Input for the static analysis can be in the form of nodal or element load patterns. Input for the dynamic analysis can be in the form of ground acceleration records, ground displacement records, nodal force records, velocity patterns, and response spectra. For the ramp analysis, static analysis was first performed with gravity loads at the nodes. The structure was then excited dynamically with the Sylmar and ATC acceleration records at three magnitudes, 0.5x, 1.0x, and 2.0x.

The nodal configuration of the model is shown in Figs. 5-10 and 5-11. The origin is located at the superstructure centerline at the west end of the ramp. Nodal layout of a typical hinge detail is shown in Fig. 5-11. Soil springs were added to the footings to obtain more accurate modeling of soil flexibility than for the preliminary model that was

fixed at the column bases. Also this model included longitudinal springs at the ends of the structure to model the abutment stiffness and the stiffness of the main bridge structure.

The superstructure and bent caps were modeled with elastic beam-column elements (Type 17). This is because of the rigid and strong nature of the superstructure with respect to the substructure. Similarly to the elastic region of the columns, the superstructure elements were defined with un-cracked properties of the superstructure. Mass of the superstructure was calculated as the unit weight of concrete and was distributed to nodes by tributary area. Rotational mass inertia was not included.

The method proposed by Darwish et al.[46] was used to calculate the stiffness of soil springs to model the soil-structure interaction at the base of the columns. Damping was modeled through both mass proportional and stiffness proportional damping. Modal analysis of the model was conducted to determine the mode shapes and the fundamental periods of vibration. The Rayleigh damping method[50] was used to calculate the damping coefficients of the classical damping matrix based on the periods of the first and third modes.

5.6.1 Analysis Results

The transverse displacement ductility capacities are compared to the demands from Sylmar and ATC in Tables 5-7 and 5-8, respectively. It was assumed that the effect of the soil springs on the column was such that the change of displacement ductility they caused was negligible. A static pushover analysis of each column in the Drain model was conducted to determine the yield displacements. Overall, Sylmar record showed to be a more demanding ground motion on the structure. At 1.0xSylmar all columns except

column 7DW are shown to have a capacity-demand ratio (C/D) of less than one, indicating potential failure. The columns that are shown to be most susceptible to failure are columns 5DW and 8DW for columns with pedestals and column 10DW for columns without pedestals.

5.7 Conclusions

The following conclusions are based on the study presented in this chapter:

1. The embedment of the longitudinal reinforcement at the column-pedestal interface and pedestal-footing interface for columns in Ramp DW is sufficient for development.
2. The lateral reinforcement of the pedestals was highly deficient and could not provide the strength to make the column and pedestal work as an integral unit.
3. Design of the pedestal extension retrofit and the addition of reinforcement outside pedestal were sufficient to prevent pedestal deterioration and to integrate the pedestal with the column.
4. When plastic hinging was shifted to the columns above the pedestal, the plastic shear demand was increased and exceeded the shear capacity of the column under moderate displacement ductilities.
5. Severing selected longitudinal bars at the base of the column adequately reduced the plastic shear demand.
6. Severing of longitudinal bars to reduce the shear demand, without the addition of shear reinforcement was not sufficient to prevent a column shear failure. It

became clear that a minimal column jacket is necessary to change the failure mode to flexure and to increase the displacement ductility beyond 5.9.

7. A column retrofit including pedestal extension, pedestal reinforcement, severed bars, and sufficient shear reinforcement should be effective to dramatically improve the column response.

8. Under a moderate earthquake, displacement ductility capacity-demand ratios from specimen testing and nonlinear modeling indicated potential failure of columns 5DW, 8DW, and 10DW. Modeling suggests these columns to be the most susceptible to earthquake damage.

CHAPTER 6

Seismic Retrofit of Two-Column Bents with Diamond Shape Columns

6.1 Introduction

The experimental study of the seismic vulnerability of the main structure of the Las Vegas Downtown Viaduct is presented in this chapter. The selection of the critical bent, and the sizing and construction of the as-built specimen are discussed. Details of retrofitted specimen, including selection of fiber reinforced plastics (FRP) and material properties are also presented in this chapter. The experimental results are explained using analytical methods. Based on the experimental results and analytical studies, a step-by-step retrofit design method is presented. This chapter presents the highlights of the study presented in Ref. 4.

6.2 Test Specimens

6.2.1 Identification of Critical Bent

The main structure has 24 spans and incorporates piers with two, three, or four column bents. The columns are diamond shape. The critical pier in the main structure was selected based on the highest shear demand on the columns. The initial evaluation was done by Dong et al[51]. Pier 16 west, a two column bent was found to be the critical pier. This is the prototype that was scaled down and tested on the shake table.

6.2.2 As built specimen

As-built specimen was a quarter scale model of the prototype. This scale was chosen so that maximum specimen ductility could be achieved without exceeding shake table capacity. The model was designated B2DA for bent with 2 columns of diamond shape with as-built details. Figure 6.1 shows the elevation view of the specimen. The general

reinforcement layout of the specimen is given in Fig. 6.2. Figure 6.3 and Fig. 6.4 show the reinforcement pattern in the column and the beam, respectively. Reinforcement at the bottom and top of the deck slab over a width of eight times the slab thickness on each side of the beam was assumed to contribute to the bent cap of the prototype and were accounted for by placing equivalent reinforcement in the bent cap of the specimen.

6.2.3 Retrofitted Specimen

The results obtained from testing the as-built model have suggested that only columns require retrofit to enhance their shear capacity (see subsequent sections). Steel jacket or fiber-reinforced plastic (FRP) wrap were the possible alternatives for column retrofit. FRP systems were easier to install on a column of diamond shape than steel jackets. Steel jackets would have to be oval shape thus changing the appearance of the columns. They also require grouting. Therefore it was decided to use FRP wraps as the method of retrofit for the columns. The FRP wraps were applied directly to the surface of the column and did not require grout. Uni-directional FRP systems allow the designer to increase the shear capacity without having significant increase in flexural capacity or stiffness.

Commonly used composite jackets to retrofit bridges are glass fiber reinforced plastic (GFRP) or carbon fiber reinforced plastic (CFRP). Selection of the type of FRP was based on the cost of the retrofit and the number of layers of wrap required. Number of required layers of GFRP and CFRP was calculated and the relevant cost was obtained from different suppliers. The cost of CFRP was considerably higher than GFRP but the number of layers of CFRP required was substantially less than that of GFRP. Based on cost analysis, it was finally decided to use carbon fiber (SCH-41) supplied by Fyfe Co. LLC.

6-2-4 Material properties

The average 28 day measured concrete compressive strength of specimens were 5000 psi (34.4 MPa), 6250 psi (43.1 MPa), and 4960 psi (34.2 MPa) for footing, columns and the beam respectively.

The grade 40 steel that was needed for the specimen could not be directly purchased from the supplier, as that particular grade of steel was no longer in production. Therefore Grade 60 steel was ordered and annealed to obtain the desired yield stress. The annealing process was done by trial and error, and after several repetitions the appropriate temperature ramp was obtained for the reinforcement and the wires. The carbon fiber used for the retrofit was also tested to obtain the material properties.

6.3 Test Procedure and Results

6.3.1 Test setup and Instrumentation

A photo of the actual test setup is shown in Fig. 6.5. The test setup for both specimens was the same. Before placing the specimen on the shake table, a steel beam was placed on the bent cap. The steel beam transfers the forces from the mass rig and the vertical jacks to the bent. The bent was connected to an inertial frame by a link and this completed the lateral loading system for the specimen. The inertial frame is called the mass rig and its design is discussed in Ref. 52. Once the link was attached to the specimen, the diagonal braces in the mass rig were removed and thus the mass rig was able to transmit inertial forces to the specimen.

The test specimens were instrumented with strain gages and displacement transducers. The strain gages were placed to measure the actual strains in the longitudinal and

transverse reinforcement and in the CFRP jackets. In addition, instruments were placed to measure lateral forces and displacements, vertical loads, and accelerations generated due to the earthquake motion. Finally all the instruments were connected to the data acquisition system. The data were collected at the rate of 160 samples per second.

6.3.2 Test Schedule

The earthquake that was simulated for this study was the 1994 Northridge earthquake measured at the parking lot of the Sylmar Hospital. The earthquake record was adjusted to account for the scale of the specimen and the loading. The peak acceleration of the Sylmar earthquake is 0.6g. The testing protocol was decided so that elastic and inelastic responses of the bent could be measured. Testing was done using scaled versions of the strong motion acceleration in increments until the failure of the specimen. The sequence of events for the as-built specimen is shown in Table 6-1.

6.3.3 Observed Behavior of As-built Specimen

First minor flexural cracks were observed at the top of the south column during Run 5. A permanent deformation of the specimen was seen after 1.0xSylmar and it increased with each subsequent run. A long shear crack was observed on the south column during Run 21 (with 1.75 x Sylmar). It was the first significant shear crack observed in the columns. The peak target table acceleration for the second to the last event (Run 22) was 1.2g, with peak amplitude that was 200 percent of the original Sylmar record. The permanent bent displacement was 1.59 in (41mm).

Measured force-displacement envelopes were idealized to elasto-plastic curves to calculate the displacement ductility of the specimen. The elastic portion of the curve starts at the origin and passes through the event at which the first column reinforcement

yielded. Then the yield level was established by equalizing the area between the measured and idealized curves. The idealized force-displacement curve is shown in Fig. 6-6. The specimen failed due to shear of the south column during the final run, which had a displacement ductility of 5.5. Figure 6-7 shows the failure of the south column. It was observed that seven tie bars ruptured and two tie bar hooks opened up.

6.3.4 Observed Behavior of Retrofitted Specimen

Small flexural cracks were observed in the joint region during Run 4. At 1.0xSylmar, long but thin shear cracks formed on both sides of the south beam near the edge of the column. There was no spalling of concrete in either the beam or the column until Run 17. The peak acceleration achieved during this event was 1.65g, which was 275 percent of the original Sylmar record. In the last event the peak lateral force was 36.2 kips (161 kN) and the maximum displacement was 4.96 in.(126mm). The full motion of the target earthquake could not be completed as the specimen formed a mechanism and became unstable. But this was only after the joint region was severely damaged due to spalling of concrete and column bar bond strength loss. The permanent bent displacement was 0.26 in (7 mm). The envelope based on the measured peak forces and the corresponding displacements and the elasto-plastic idealization is shown in Fig.6-8. The displacement at specimen failure was 4.02 in (102 mm) and this corresponds to a 20% decrease in peak load from all the runs. The measured displacement ductility of the retrofitted specimen was 9.6.

The flexural capacity of the retrofitted bent was close to that of the as built specimen. The maximum lateral loads on both specimens were just above 49 kips (218 kN). This ensured that the shear demands on the columns of both specimens were approximately

equal. Figure 6-9 and 6-10 show that the yield displacements are approximately the same from elasto-plastic idealization and the measured load-displacement envelopes. The ultimate displacement of B2DC was 61% larger than the value obtained from B2DA thus increasing the displacement ductility from 5.5 to 9.6, a 75% increase.

6.4 Analysis of Test Specimens

6.4.1 Moment Curvature Analysis

The moment curvature analysis was performed for members of both As-built (B2DA) and retrofitted (B2DC) specimens, using program RCMC[38]. This program is based on cross sectional property analysis. The program allows for the consideration of confined and unconfined concrete. The concrete was assumed to be unconfined in the as-built columns due to the large spacing and low amount of ties and stirrups in the column and beam sections. The bases of columns, however, were assumed to be confined. The column bases were two-way hinges and the confinement is provided by the footing and the column concrete. A new simple confinement model was used to calculate the confined concrete material properties of the retrofitted columns (B2DC). Moment curvature properties for the beam sections were the same as those obtained for B2DA since no retrofit was done on the beam. The columns, however, had different M-ϕ properties, due to the confinement provided by the CFRP jacket wrapped around the column.

6.4.2 Pushover Analysis

The lateral load carrying capacity of the as built and retrofitted specimens was studied using pushover analysis. Program DRAIN-3DX[5] was used for this purpose. Linear

elements were modeled as elastic line elements and non-linear elements (plastic hinges) as fiber elements.

Figure 6-9 shows the comparison of theoretical and experimental load-displacement curves for B2DA.The results compare well especially during pre-yield and partially into the post yield of the specimen. The input model for B2DC was the same as that used to analyze the as built specimen by DRAIN-3DX program, except for the concrete properties at the top of the column. The confined concrete properties were used. The load-displacement curves obtained from two Drain models were compared to experimental curve in Fig. 6-10. It is seen that the pre-yield values are comparable to the theoretical experimental curves. The theoretical lateral load capacity of the bent agreed with the experimental results when the column bases were treated as pins with no flexural capacity.

6.5 Retrofit Design Guidelines for Diamond Shape Columns

The performance of the retrofitted specimen suggests that the column retrofit was successful and met the retrofit objectives for the bents. A step-by-step guideline with a design example for retrofit design of multi-column bents with diamond shape columns are shown in Appendix B. The flow chart is shown in Fig. 6-11.

6.6 Conclusion Remarks

The following observations and conclusions were drawn from the experimental and analyses performed in the course for this chapter.

1. Although the structure was designed prior to 1970 and did not have adequate shear reinforcement and good detailing, the performance of the as-built specimen in terms of displacement ductility was considerably better than expected. Usually structures built during that period have displacement ductility capacity of approximately 2. However, the measured displacement ductility capacity of the as-built bent was 5.5.
2. The column retrofit was based on improving the shear capacity of the columns even though confinement requirement controlled the retrofit design. The cap beams did not need to be retrofitted. It was demonstrated that the increase in the column shear capacity by the CFRP jacket was sufficient to change the mode of failure from shear to flexural failure even though the confinement requirements were not met. This led to substantial saving in the cost of retrofit.
3. The displacement ductility capacity of the retrofitted bent was 9.6. This is a 75% increase in displacement ductility compared to that achieved by the as built specimen. This confirms the effectiveness of this retrofit method to improve the seismic performance of the bent.

CHAPTER 7

Summary and Conclusions

7.1 Summary

This study was primarily focused on the seismic vulnerability assessment of the Las Vegas Downtown Viaduct structures. The development of the seismic retrofit strategies for the piers was the main goal of the study. Several aspects of the behavior of the bridge were studied both at the system level and at component level. The studies at the system level included pushover analysis of the entire structure and an evaluation of the ductility demand. Another aspect of the system behavior was a general study of the effects of incoherent ground motions on the forces and displacements of the bridge. Other segments of the study included the seismic evaluation of the ramp structures, the development of retrofit strategies for single-column bents, and the development of retrofit details for multi-column bents. Several research reports providing the details of the above aspects of the study have been prepared. This report presents a brief summary of the highlights of those studies.

The viaduct structure is typical of bridge structures built before 1970. It has insufficient transverse reinforcement in the columns and the cap beam, poor seismic detailing, no joint shear reinforcement, and inadequate configuration of the confinement reinforcement. The viaduct consists of a main bridge, two off-ramps, and one on-ramp structure. The main bridge substructure consists of two, three and four column bents. The columns were diamond shaped. The push-over analysis was conducted on the main bridge in the longitudinal and transverse directions, using Drain-3DX software, to identify the most critical pier. The maximum displacement for each pier was calculated

directly from the push-over diagram while the yield displacement was determined from the geometrical and material properties of the pier.

The analytical study to determine the influence of the incoherency of earthquake ground motions on the main bridge included three sources of incoherency: (1) the geometry incoherency effect, (2) the wave-passage effect and (3) the local site effect. The influence of each factor and a combination of the factors were studied. A linear model was used for response history analysis of the longitudinal response of the bridge. It was shown that the incoherency motions can have a dramatic influence on the structural response by modifying the dynamic response of uniform excitation and inducing pseudo-static response, which does not exist in structures subjected to uniform excitation.

As a part of this extensive investigation, the seismic vulnerability of two off-ramp bridge structures of Las Vegas downtown viaduct was also investigated. . The 1RWD off-ramp superstructure is supported by two piers, while the 1RWL-2RWL off-ramp superstructure is supported by three piers. All the piers consisted of single octagonal shape columns. The maximum shear and moment capacities of the columns of the off-ramp structures were determined by moment-curvature analysis. The existing deign of the bridge columns were also checked against the seismic provisions of the ACI, AASHTO, Caltrans, and ATC-32 recent bridge design codes. A comparison was made among the minimum required steel confinement, according to the codes, and the confinement steel provided in the columns. A comparison was also made between existing bridge column shear, moment and deformation capacities with the shear, moment and deformation demands as determined using the AASHTO, and UBC codes. Three dimensional non-linear finite element models of the both off-ramp bridge structures were conducted using. Drain-3DX

program. Two different earthquakes, Sylmar and ATC, were applied to the bridges for the analysis. The shear, moment and deformation demands found from the finite element analyses of the bridges were compared and the shear demands were found to exceed the capacities. Column retrofit design guidelines provided by Catrans were used for retrofit design. Two types of composite wraps, Carbon Fiber Reinforced Polymer (CFRP) and Glass Fiber Reinforced Polymer (GFRP) were used for retrofit design. Finally, the number of layers of composite wrap required for each column was determined to meet all the minimum requirements of the Caltrans design guidelines.

The on-ramp structure of Las Vegas Downtown Viaduct was studied by both shake table testing of the columns and analytical evaluation of the bridge. The study focused on developing retrofit methods for octagonal single column piers. Three identical quarter-scale specimens of the critical column (8DW) were built. They were tested on the shake table using the 1994 Northridge Sylmar earthquake record. The first of the three columns, OLVA was tested as-built. The other two, OLVR-1 and OLVR-2 were retrofitted and tested for the same input to determine retrofit effectiveness. Testing of OLVA revealed cracking at the vertical column-pedestal interface at 0.75xSylmar due to lack of lateral pedestal reinforcement, and failure at this location under 2.0xSylmar at a ductility level of 6.9. The pedestal cracking was cause for concern since it began at a small ground motion at a ductility of only 0.63 and large pedestal cracking began at a ductility of only 1.46. The pedestal in OLVR-1 was retrofitted to improve its performance and shift hinging into the column. The retrofit consisted of an extension of the pedestal and one-way hinge, and also the addition of a GFRP (glass fiber reinforcement plastic) jacket as lateral pedestal reinforcement. No retrofit was applied on

the column above the pedestal. OLVR-1 was tested up to 2.75xSylmar until the column failed in shear under a displacement ductility of 4.6. It was decided for the OLVR-2 retrofit to include the OLVR-1 pedestal retrofit and also to severe some of the longitudinal bars to reduce the shear demand. OLVR-2 achieved an increase displacement capacity compared to OLVR-1 from 4.6 to 5.9. Final recommendations to retrofit the columns with pedestals include the pedestal and severed bar retrofits applied to OLVR-2 plus a minimum number of FRP layers to further enhance the shear capacity and ductility.

A two column bent (Pier 16 West) with the highest shear demand was selected as the critical one. Two quarter scale models of the prototype bent were constructed and tested on the shake table subjected to the 1994 Northridge Sylmar earthquake. One of the specimens tested as built and the other one was retrofitted using unidirectional carbon fiber reinforced plastic (CFRP) jacket. The columns in the as built specimen failed in shear at 2.25xSylmar with the displacement ductility capacity of 5.5. The as-built specimen showed that the cap beams may be left without retrofit thus reducing the retrofit cost substantially. The failure of the retrofitted specimen was at the beam column joint with a displacement ductility capacity of 9.6. The experimental results proved the retrofit to be very effective in increasing the displacement ductility capacity by 75%.

7.2 Conclusions

The following conclusions are based on the study presented in this report:

1. Push-over analysis showed that the displacement ductility demand in the majority of the columns exceeds the capacity of the columns. The shear capacity is also marginal in the columns.

2. The limited study of earthquake incoherency at different supports of the viaduct showed that the response at the majority of locations may exceed that of uniform ground motion. This effect needs to be accounted for in the retrofit design.

3. Although the main structure did not have adequate shear reinforcement and good detailing, the performance of the as-built specimen in terms of displacement ductility was considerably better than expected. This led to the conclusion that the cap beams in the bridge do not need to be retrofitted and substantial saving in the cost of retrofit can be made accordingly.

4. The CFRP jackets provided a large increase in shear capacity of the column of the main structure and thus changed the mode of failure from shear to flexure. The displacement ductility capacity of the retrofitted bent was 9.6 even though only one layer (corresponding to four layers in the actual bridge) of CFRP composite was used in the retrofit of the model frame.

5. The embedment of the longitudinal reinforcement at the column-pedestal interface and pedestal-footing interface for columns in on-ramp structure is sufficient for adequate development, while the lateral reinforcement of the pedestals was highly deficient and could not provide the strength to make the column and pedestal work as an integral unit. The design of the pedestal extension retrofit and the addition of reinforcement outside pedestal for on-ramp structure were sufficient to prevent pedestal deterioration and to integrate the pedestal with the column.

REFERENCES

1- Yang, Q., Saiidi, M., Wang,H., and Itani, A.,"Influence of Ground Motion Incoherency on Earthquake Response of Multi-Support Structures", Civil Engineering Department, Report No. CCEER-02-2, University of Nevada, Reno, May 2002.

2- Hassan, M., "Seismic Vulnerability Assessment of Off-Ramp Structures of the Las Vegas Downtown Viaduct", MSc Thesis, Department of Civil and Environmental Engineering, University of Nevada, Las Vegas, Dec. 2002.

3- Johnson, N., Saiidi, M., Itani, A. and Ladkani, S., "Seismic Retrofit of Octagonal Columns with Pedestal and One-Way Hinge at the Base," Civil Engineering Department, Report No. CCEER-03-05, University of Nevada, Reno, 2003.

4- Sureshkumar, K., Saiidi, M., Itani, A. and Ladkani, S.,"Seismic Retrofit of Two-Column Bents with Diamond Shape Columns," Civil Engineering Department, Report No. CCEER-04-09, University of Nevada, Reno, 2004.

5- Prakash, V., Powell, G., and Cambell, S., "DRAIN-3DX: Base Program User Guide, V1.1", Structural Engineering Mechanics and Materials, Department of Civil Engineering, University of California, Berkely, November 1993.

6- Priestley, M., Seible, F., and Calvi, G., "Seismic Design and Retrofit of Bridges", Wiley, 1996.

7- Yang Q., and Chen Y., 'A Practical Coherency Model for Spatially Varying Ground Motions', Structural Engineering and Mechanics, 9(2), pp 141-152, 2000.

8- Yang Q., and Jiang H., 'Generation of Ground Motion Non-Stationary Both in Time and Frequency Domains Based on Phase Difference Spectrum', Earthquake Engineering and Engineering Vibration, 21(3), pp 10-16, 2001.

9- Bogdanoff J., Goldberg J., and Schiff E. "The Effect of Ground Transmission Time on the Response of Long Structures". Bull Seism Soc Am, 55(3), pp 627-640, 1965.

10- Luco J., and Wong L., 'Response of a Rigid Foundation to a Spatially Random Ground Motion', Earthquake Engineering and Structural Dynamics, 14, pp 891-908, 1986.

11- Perotti, F., 'Structural Response to Non-Stationary Multiple-Support Random Excitation', Earthquake Engineering and Structural Dynamics, 19(4), pp 513-527, 1990.

12- Zerva A., 'Response of Multi-Span Beams to Spatially Incoherent Seismic Ground Motions', Earthquake Engineering and Structural Dynamics, 19, pp 819-832, 1990.

13- Hao H., and Zhang S., 'Spatial Ground Motion Effect on Relative Displacement of Adjacent Building Structures', Earthquake Engineering and Structural Dynamics, 28, pp 333-349, 1999.

14- Harichandran R., Hawwari A., and Sweiden B., 'Response of Long-Span Bridges to Spatially Varying Ground Motion', J. of Structural Engineering, 122(5), pp 476-484, 1996.

15- Kahn M., Gibert R., and Bard P., "Influence of Seismic Waves Spatial Variability on Bridges: A Sensitivity Analysis". Earthquake Engineering & Structural Dynamic. 25(4), pp 795-814, 1996.
16- Shrikhande M., and Gupta V., 'Dynamic Soil-Structure Interaction Effects on the Seismic Response of Suspension Bridges', Earthquake Engineering and Structural Dynamics, 28, pp 1383-1403, 1999.
17- Ettouney, M, Hapij A., and Gajer, R., 'Frequency Domain Analysis of Long-Span Bridges Subjected to Non Uniform Seismic Motions', J. of Bridge Engineering, 6(6), pp 577-586 ,2001.
18- Nazmy A., and Abdel-Ghaffar A., 'Effect of Ground Motion Spatial Variability on the Response of Cable-Stayed Bridges' Earthquake Engineering and Structural Dynamics, 21, pp 1-20, 1992.
19- Abdel-Ghaffar A., and Nazmy A., '3-D Nonlinear Seismic Behavior of Cable-Stayed Bridge', Journal of Structural Engineering, ASCE 117(11), pp 3456-3476, 1991.
20- Price T., and Eberhard M., 'Effects of Spatially Varying Ground Motions on Short Bridges', J. Structural Engineering, 124(8), pp 948-955, 1998.
21- Hao H., 'Response of Two-Way Eccentric Building to Nonuniform Base Excitations', Engineering Structures, 20(8), pp 677-684, 1998.
22- Behnamfar F., and Sugimura Y., 'Dynamic Response of Adjacent Structures Under Spatially Variable Seismic', Probabilistic Engineering Mechanics, 14, pp 33-44, 1999.
23- Betti R., and Panariello G., 'Active Tendon Control Systems for Structures Subjected to Multiple Support Excitation', Smart Materials and Structures, 4, pp 153-163, 1995.
24- Betti R., Abdel-Ghaffar A., and Nazmy A., 'Kinematic Soil-Structure Interaction for Long-Span Cable-Supported Bridges', Earthquake Engineering and Structural Dynamics, 22, pp 415-430, 1993.
25- Bolt B., 'The Variation of Strong Ground Motion over Short Distance', 8th WCEE, San Francisco, Vol.2, pp183-189 (1984); EERC Report No. UCB/EERC-84/13,1984.
26- Abrahamson N., 'Spatial Variation of Multiple Support Inputs', Proc. 1st U.S. Seminar Seismic Evaluation and Retrofit of Steel Bridges, University of California, Berkeley, 1993.
27- Harichandran R., and Vanmarke E., 'Stochastic Variation of Earthquake Ground Motion in Space and Time', J. of Engineering Mechanics, 112(2), pp 154-174, 1986.
28- Abrahamson N., Schneider J., and Stepp J., 'Empirical Spatial Coherency Function for Application to Soil-Structure Interaction Analysis', Earthquake Spectra, 7, pp 1-28, 1991.
29- Loh C., and Yeh T., 'Spatial Variation and Stochastic Modeling of Seismic Differential Ground Movement', Earthquake Engineering and Structural Dynamics, 16, pp 583-596, 1988.
30- Hao H., Oliveira C., and Penzien J., 'Multiple-Station Ground Motion Processing and Simulation Based on SMART-1 Array Data', Nuclear Engineering And Design, 111, pp 293-310, 1989.

31- Oliveira C., Hao H., and Penzien J., 'Ground Motion Modeling For Multiple-Input Structural Analysis', Structural Safety, 10, pp 79-93, 1991.
32- Der Kiureghian A., 'A Coherency Model for Spatially Varying Ground Motions', Earthquake Engineering and Structural Dynamics, 25, pp 99-111, 1996.
33- Laouami N., and Labbe P., 'Analytical Approach for Evaluation of the Seismic Ground Motion Coherency Function', Soil Dynamics and Earthquake Engineering, 21, pp 727-733, 2001.
34- Boissieres H., and Vanmarcke E., 'Estimation of Lags for a Seismograph Array: Wave Propagation and Composite Correlation', Soil Dynamics and Earthquake Engineering, 14, pp 5-21, 1995.
35- Boissieres H., and Vanmarcke E., 'Spatial Correlation of Earthquake Ground Motion: Non-Parametric Estimation', Soil Dynamics and Earthquake Engineering, 14, pp 23-31, 1995.
36- Monti G., Nuti C., and Pinto P., 'Nonlinear Response of Bridges under Multi-Support Excitation', J. Structural Engineering, 122(10), pp 1147-1159, 1996.
37- California Department of Transportation", Memo to Designers 20-4 Attachment B", Engineering Service Center, Earthquake Engineering Branch, California, November, 1996.
38- Wehbe, N. and Saiidi, M., " User's Manual for RCMC v1.2, A Computer Program for Moment-Curvature Analysis of Confined and Unconfined Reinforced Concrete Sections", Civil Engineering Department, University of Nevada, Reno, May 1999.
39- California Department of Transportation, " Memo to Designers 20-4 Attachment B", Engineering Service Center, Earthquake Engineering Branch, California, July 1999.
40- Federal Highway Administration, "Seismic Retrofitting Manual for Highway Bridges", Publication No. FHWA-RD-94-052,Virginia, May 1995.
41- Wehbe, N., Saiidi, M., and Sanders, D., "Effects of confinement and flares on the seismic performance of reinforced concrete bridge columns", Report No. 97-2,CCEER. Department of Civil Engineering, University of Nevada, Reno, September1997.
42- Williams, A.,"Seismic design of Buildings and Bridges'., Second edition, Engineering press, Austin, Texas,1998.
43- Ladkany, S. and Ahmed, A.," Case Study for the Dynamic Earthquake Response of Hybrid Two Stories Tower.", Proceedings of the DOE/ESCORT conference, Las Vegas, Nevada, 2000.
44- International Conference Building Officials," Uniform Building Code 1997", Whittier, California, 1997.
45- Clough, R. and Pension, J., "Dynamics of Structures.", Second Edition, MacGraw-Hill, Inc.,1993.
46- Darwish, I., Saiidi,M., Norris,G., and Maragakis,E.,"Determination of In-Situ Footing Stiffness Using Full-Scale Dynamic Field Testing", Center for Civil Engineering and Earthquake Research, Report No. CCEER-97-03, Department of Civil Engineering, University of Nevada, Reno, October,1997.
47- Federal Highway Administration, " Highway Bridge Foundation Design to Resist Earthquake Motion", Report No. FHWA/RD/86-102, Washington, D.C, 1986.

48- Dorby, R. and Gazetas, G., "Dynamic Response of Arbitrarily Shaped Foundations", Journal of Geotechnical Engineering, ASCE, 112(2), pp. 109-135, February 1986.
49- Dorby,R. and Gazetas,G., and Stokoe, K.H., "Dynamic Response of Arbitrarily Shaped Foundations: Experimental Verification", Journal of Geotechnical Engineering, ASCE, 112(2), pp. 136-149, February 1986,
50- Chopra, A., Dynamics of Structures, Prentice Hall, USA, 1995.
51- Dong, G., "Report on the Analysis of Downtown Las Vegas Viaduct," A Special Project Report Submitted to the Civil Engineering Department, University of Nevada, Reno, December 2003.
52- Laplace, P., Sanders, D., Douglas, B., and Saiidi, M., "Shake Table Testing of Flexure Dominated Reinforced Concrete Bridge Columns", Report No. CCEER-99-13, University of Nevada, Reno, 1999.
53- California Department of Transportation, " Seismic Design Criteria Version 1.2",Engineering Service Center, Earthquake Engineering Branch, California, December 2001.
54- American Association of State Highway and Transportation Officials, "Standard Specifications for Highway Bridges", AASHTO, Washington D.C., 1996.
55- Sexmith, R., Anderson, D., and English, D., "Cyclic Behavior of Concrete Bridge Bents", ACI Structural Journal, 94(2), pp 103-1133, March-April 1997.
56- Iacobucci, R., Sheikh, S., and Bayrak, O., "Retrofit of Square Concrete Columns with Carbon Fiber-Reinforced Polymer for Seismic Resistance", ACI Structural Journal, 100(6), pp 785-794, November-December 2003.

Table 2-1a: Displacement Ductility Demands for East Viaduct Bound

Viaduct Pier	Corresponding Frame	Yield Displacement, Δ_y		Displacement Ductility	
		In Weak Direction	In Strong Direction	In Weak Direction	In Strong Direction
P1A	Frame 1	0.83' (253)	0.51' (155)	0.92	1.22
P1		0.75' (229)	0.46' (140)	0.87	**1.59**
P2		0.72' (219)	0.44' (134)	0.90	**1.98**
P3	Frame 2	0.46' (140)	0.25' (76)	1.11	**2.56**
P4		0.40' (122)	0.23' (70)	1.28	**1.63**
P5	Frame 3	0.35' (107)	0.2' (61)	1.14	1.43
P6		0.26' (79)	0.16' (49)	**1.54**	1.38
P7		0.21' (64)	0.13' (40)	**1.90**	1.15
P8	Frame 4	0.36' (110)	0.22' (67)	**1.56**	**3.91**
P9		0.37' (113)	0.22' (67)	**1.51**	**4.00**
P10	Frame 5	0.36' (110)	0.22'(67)	1.22	**2.05**
P11		0.27' (82)	0.17' (52)	**1.63**	**2.06**
P12		0.27' (82)	0.16' (49)	**1.63**	**1.63**
P13	Frame 6	0.27' (82)	0.15' (46)	**2.04**	**1.87**
P14		0.24' (73)	0.14' (43)	**2.29**	**1.93**
P15	Frame 7	0.26' (79)	0.16" (49)	**1.65**	1.00
P16		0.26' (79)	0.16' (49)	**1.65**	0.80
P17	Frame 7A	0.27' (82)	0.16" (49)	**1.59**	0.69
P18	Frame 8	0.29' (88)	0.04' (12)	**2.00**	0.85
P20		----------	----------	----------	----------
P21		0.29' (88)	0.04' (12)	**2.00**	0.85
P22		0.32' (97)	0.19' (58)	**1.84**	0.18

Table 2-1b: Displacement Ductility Demands for West Viaduct Bound

Viaduct Pier	Corresponding Frame	Yield Displacement, Δ_y		Displacement Ductility	
		In Weak Direction	In Strong Direction	In Weak Direction	In Strong Direction
P1A	Frame 1	0.73’ (222)	0.44’ (134)	0.40	1.16
P1		0.66’ (201)	0.40’ (122)	0.48	**1.60**
P2		0.61’ (186)	0.37’ (133)	0.56	**2.10**
P3	Frame 2	0.53’ (162)	0.32’ (98)	0.55	**1.97**
P4		0.49’ (149)	0.29’ (88)	0.53	**1.93**
P5	Frame 3	0.44’ (134)	0.24’ (73)	0.95	**3.38**
P6		0.33’ (100)	0.19’ (58)	1.27	**2.63**
P7		0.28’ (85)	0.16’ (49)	**1.50**	1.44
P8	Frame 4	0.34’ (104)	0.2’ (61)	**1.60**	**3.70**
P9		0.41’ (125)	0.25’ (76)	1.32	**3.00**
P10	Frame 5	0.35’(107)	0.22’ (67)	1.20	**1.55**
P11		0.27’ (82)	0.16’ (49)	**1.56**	**1.56**
P12		0.27’ (82)	0.16’ (49)	**1.56**	1.06
P13	Frame 6	0.26’ (79)	0.16’ (49)	1.12	**1.81**
P14		0.25’ (76)	0.15’ (46)	1.16	**2.27**
P15	Frame 7	0.23’ (70)	0.14’ (43)	**1.87**	**2.80**
P16		0.23’ (70)	0.14’ (43)	**1.81**	**5.00**
P17	Frame 7A	0.26’ (79)	0.03’ (9)	**2.23**	0.83
P18	Frame 8	----------	----------	----------	----------
P20		0.21’ (64)	0.02’ (6)	**2.81**	**2.00**
P21		----------	----------	----------	----------
P22		0.25’ (76)	0.15’ (46)	**2.40**	0.53

Table 2-2a: Column Shear Demand and Capacity for the East Viaduct Bound

Viaduct Pier	Frame	Shear Capacity for the Critical Column		Shear Demand for the Critical Column		Demand/ Capacity in 2	Demand/ Capacity in 1
		Direction 2	Direction 1	Direction 2	Direction 1		
P1A	Frame 1	509	500	60	202	0.12	0.40
P1		516	506	76	258	0.15	0.51
P2		517	507	84	286	0.16	0.56
P3	Frame 2	500	493	97	230	0.19	0.47
P4		504	496	93	268	0.18	0.54
P5	Frame 3	507	499	84	239	0.17	0.48
P6		513	503	118	242	0.23	0.48
P7		513	503	158	251	0.31	0.50
P8	Frame 4	520	510	132	323	0.25	0.63
P9		516	507	133	338	0.26	0.67
P10	Frame 5	513	503	97	288	0.19	0.57
P11		512	503	145	316	0.28	0.63
P12		516	507	143	291	0.28	0.57
P13	Frame 6	506	498	134	273	0.26	0.55
P14		512	503	103	264	0.20	0.52
P15	Frame 7	516	506	105	246	0.20	0.49
P16		519	508	106	202	0.20	0.40
P17	7A	514	504	164	190	0.32	0.38
P18	Frame 8			234	1320		
P20		----------	----------	----------	----------		
P21				256	1210		
P22		485	480	154	48	0.32	0.10

Table 2-2b: Column Shear Demand and Capacity for the West Viaduct Bound

Viaduct Pier	Frame	Shear Capacity for the Critical Column		Shear Demand for the Critical Column		Demand/ Capacity in 2	Demand/ Capacity in 1
		Direction 2	Direction 1	Direction 2	Direction 1		
P1A	Frame 1	498	491	24	200	0.05	0.41
P1		504	497	46	275	0.09	0.55
P2		420	411	53	152	0.13	0.37
P3	Frame 2	512	503	59	247	0.12	0.49
P4		509	500	30	252	0.06	0.50
P5	Frame 3	511	503	58	253	0.11	0.50
P6		512	503	95	283	0.19	0.56
P7		513	503	118	214	0.23	0.43
P8	Frame 4	512	503	114	311	0.22	0.62
P9		512	503	105	290	0.21	0.58
P10	Frame 5	512	503	95	268	0.19	0.53
P11		512	503	146	288	0.29	0.57
P12		512	503	143	234	0.28	0.47
P13	Frame 6	512	503	61	227	0.12	0.45
P14		512	503	130	358	0.25	0.71
P15	Frame 7	509	500	122	340	0.24	0.68
P16		507	499	89	362	0.18	0.73
P17	7A			350	816		
P18	Frame 8	----------	----------	----------	----------		
P20				413	1900		
P21		----------	----------	----------	----------		
P22		503	496	187	181	0.37	0.36

Table 3.1 Structural Parameters

Node/column	1	2	3	4	5	6	7	8
Mass ($\times 10^3$ Kg)	1642	1140	2365	1572	1683	2000	2642	1303
Length (m)	10.69	9.14	9.14	7.62	7.62	7.62	7.62	6.01
Area (m^2)	7.433	7.433	11.150	4.956	7.433	7.433	7.433	11.768
I_Z (m^4)	0.460	0.460	0.691	0.307	0.460	0.460	0.460	1.0007

Table 3.2 Dynamic Properties

Damping Ratio	The first four natural frequencies□rad/s□				Rayleigh damping coefficients	
	ω_1	ω_2	ω_3	ω_4	α	β
0.05	8.268	25.872	50.753	69.065	0.627	0.00293

Table 3.3 Generated Acceleration Records

Acc. No.	1	2	3	4	5	6	7	8
Amplitude (m/s^2)	3.7845	3.8053	3.8845	3.8553	3.8945	3.7502	3.8245	4.0607
Time (s)	17.92	18.28	17.52	16.08	18.84	19.88	18.02	19.50

Table 3.4 Cases with Different Soil Characteristics

Case	1	2	3 (Multi-input, Figure 3.7)	
input	Uniform input a_{s5}	Uniform input a_{m5}	Supports 1—3 a_{s5}	Supports 4—8 a_{m5}

Table 3.5 R_d of the Top Nodes for Uniform Excitations (m)

Node position	Case 1	Case 2	Case 5*
9	0.08645	0.04970	0.06808
11	0.08551	0.04911	0.06731
13	0.08423	0.04827	0.06625
15	0.08246	0.04708	0.06477
17	0.08025	0.04560	0.06293
19	0.07781	0.04401	0.06091
21	0.07503	0.04225	0.05864
23	0.07127	0.04005	0.05566

* Case 5* is the average of the maximum responses of Case 1 and Case 2.

Table 3.6 Maximum Absolute Displacements of Case 3

Node Position	D_d (m)	R_p (m)	R_d (m)	D_d/R_d (%)	R_p/R_d (%)	R_d/D^{5*}(%)
9	0.05658	0.01949	0.05851	96.7	33.3	85.9
11	0.05593	0.01958	0.05788	96.6	33.8	86.0
13	0.05502	0.01982	0.05700	96.5	34.8	86.0
15	0.05375	0.01025	0.05301	101.4	19.3	81.8
17	0.05219	0.00962	0.05149	101.4	18.7	81.8
19	0.05051	0.00909	0.04985	101.3	18.2	81.8
21	0.04864	0.00866	0.04802	101.3	18.0	81.9
23	0.04618	0.00831	0.04560	101.3	18.2	81.9

Table 3.7 Arrival Time Differences between Adjacent Supports

Δt_1	Δt_2	Δt_3	Δt_4	Δt_5	Δt_6	Δt_7
0.10	0.12	0.14	0.12	0.12	0.12	0.12

Table 3.8 Cases with Traveling Wave Effects

Case	4 (Propagating direction 8→1)							
support	1	2	3	4	5	6	7	8
input	a_{s5} (t-0.84s)	a_{s5} (t-0.74s)	a_{s5} (t-0.62s)	a_{m5} (t-0.48s)	a_{m5} (t-0.36s)	a_{m5} (t-0.24s)	a_{m5} (t-0.12s)	a_{m5} (t)
Case	5□Propagating direction 1→8							
support	1	2	3	4	5	6	7	8
Input	a_{s5} (t)	a_{s5} (t-0.10s)	a_{s5} (t-0.22s)	a_{m5} (t-0.36s)	a_{m5} (t-0.48s)	a_{m5} (t-0.60s)	a_{m5} (t-0.72s)	a_{m5} (t-0.84s)

Table 3.9 Maximum Absolute Displacements of Case 4

Node Position	D_d (m)	R_p (m)	R_d (m)	D_d/R_d (%)	R_p/R_d (%)	R_d/D^{5*} (%)
9	0.03537	0.03932	0.07624	46.4	51.6	112.0
11	0.03460	0.05306	0.06194	55.9	85.7	92.0
13	0.03343	0.04035	0.06089	54.9	66.3	91.9
15	0.03155	0.03189	0.04927	64.0	64.7	76.1
17	0.02989	0.02584	0.03201	93.4	80.7	50.9
19	0.02876	0.01850	0.02389	120.4	77.4	39.2
21	0.02756	0.01829	0.03941	69.9	46.4	67.2
23	0.02611	0.02837	0.04322	60.4	65.6	77.7

Table 3.10 Maximum Absolute Displacements of Case 5

Node Position	D_d (m)	R_p (m)	R_d (m)	D_d/R_d (%)	R_p/R_d (%)	R_d/D^{5*} (%)
9	0.03142	0.06262	0.07546	41.6	83.0	110.8
11	0.03108	0.05872	0.05979	52.0	98.0	88.8
13	0.03062	0.05669	0.05348	57.3	106.0	80.7
15	0.02999	0.03054	0.03622	82.8	84.3	55.9
17	0.02918	0.02422	0.02916	100.0	83.0	46.3
19	0.02827	0.02366	0.02447	115.5	96.7	40.2
21	0.02722	0.02550	0.03153	86.3	80.9	53.8
23	0.02581	0.02902	0.04454	57.9	65.2	80.0

Table 3.11 Maximum Absolute Displacements of Case 6

Node Position	D_d (m)	R_p (m)	R_d (m)	D_d/R_d (%)	R_p/R_d (%)	R_d/D^{5*} (%)
9	0.03297	0.07479	0.07357	44.8	101.6	108.1
11	0.03247	0.07343	0.08016	54.0	92.0	119.1
13	0.03173	0.08262	0.08431	37.6	98.0	127.3
15	0.03062	0.07217	0.08524	35.9	84.7	131.6
17	0.02933	0.05358	0.06445	45.5	83.1	102.4
19	0.02800	0.06278	0.06641	42.2	94.5	109.0
21	0.02667	0.08963	0.09269	28.8	96.7	158.1
23	0.02520	0.06059	0.05919	42.6	102.3	106.3

Table 3.12 Cases with Combined Effects

Case	7□Propagating direction 8→1□							
Supports	1	2	3	4	5	6	7	8
Input	a_{s1} (t-0.84s)	a_{s2} (t-0.74s)	a_{s3} (t-0.62s)	a_{m4} (t-0.48s)	a_{m5} (t-0.36s)	a_{m6} (t-0.24s)	a_{m7} (t-0.12s)	a_{m8} (t)
Case	8□Propagating direction 1→8□							
Supports	1	2	3	4	5	6	7	8
Input	a_{s1} (t)	a_{s2} (t-0.10s)	a_{s3} (t-0.22s)	a_{m4} (t-0.36s)	a_{m5} (t-0.48s)	a_{m6} (t-0.60s)	a_{m7} (t-0.72s)	a_{m8} (t-0.84s)

Table 3.13 Maximum Absolute Displacements of Case 7

Node Position	D_d (m)	R_p (m)	R_d (m)	D_d/R_d (%)	R_p/R_d (%)	R_d/D^{5*} (%)
9	0.03635	0.06342	0.07088	51.3	89.5	104.1
11	0.03584	0.06307	0.06593	54.4	95.7	97.9
13	0.03511	0.08522	0.08348	42.1	102.1	126.0
15	0.03406	0.08253	0.08677	39.3	95.1	134.0
17	0.03284	0.03447	0.03775	87.0	91.3	60.0
19	0.03157	0.08868	0.09223	34.2	96.2	151.4
21	0.03023	0.10070	0.10137	29.8	99.3	172.9
23	0.02864	0.05466	0.05712	50.1	95.7	102.6

Table 3.14 Maximum Absolute Displacements of Case 8

Node Position	D_d (m)	R_p (m)	R_d (m)	D_d/R_d (%)	R_p/R_d (%)	R_d/D^{5**} (%)
9	0.03346	0.07271	0.07985	41.9	91.0	117.3
11	0.03261	0.08640	0.10583	30.8	81.6	157.2
13	0.03131	0.06643	0.09204	34.0	72.2	138.9
15	0.02936	0.07018	0.07478	39.3	93.8	115.5
17	0.02823	0.07703	0.09089	31.1	84.8	144.4
19	0.02704	0.04460	0.05398	50.1	82.6	88.6
21	0.02594	0.09150	0.10741	24.2	85.2	183.2
23	0.02467	0.05969	0.06760	34.5	88.3	121.5

Table 4.1: Maximum moment and displacement capacities of the columns determined using RCMC program

Name of the Off-Ramp	Name of the Column	Maximum Moment in Strong Direction (kip-ft)	Maximum Moment in Weak Direction (kip-ft)	Displacement in strong Direction (inch)	Displacement in Weak Direction (inch)
1RWD	8WD	10590	4702	1.60	3.39
	9WD	10590	4702	1.35	2.86
1RWL-2RWL	19WL	22119	7090	1.32	5.84
	22WL	22119	7090	1.29	5.68
	23WL	22119	7090	0.98	4.29

Table 4.2: Maximum shear capacity of the columns using CALTRANS, FHWA and Wehbe methods

Name of the Off-Ramp	Name of the Column	Axial Load on the Column (kip)	Shear Capacity (kip)		
			CALTRANS	FHWA	Wehbe
1RWD	8WD	557	220.0	360.3	220.3
	9WD	534	219.8	364.2	220.2
1RWL-2RWL	19WL	737	269.8	447.1	270.2
	22WL	803	269.8	457.0	270.2
	23WL	740	269.8	464.5	270.3

Table 4.3: Shear, moment and displacement demands on the bridge, calculated using seismic provision of UBC 1997

Name of the Off-Ramps	Name of the Columns	Shear Demand (kip)		Moment Demand (kip-ft)		Displacement (inch)	
		Strong Direction (transverse direction)	Weak Direction (longitudinal direction)	Strong Direction (transverse direction)	Weak Direction (longitudinal direction)	Strong Direction (transverse direction)	Weak Direction (longitudinal direction)
1RWD	8WD	420	390	8610	7995	0.498	1.534
	9WD	652	373	12192	6975	0.289	1.534
1RWL-2RWL	19WL	457	453	12517	12408	0.446	4.195
	22WL	601	561	16227	15147	0.306	4.195
	23WL	517	517	12005	12005	0.232	1.839

Table 4.4: Corrected footing stiffness values for the columns

Name of the column	Kx (kip/in)	Ky (kip/in)	K(rocking,x) (kip-in/radian)	K(rocking,y) (kip-in/radian)
19WL	6.48E+05	6.57E+05	1.10E+08	4.14E+07
22WL	6.74E+05	6.83E+05	1.15E+08	4.33E+07
23WL	6.39E+05	6.48E+05	1.09E+08	4.12E+07
8WD	8.35E+05	8.59E+05	9.56E+07	4.54E+07
9WD	6.94E+05	7.13E+05	7.94E+07	3.77E+07

Table 4.5 :Summary of Drain Output for Sylmar x 0.5

	Column	19WL	22WL	23WL	8WD	9WD
Demand	Maximum moment,strong direction (kip-ft)	12690	9318	9921	4158	3620
	Maximum moment,weak direction (kip-ft)	6545	7111	6068	2482	2816
	Maximum shear, strong direction (kip)	597	438	457	196	236
	Maximum shear, weak direction (kip)	336	354	292	178	163
	Maximum displacemet, strong direction(inch)	0.3400	0.2411	0.2236	0.0961	0.0766
	Maximum displacement, weak direction (inch)	1.0824	1.0823	0.8286	0.2672	0.2637
Capacity	Shear capacity (CALTRANS method),Kip	270	270	270	220	220
	Displacement capacity,strong direction(inch)	1.32	1.29	0.98	1.60	1.35
	Displacement capacity,weak direction(inch)	5.84	5.68	4.29	3.39	2.86
	Moment capacity, strong direction (Moment-Curvature analysis (kip-ft)	22119	22119	22119	10590	10590
	Moment capacity, weak direction (moment-curvature analysis) (kip-ft)	7090	7090	7090	4702	4702

Table 4.6 :Summary of drain output for Sylmar x 1.0

	Column	19WL	22WL	23WL	8WD	9WD
Demand	Maximum moment,strong direction (kip-ft)	17260	16360	17600	8267	7225
	Maximum moment,weak direction (kip-ft)	7999	8739	9140	4358	4643
	Maximum shear, strong direction (kip)	886	725	952	390	405
	Maximum shear, weak direction (kip)	525	551	611	346	202
	Maximum displacement, strong direction(inch)	0.6696	0.5345	0.5139	0.2307	0.1888
	Maximum displacement, weak direction (inch)	1.9781	1.9855	1.8307	0.5575	0.5560
Capacity	Shear capacity (CALTRANS method) (Kip)	270	270	270	220	220
	Displacement capacity, strong direction(inch)	1.32	1.29	0.98	1.60	1.35
	Displacement capacity, weak direction(inch)	5.84	5.68	4.29	3.39	2.86
	Moment capacity, strong direction (Moment-Curvature Analysis) (kip-ft)	22119	22119	22119	10590	10590
	Moment capacity, weak direction (Moment-Curvature Analysis) (kip-ft)	7090	7090	7090	4702	4702

Table 4.7 :Summary of drain output for Sylmar x 2.0

	Column	19WL	22WL	23WL	8WD	9WD
Demand	Maximum moment,strong direction (kip-ft)	30830	34090	30500	13170	12290
	Maximum moment,weak direction (kip-ft)	15540	11530	15750	5803	5325
	Maximum shear, strong direction (kip)	1507	1176	1488	633	561
	Maximum shear, weak direction (kip)	638	700	822	432	426
	Maximum Displacement, strong direction(inch)	1.7008	1.3057	1.2156	0.7258	0.5342
	Maximum displacement, weak direction (inch)	3.8939	3.9005	4.0412	0.9689	0.9684
Capacity	Shear capacity (CALTRANS method),Kip	270	270	270	220	220
	Displacement capacity,strong direction(inch)	1.32	1.29	0.98	1.60	1.35
	Displacement capacity,weak direction(inch)	5.84	5.68	4.29	3.39	2.86
	Moment capacity,strong direction (Moment-Curvature Analysis (kip-ft)	22119	22119	22119	10590	10590
	Moment capacity, strong direction (Moment-Curvature Analysis (kip-ft)	7090	7090	7090	4702	4702

Table 4.8: Summary of Drain Output for ATC x 0.5

	Column	19WL	22WL	23WL	8WD	9WD
Demand	Maximum moment,strong direction (kip-ft)	14200	9361	11210	9201	8631
	Maximum moment,weak direction (kip-ft)	4958	5118	4155	4680	3428
	Maximum shear, strong direction (kip)	657	391	496	527	504
	Maximum shear, weak direction (kip)	208	220	218	386	343
	Maximum displacement, strong direction(inch)	0.3458	0.2523	0.2013	0.1148	0.0941
	Maximum displacement, weak direction (inch)	1.2180	1.2179	0.9794	0.2862	0.2850
Capacity	Shear capacity (CALTRANS method),Kip	270	270	270	220	220
	Displacement capacity, strong direction(inch)	1.32	1.29	0.98	1.60	1.35
	Displacement capacity, weak direction(inch)	5.84	5.68	4.29	3.39	2.86
	Moment capacity, strong direction (Moment-Curvature Analysis (kip-ft)	22119	22119	22119	10590	10590
	Moment capacity,strong direction (Moment-Curvature Analysis (kip-ft)	7090	7090	7090	4702	4702

Table 4.9 :Summary of Drain Output for ATC x 1.0

	Column	19WL	22WL	23WL	8WD	9WD
Demand	Maximum moment,strong direction (kip-ft)	19370	17030	18390	11740	12390
	Maximum moment,weak direction (kip-ft)	9639	10200	8575	6064	4991
	Maximum shear, strong direction (kip)	906	744	841	579	628
	Maximum shear, weak direction (kip)	405	441	420	500	487
	Maximum displacement, strong direction(inch)	0.5716	0.5251	0.4247	0.5133	0.4135
	Maximum displacement, weak direction (inch)	2.4102	2.4176	1.9882	0.9313	0.9310
Capacity	Shear capacity (CALTRANS method),Kip	270	270	270	220	220
	Displacement capacity,strong direction(inch)	1.32	1.29	0.98	1.60	1.35
	Displacement capacity, weak direction(inch)	5.84	5.68	4.29	3.39	2.86
	Moment capacity, strong direction (Moment-Curvature Analysis (kip-ft)	22119	22119	22119	10590	10590
	Moment capacity,strong direction (Moment-Curvature Analysis (kip-ft)	7090	7090	7090	4702	4702

Table 4.10: Summary of drain output for ATC x 2.0

	Column	19WL	22WL	23WL	8WD	9WD
Demand	Maximum moment,strong direction (kip-ft)	32640	30120	34130	16600	16720
	Maximum moment,weak direction (kip-ft)	16010	11800	15340	6370	5447
	Maximum shear, strong direction (kip)	1536	1252	1542	805	846
	Maximum shear, weak direction (kip)	671	677	820	586	574
	Maximum displacement, strong direction(inch)	1.2174	1.1726	0.9030	1.2324	1.0658
	Maximum Displacement, weak direction (inch)	3.8944	3.8540	3.5095	1.6868	1.5371
Capacity	Shear capacity (CALTRANS method),Kip	270	270	270	220	220
	Displacement capacity,strong direction(inch)	1.32	1.29	0.98	1.60	1.35
	Displacement capacity, weak direction(inch)	5.84	5.68	4.29	3.39	2.86
	Moment capacity,strong direction (Moment-Curvature Analysis (kip-ft)	22119	22119	22119	10590	10590
	Moment capacity,strong direction (Moment-Curvature Analysis (kip-ft)	7090	7090	7090	4702	4702

Table 4.11 : Material properties of CFRP and GFRP

CFRP	CALTRANS System	5
	Ultimate Tensile Strength in Primary Fiber Direction	555 ksi
	Yield Strength in primary fiber direction	322 ksi
	Strain at strain hardening	0.01
	Ultimate strain	1.48 in/in
	Tensile Modulus of Primary Fibers	29.2×10^3 ksi
	Dry Fiber Thickness	0.0065 inch
GFRP	Ultimate Tensile Strength in Primary Fiber Direction	220 ksi
	Yield strength in primary fiber direction	170 ksi
	Yield strain	0.017 in/in
	Ultimate strain	0.021 in/in
	Tensile Modulus of Primary Fibers	10.5×10^3 ksi
	Dry Fiber Thickness	0.0139 inch

Table 4.12 : Retrofit design based on minimum confinement requirements for 1RWD off-ramp columns.

Type of Retrofit (1RWD Columns)	Design Parameters	Plastic Hinge Region	Outside Plastic Hinge Region
CFRP	f_l	300 psi	150 psi
	ε_j	0.004	0.004
	No.of Layers	17	9
	Thickness provided (inch)	0.1105	0.0585
	Thickness required (inch)	0.1096	0.0548
	$t_{provided}/t_{required}$	1.0083	1.0676
GFRP	f_l	300 psi	150 psi
	ε_j	0.004	0.004
	No.of Layers	22	11
	Thickness provided (inch)	0.3058	0.1529
	Thickness required (inch)	0.3048	0.1524
	$t_{provided}/t_{required}$	1.0034	1.0034

Table 4.13:Retrofit design based on minimum confinement requirements for 1RWL-2RWL off-ramp columns.

Type of Retrofit (1RWL-2RWL Columns)	Design Parameters	Plastic Hinge Region	Outside Plastic Hinge Region
CFRP	f_l	300 psi	150 psi
	ε_j	0.004	0.004
	No.of Layers	19	10
	Thickness provided (inch)	0.1235	0.0650
	Thickness required (inch)	0.1174	0.0587
	$t_{provided}/t_{required}$	1.0518	1.1072
GFRP	f_l	300 psi	150 psi
	ε_j	0.004	0.004
	No.of Layers	24	12
	Thickness provided (inch)	0.3336	0.1668
	Thickness required (inch)	0.3265	0.1633
	$t_{provided}/t_{required}$	1.0217	1.0217

Table 4.14 : Retrofit design based on minimum ductility requirements

Type of Retrofit (1RWD Columns)	Design Parameters	Plastic Hinge Region
CFRP	f_l	300 psi
	ε_j	0.004
	No.of Layers	1
	Thickness provided (inch)	0.0065
	Thickness required (inch)	0.0001
	$t_{provided}/t_{required}$	76.8250
GFRP	f_l	300 psi
	ε_j	0.004
	No.of Layers	1
	Thickness provided (inch)	0.0139
	Thickness required (inch)	0.0002
	$t_{provided}/t_{required}$	65.1229

Table 4.15 : Retrofit design based on minimum ductility requirements

Type of Retrofit (1RWL-2RWL Columns)	Design Parameters	Plastic Hinge Region
CFRP	f_l	300 psi
	ε_j	0.004
	No.of Layers	1
	Thickness provided (inch)	0.0065
	Thickness required (inch)	0.0002
	$t_{provided}/t_{required}$	36.7341
GFRP	f_l	300 psi
	ε_j	0.004
	No.of Layers	1
	Thickness provided (inch)	0.0139
	Thickness required (inch)	0.0004
	$t_{provided}/t_{required}$	31.1387

Table 4.16: Summary of Column Retrofit Design Summary.

Type of Retrofit	Name of the Column	Maximum Shear Demand from ATC x 2.0 (kip)	Number of Layers Required for Maximum Shear Demand	Number of Layers Required for Minimum Confinement Requirement		Number of Layers Required for Minimum Ductility Requirements (inside plastic hinge Region)
				Inside Plastic Hinge Region	Outside Plastic Hinge Region	
CFRP	1RWD Off-Ramp	846	4	17	9	4
	1RWL-2RWL Off-Ramp	1542	8	19	10	8
GFRP	1RWD Off-Ramp	846	5	22	11	5
	1RWL-2RWL Off-Ramp	1542	9	24	12	9

Table 4.17: Length of plastic hinge regions on the top and bottom of the columns

	19WL	22WL	23WL	8WD	9WD
Length of the Column (ft)	27.39	27.00	23.22	20.50	18.70
Length of Plastic Hinge Region (inch)	35.60	35.23	31.60	28.99	27.26

Table 4.18: Moment capacity of columns with jackets using RCMC model

Type of Jacket	Name of the off-Ramp columns	Maximum moment demand in strong direction (kip-ft)	Maximum moment capacity in strong Direction (kip-ft)	Maximum moment demand in weak direction (kip-ft)	Maximum moment in weak direction (kip-ft)
CFRP	1RWD	16720	17362	6370	8542
	1RWL-2RWL	34130	47573	16010	16173
GFRP	1RWD	16720	17426	6370	8577
	1RWL-2RWL	34130	45467	16010	16174

Table 4.19: Shear strength of jackets.

Type of Jacket	Name of the Off-Ramp	Maximum shear demand on the columns (kip)	Required jacket shear strength (kip)	Shear strength provided by jacket (kip)
CFRP	1RWD	846	775	3532
	1RWL-2RWL	1542	1544	3948
GFRP	1RWD	846	775	3875
	1RWL-2RWL	1542	1544	4227

Table 5-1 Properties of Ramp DW Columns

Column	Height		*Vertical Stress in Column		**Axial Load Index			Vertical Steel Ratio	Lateral Steel Ratio	Plastic Shear Demand	
					Top of Column	Top of Pedestal	Top of Footing				
	(ft)	(m)	(psi)	(MPa)						(Kips)	(kN)
5DW	29.56	9.01	196	1.35	0.039	0.045	0.078	0.0239	0.0078	490	2180
6DW	25.68	7.83	198	1.37	0.040	0.045	0.078	0.0239	0.0078	546	2429
7DW	21.11	6.43	194	1.34	0.039	0.043	0.075	0.0239	0.0078	631	2807
8DW	**17.12**	**5.22**	**188**	1.30	**0.038**	**0.041**	**0.071**	**0.0239**	**0.0078**	739	3287
9DW	20.06	6.11	190	1.31	0.038	0.042	0.068	0.0157	0.0078	284	1263
10DW	15.48	4.72	169	1.17	0.034	0.037	0.060	0.0157	0.0078	339	1508

* Based on concrete weight from deck tributary loading

** Compressive axial force over the product of cross sectional area and the concrete compressive strength

Table 5-2 Measured Steel Properties

Rebar Size	Yield Stress ksi	MPa	Yield Strain*	Strain at Hardening	Maximum Stress ksi	MPa	Maximum Strain
#3	41.7	288	0.00144	0.0129	72.7	501	0.193
W2.9	39.4	272	0.00136	N/A	53.3	367	0.220
W2	40.7	281	0.00140	N/A	55.1	380	0.217
W1.4	41.3	285	0.00142	N/A	55.0	379	0.220

* Based on E = 29000 ksi (200MPa)

Table 5-3 Test Schedule for Specimen OLVA

Event	a_{max} (g)	x sylmar	Estimated Δ_{max} (in)	(cm)	Comments
A		SNAP RAMP			Measure Frequency and Damping
		TUNING			
B		SNAP RAMP			Measure Frequency and Damping
		TUNING at 0.2 x Sylmar			
C		SNAP RAMP			Measure Frequency and Damping
1	0.15	0.25	0.11	0.28	Initial Stiffness
2	0.30	0.50	0.22	0.56	
3	0.45	0.75	0.33	0.85	Estimated Pre-Yield Run
4	0.61	1.00	0.43	1.10	Estimated Yield Run
5	0.76	1.25	0.60	1.52	
D		SNAP RAMP			Measure Frequency and Damping
6	0.91	1.50	1.14	2.89	
7	1.06	1.75	1.39	3.54	
E		SNAP RAMP			Measure Frequency and Damping
8	1.21	2.00	1.89	4.80	

Table 5-4 Summary of Measured Peak Forces and Displacements for OLVA

	0.25 x Sylmar				0.50 x Sylmar				0.75 x Sylmar				1.0 x Sylmar			
	Disp.		Force		Disp.		Force		Disp.		Force		Disp.		Force	
	in	mm	Kips	kN	in	mm	Kips	kN	in	mm	Kips	kN	in	mm	Kips	kN
Min. Disp.	-0.06	-1.5	-7.5	-33.5	-0.11	-2.7	-12.2	-54.3	-0.17	-4.2	-20.7	-92.0	-0.28	-7.2	-35.8	-159.3
Max. Disp.	0.07	1.8	6.9	30.8	0.10	2.4	10.4	46.4	0.14	3.5	14.7	65.5	0.21	5.2	22.9	101.7
Min. Force.	-0.03	-0.7	-11.8	-52.5	-0.08	-2.1	-20.2	-89.8	-0.15	-3.8	-28.0	-124.6	-0.26	-6.5	-39.0	-173.3
Max. Force.	0.01	0.3	8.9	39.5	0.03	0.7	15.8	70.1	0.04	1.0	21.3	94.5	0.05	1.3	27.3	121.3

	1.25 x Sylmar				1.50 x Sylmar				1.75 x Sylmar				2.0 x Sylmar			
	Disp.		Force		Disp.		Force		Disp.		Force		Disp.		Force	
	in	mm	Kips	kN	in	mm	Kips	kN	in	mm	Kips	kN	in	mm	Kips	kN
Min. Disp.	-0.58	-14.7	-27.0	-120.2	-0.95	-24.0	-32.2	-143.0	-1.24	-31.5	-35.8	-159.4	-1.96	-49.7	-36.5	-162.4
Max. Disp.	0.23	6.0	22.7	101.0	0.28	7.1	29.9	133.1	0.42	10.6	33.3	148.0	0.44	11.3	30.2	134.6
Min. Force.	-0.35	-8.8	-42.9	-191.0	-0.81	-20.7	-46.5	-206.7	-1.14	-29.1	-44.8	-199.2	-1.65	-41.9	-44.5	-198.1
Max. Force.	0.07	1.7	30.1	134.0	0.25	6.4	32.1	142.7	0.39	9.8	33.8	150.3	0.41	10.5	32.5	144.4

Table 5-5 Summary of Measured Peak Forces and Displacements for OLVR-1

	0.25 x Sylmar				0.50 x Sylmar				0.75 x Sylmar				1.0 x Sylmar			
	Disp.		Force		Disp.		Force		Disp.		Force		Disp.		Force	
	in	mm	Kips	kN	in	mm	Kips	kN	in	mm	Kips	kN	in	mm	Kips	kN
Min. Disp.	-0.08	-2.1	-16.4	-73.0	-0.10	-2.6	-19.6	-87.0	-0.15	-3.9	-22.9	-102.1	-0.21	-5.2	-33.6	-149.3
Max. Disp.	0.10	2.7	19.4	86.5	0.10	2.7	18.9	83.9	0.15	3.8	28.4	126.4	0.23	5.7	40.3	179.4
Min. Force.	-0.08	-2.1	-17.2	-76.7	-0.09	-2.2	-20.1	-89.5	-0.14	-3.5	-26.4	-117.2	-0.21	-5.2	-33.6	-149.3
Max. Force.	0.08	2.2	21.5	95.5	0.07	1.8	20.6	91.7	0.13	3.4	28.6	127.2	0.23	5.7	40.3	179.4

	1.25 x Sylmar				1.50 x Sylmar				1.75 x Sylmar				2.0 x Sylmar			
	Disp.		Force		Disp.		Force		Disp.		Force		Disp.		Force	
	in	mm	Kips	kN	in	mm	Kips	kN	in	mm	Kips	kN	in	mm	Kips	kN
Min. Disp.	-0.25	-6.2	-39.4	-175.1	-0.27	-6.9	-38.5	-171.5	-0.27	-6.7	-34.1	-151.8	-0.25	-6.4	-33.3	-148.2
Max. Disp.	0.39	9.9	51.7	229.9	0.49	12.4	56.8	252.7	0.59	15.1	58.3	259.1	0.74	18.8	61.6	274.2
Min. Force.	-0.24	-6.1	-39.6	-176.0	-0.27	-6.8	-41.5	-184.4	0.24	6.1	-38.9	-173.1	-0.22	-5.7	-37.1	-165.0
Max. Force.	0.37	9.5	51.9	230.9	0.48	12.2	57.2	254.2	0.57	14.4	59.2	263.5	0.71	18.0	62.9	279.8

	2.25 x Sylmar				2.50 x Sylmar				2.75 x Sylmar			
	Disp.		Force		Disp.		Force		Disp.		Force	
	in	mm	Kips	kN	in	mm	Kips	kN	in	mm	Kips	kN
Min. Disp.	-0.26	-6.6	-39.6	-176.2	-0.26	-6.7	-38.6	-171.6	-0.26	-6.5	-44.4	-197.6
Max. Disp.	0.90	23.0	62.6	278.7	1.08	27.5	65.7	292.1	1.34	34.0	46.3	206.1
Min. Force.	-0.25	-6.3	-40.2	-178.7	-0.23	-5.9	-42.2	-187.9	-0.26	-6.5	-44.4	-197.6
Max. Force.	0.86	21.9	65.7	292.2	1.07	27.1	66.8	297.0	1.23	31.3	66.3	295.0

Table 5-6 Summary of Measured Peak Forces and Displacements for OLVR-2

	0.25 x Sylmar				0.50 x Sylmar				0.75 x Sylmar				1.0 x Sylmar			
	Disp.		Force		Disp.		Force		Disp.		Force		Disp.		Force	
	in	mm	Kips	kN	in	mm	Kips	kN	in	mm	Kips	kN	in	mm	Kips	kN
Min. Disp.	-0.05	-1.1	-10.3	-45.8	-0.09	-2.3	-16.0	-71.1	-0.13	-3.4	-21.0	-93.5	-0.18	-4.6	-26.5	-117.9
Max. Disp.	0.06	1.6	11.4	50.6	0.11	2.8	15.4	68.6	0.15	3.8	25.6	113.9	0.25	6.5	36.2	160.8
Min. Force.	-0.03	-0.8	-11.9	-53.0	-0.07	-1.8	-17.3	-77.2	-0.13	-3.3	-22.7	-101.1	-0.17	-4.3	-28.8	-127.9
Max. Force.	0.06	1.5	11.4	50.7	0.11	2.8	17.3	76.8	0.15	3.7	25.8	114.8	0.25	6.5	36.2	160.8

	1.25 x Sylmar				1.50 x Sylmar				1.75 x Sylmar				2.0 x Sylmar			
	Disp.		Force		Disp.		Force		Disp.		Force		Disp.		Force	
	in	mm	Kips	kN	in	mm	Kips	kN	in	mm	Kips	kN	in	mm	Kips	kN
Min. Disp.	-0.25	-6.3	-31.6	-140.6	-0.30	-7.7	-33.9	-150.7	-0.39	-10.0	-35.1	-156.0	-0.41	-10.5	-39.9	-177.4
Max. Disp.	0.43	10.9	43.9	195.3	0.70	17.8	50.0	222.3	0.92	23.3	50.2	223.1	1.05	26.7	51.9	231.1
Min. Force.	-0.20	-5.1	-33.3	-148.2	-0.24	-6.1	-37.5	-166.6	-0.33	-8.4	-40.5	-180.1	-0.40	-10.2	-41.1	-183.0
Max. Force.	0.41	10.5	44.3	197.0	0.59	14.9	50.2	223.4	0.78	19.9	51.3	228.3	1.05	26.7	51.9	231.1

	2.25 x Sylmar				2.50 x Sylmar				2.75 x Sylmar			
	Disp.		Force		Disp.		Force		Disp.		Force	
	in	mm	Kips	kN	in	mm	Kips	kN	in	mm	Kips	kN
Min. Disp.	-0.44	-11.1	-40.8	-181.3	-0.44	-11.1	-39.3	-175.0	-0.39	-9.8	-36.1	-160.5
Max. Disp.	1.19	30.3	52.4	233.1	1.47	37.2	49.6	220.7	2.72	69.1	31.3	139.2
Min. Force.	-0.39	-10.0	-41.4	-184.0	-0.38	-9.6	-40.8	-181.3	-0.36	-9.3	-38.1	-169.6
Max. Force.	1.19	30.3	52.4	233.1	1.29	32.8	51.8	230.5	1.48	37.6	49.1	218.5

Table 5-7 Ramp DW Column Transverse Ductility Demand for Sylmar

	Δ_{yield} (in)	(mm)	μ_Δ capacity	0.5xSylmar Δ_{max} (in)	(mm)	μ_Δ demand	C/D Ratio	1.0xSylmar Δ_{max} (in)	(mm)	μ_Δ demand	C/D Ratio	2.0xSylmar Δ_{max} (in)	(mm)	μ_Δ demand	C/D Ratio
Column 5DW	0.84	2.1	1.46	0.720	1.8	0.86	1.71	1.521	3.9	1.81	0.81	3.510	8.9	4.17	0.35
Column 6DW	0.65	1.7	1.46	0.436	1.1	0.67	2.18	0.959	2.4	1.47	0.99	2.369	6.0	3.64	0.40
Column 7DW	0.66	1.7	1.46	0.259	0.7	0.39	3.71	0.621	1.6	0.94	1.55	1.601	4.1	2.43	0.60
Column 8DW	0.31	0.8	1.46	0.227	0.6	0.73	2.00	0.585	1.5	1.89	0.77	1.552	3.9	5.01	0.29
Column 9DW	0.29	0.7	2.4	0.205	0.5	0.72	3.34	0.715	1.8	2.50	0.96	2.116	5.4	7.40	0.32
Column 10DW	0.20	0.5	2.56	0.242	0.6	1.23	2.07	0.770	2.0	3.93	0.65	2.263	5.7	11.55	0.22

Table 5-8 Ramp DW Column Transverse Ductility Demand for ATC

	Δ_{yield} (in)	(mm)	μ_Δ capacity	0.5xATC Δ_{max} (in)	(mm)	μ_Δ demand	C/D Ratio	1.0xATC Δ_{max} (in)	(mm)	μ_Δ demand	C/D Ratio	2.0xATC Δ_{max} (in)	(mm)	μ_Δ demand	C/D Ratio
Column 5DW	0.84	2.1	1.46	0.663	1.7	0.79	1.85	1.354	3.4	1.61	0.91	2.534	6.4	3.01	0.48
Column 6DW	0.65	1.7	1.46	0.453	1.2	0.70	2.10	0.834	2.1	1.28	1.14	1.917	4.9	2.94	0.50
Column 7DW	0.66	1.7	1.46	0.239	0.6	0.36	4.02	0.483	1.2	0.73	1.99	1.108	2.8	1.68	0.87
Column 8DW	0.31	0.8	1.46	0.166	0.4	0.53	2.73	0.398	1.0	1.28	1.14	0.979	2.5	3.16	0.46
Column 9DW	0.29	0.7	2.4	0.151	0.4	0.53	4.53	0.420	1.1	1.47	1.64	1.306	3.3	4.57	0.53
Column 10DW	0.20	0.5	2.56	0.200	0.5	1.02	2.51	0.434	1.1	2.21	1.16	1.363	3.5	6.95	0.37

Table 6-1 Test Events for B2DA

Run Number	Motion	Comments/Purpose
1	Quick Release	Measure Frequency/Damping
2	Tuning	Tuning the Table
3	Quick Release	Measure Frequency/Damping
4	0.05xSylmar	
5	0.12xSylmar	
6	0.24xSylmar	
7	0.36xSylmar	
8	0.48xSylmar	
9	Quick Release	Measure Frequency/Damping
10	0.60xSylmar	
11	0.72xSylmar	
12	0.83xSylmar	
13	0.95xSylmar	
14	1.07xSylmar	
15	1.09xSylmar	
16	1.19xSylmar	
17	Quick Release	Measure Frequency/Damping
18	1.0xSylmar	
19	1.25xSylmar	
20	1.50xSylmar	
21	1.75xSylmar	
22	2.0xSylmar	
23	2.25xSylmar	

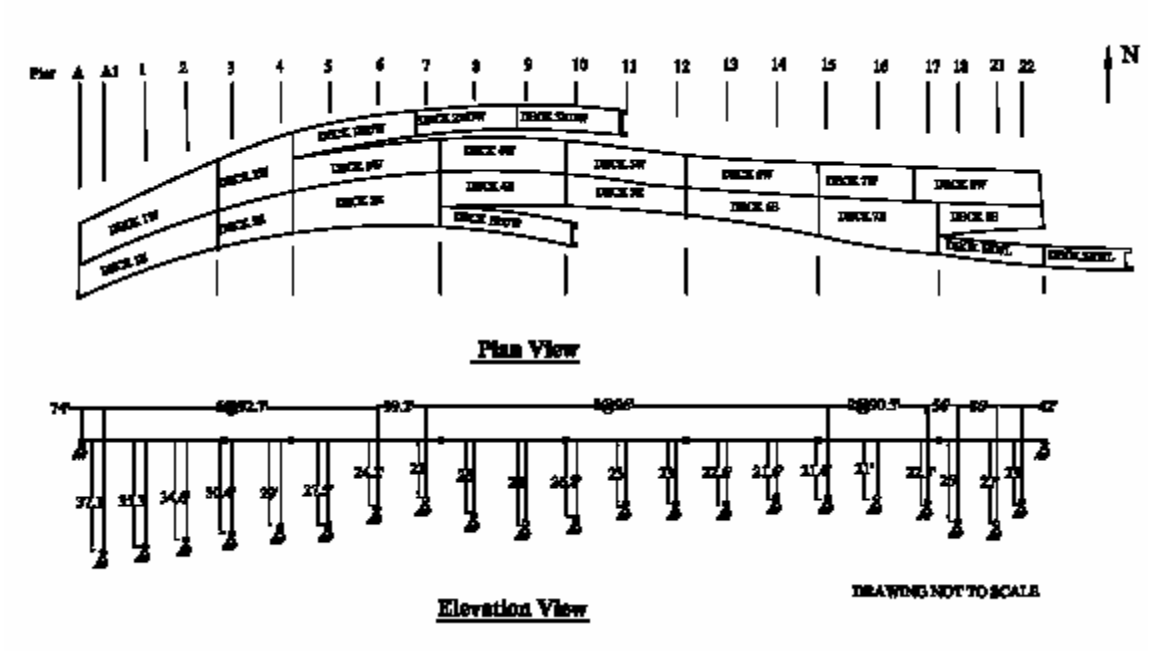

Figure 1-1 Las Vegas Viaduct Details

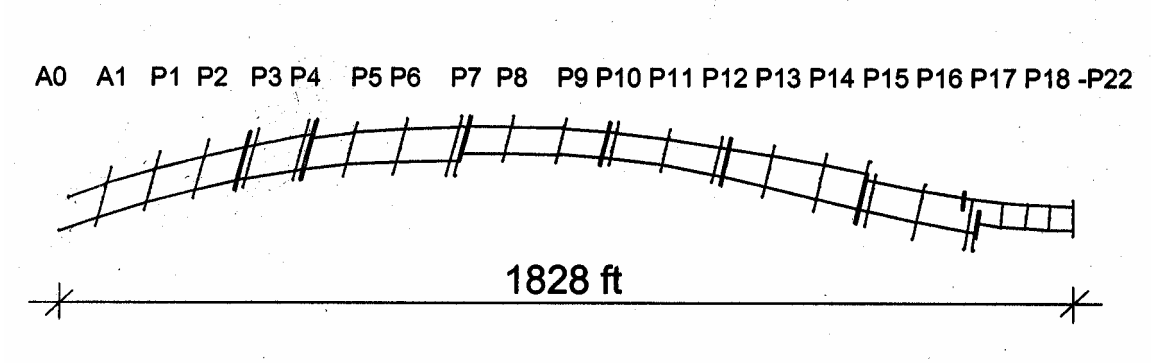

Fig. 2.1: Viaduct Main Bridge Layout

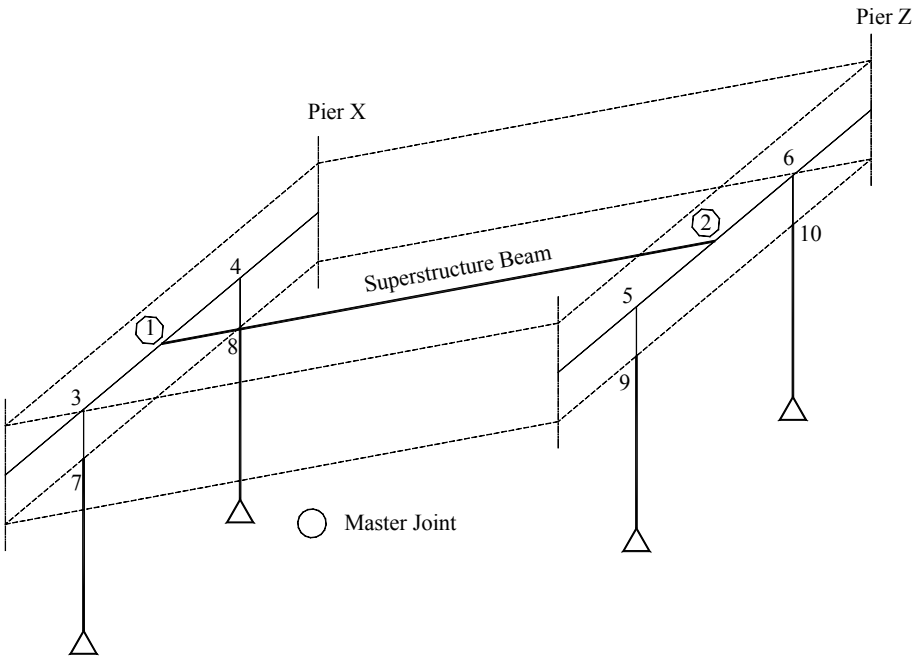

Fig. 2.2: Viaduct Spine Model

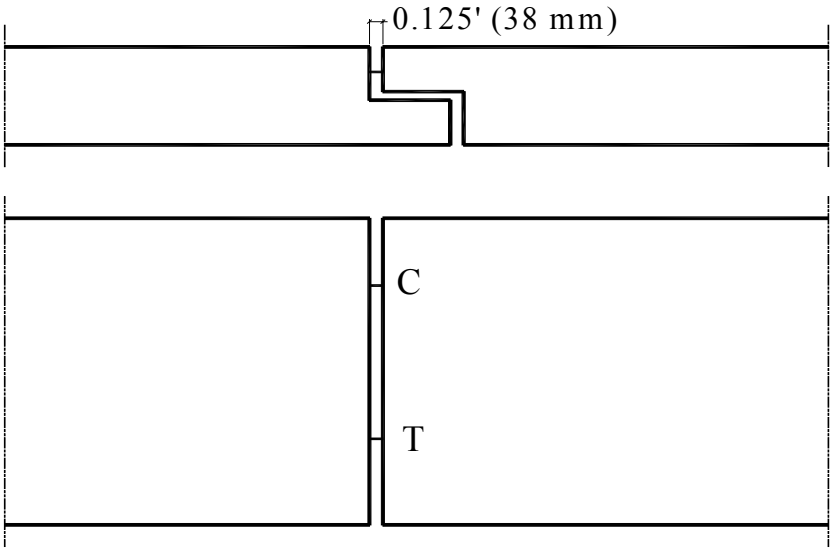

Fig. 2.3: Tension and Compression Elements at Viaduct Hinges

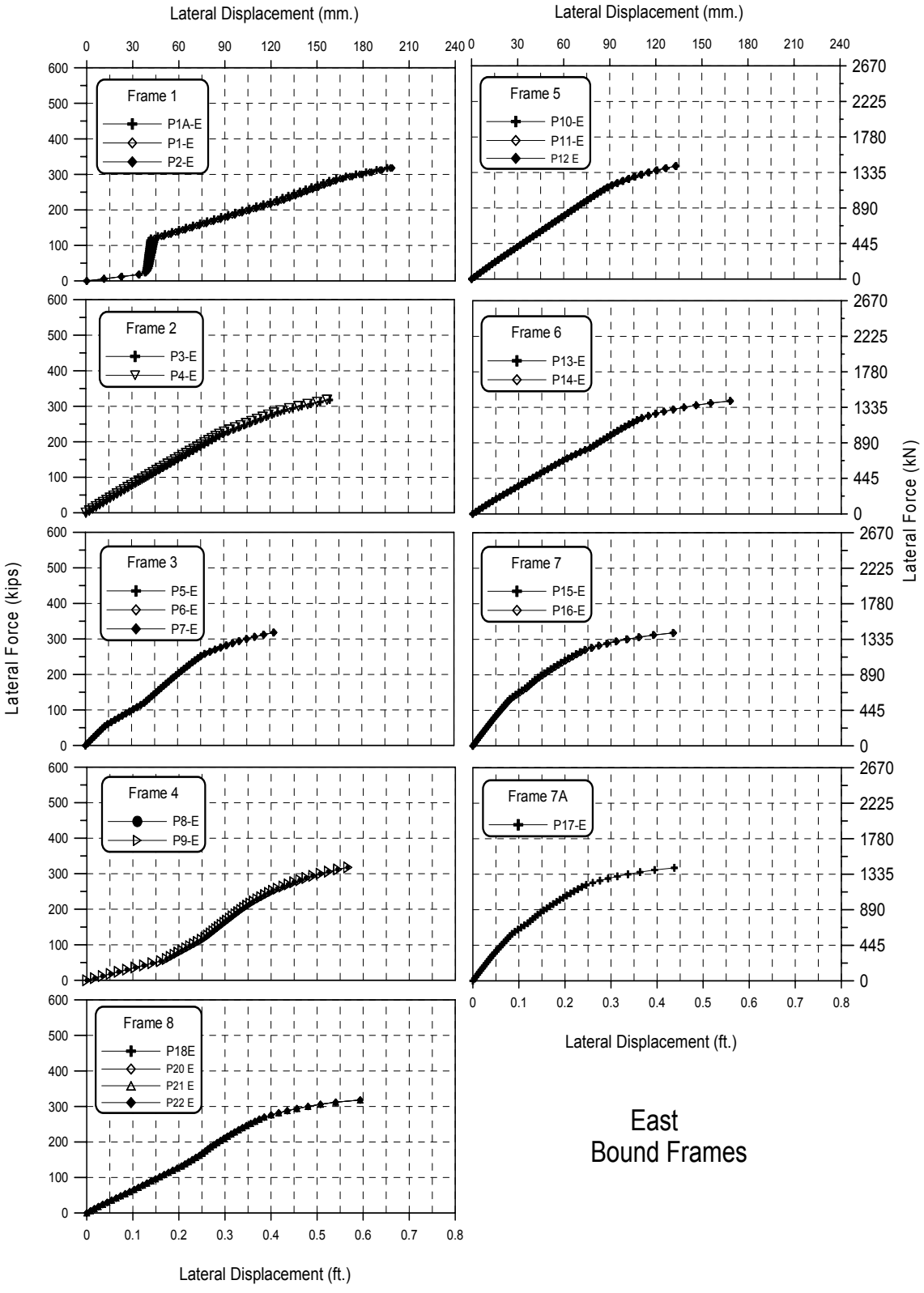

Fig. 2.4a: Push-over in X-direction for Viaduct Frames (East Bound)

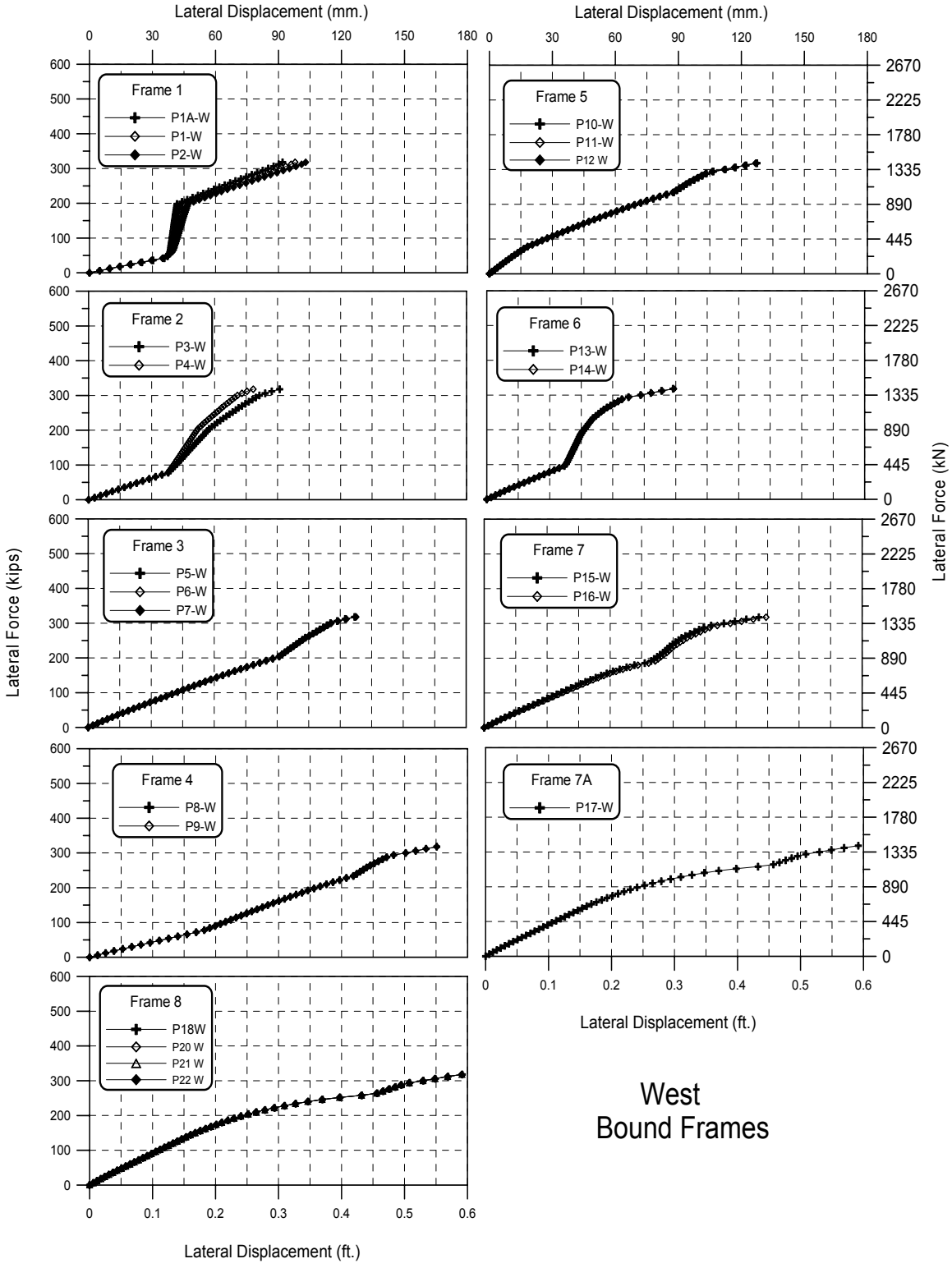

Fig. 2.4b: Push-over in X-direction for Viaduct Frames (West Bound)

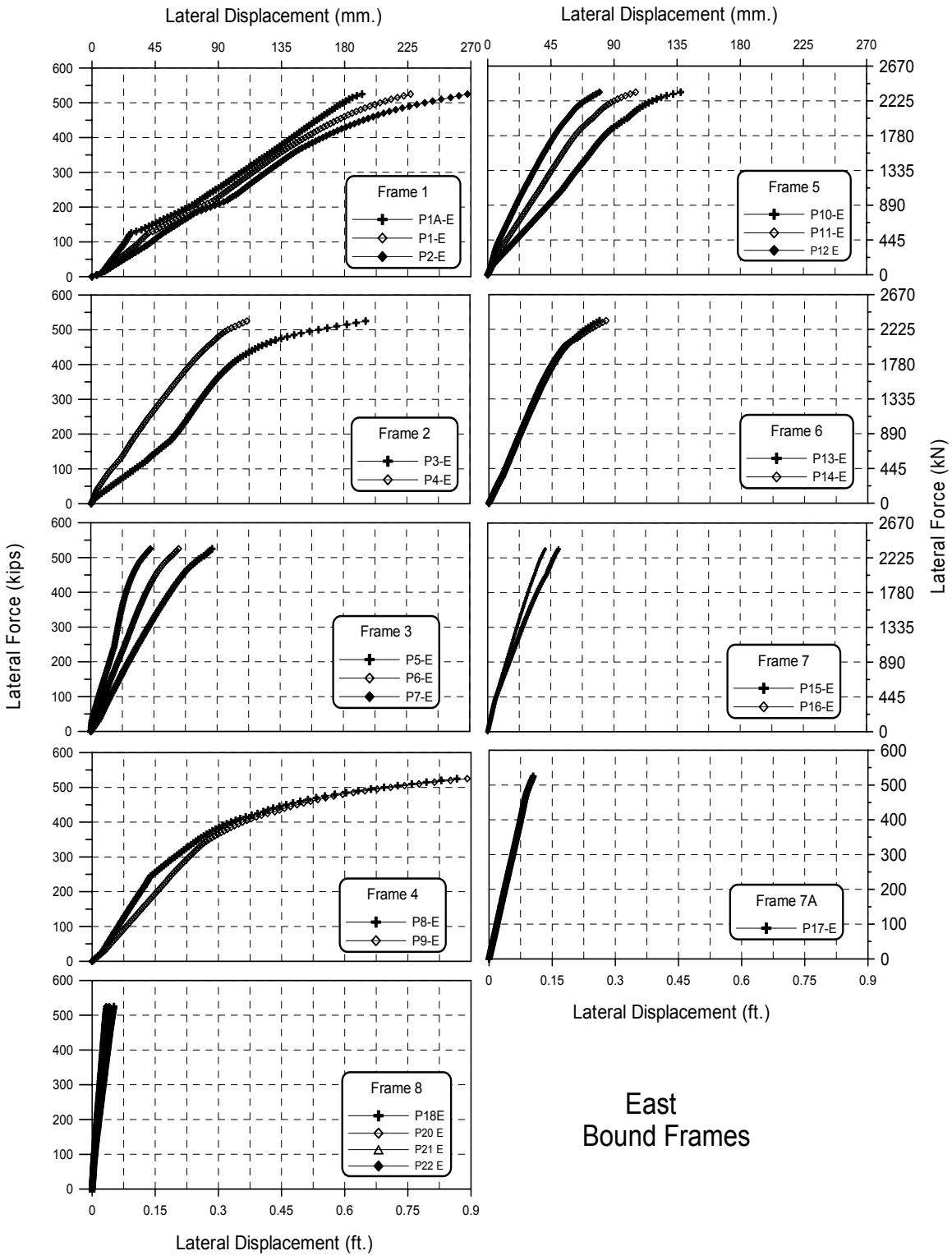

Fig. 2.5a: Push-over in Y-direction for Viaduct Frames (East Bound)

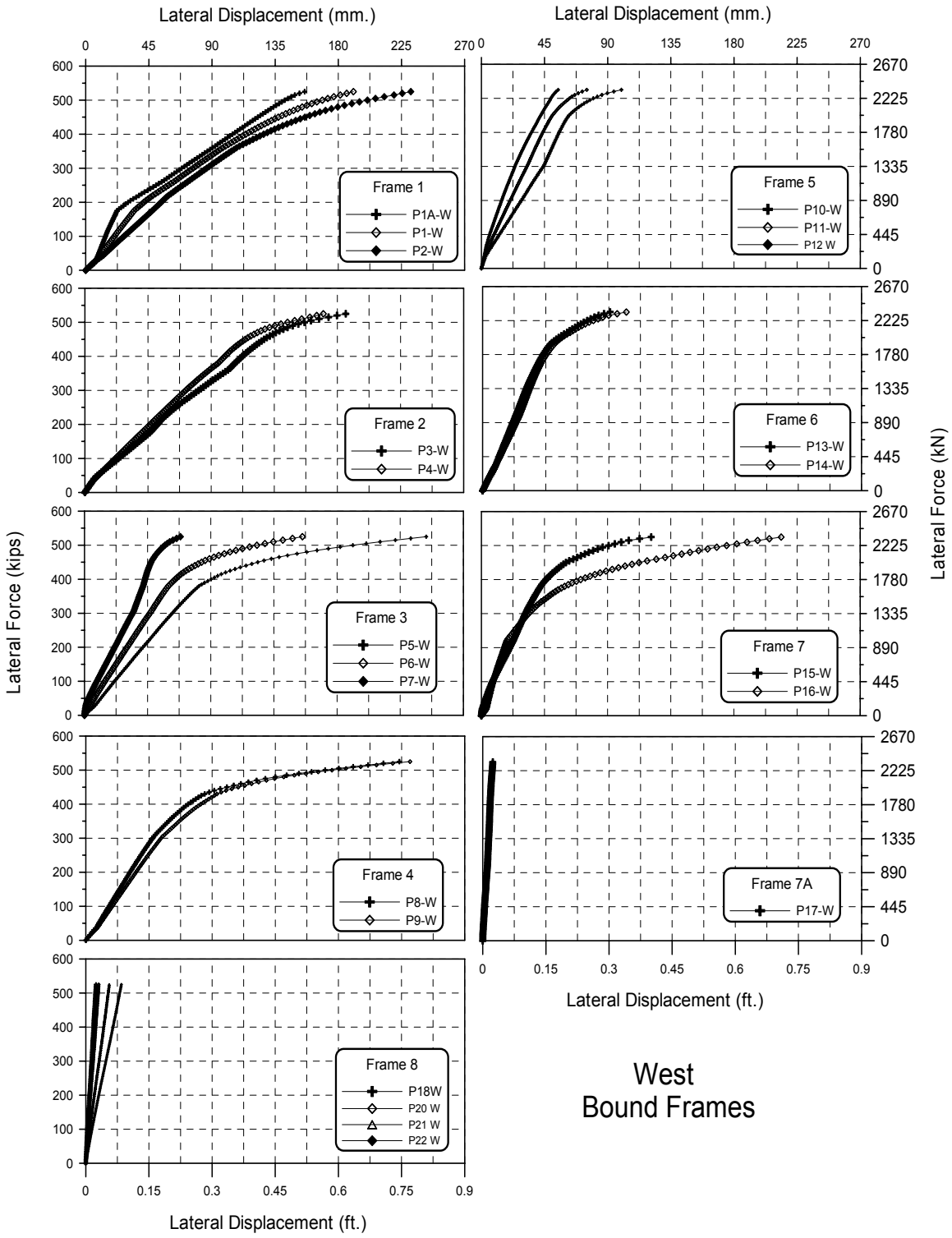

Fig. 2.5b: Push-over in Y-direction for Viaduct Frames (West Bound)

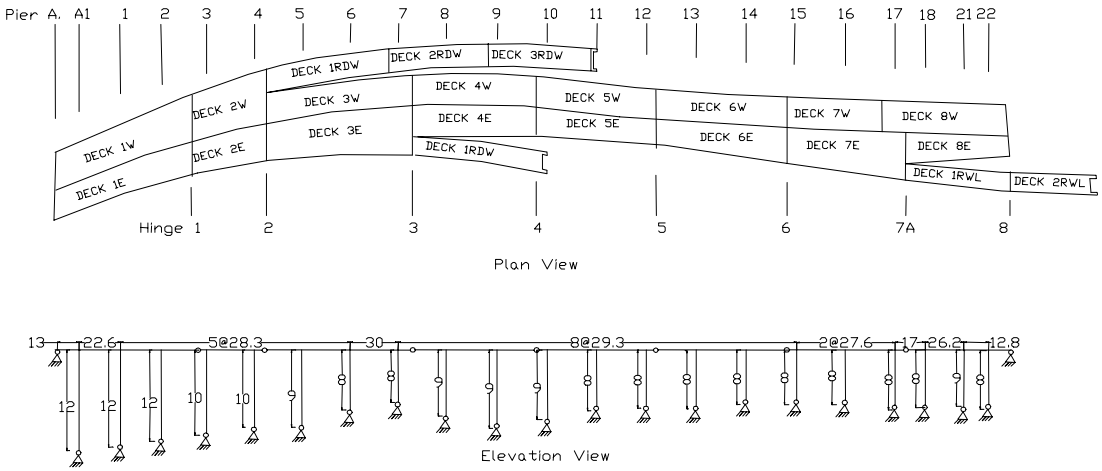

Figure 3.1 Structure Model

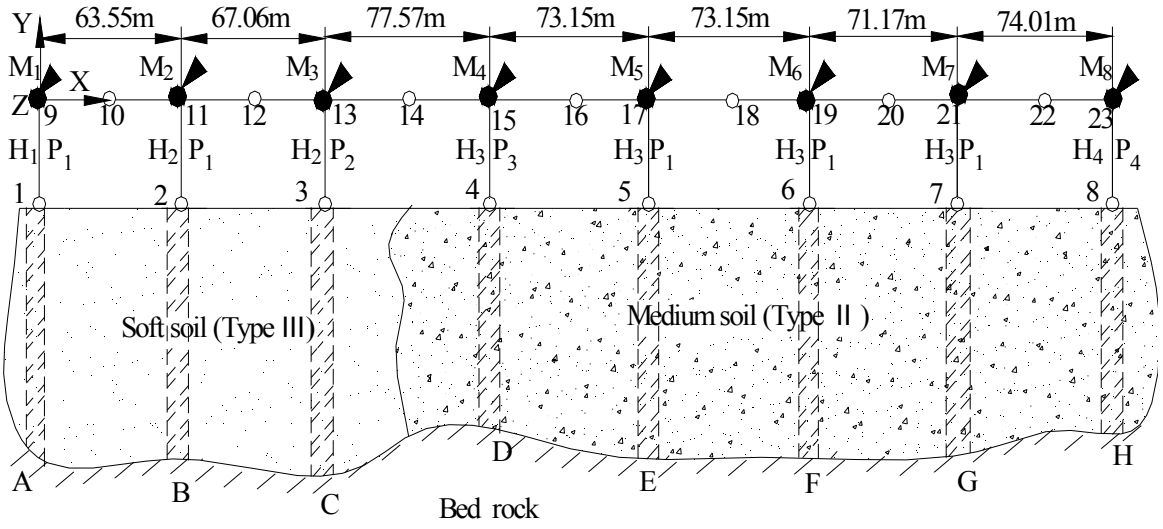

Figure 3.2 Reduced model of the bridge

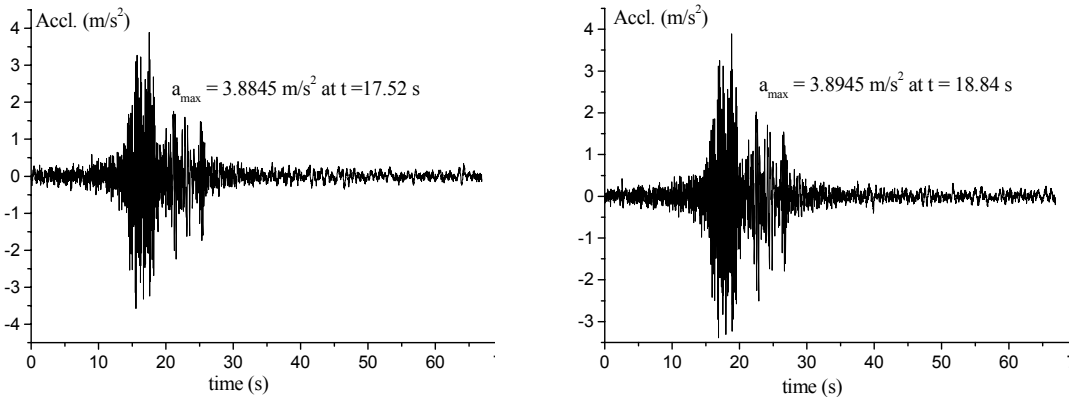

a) Acc.3 b) Acc.5

Figure 3.3 Acceleration histories of bedrock

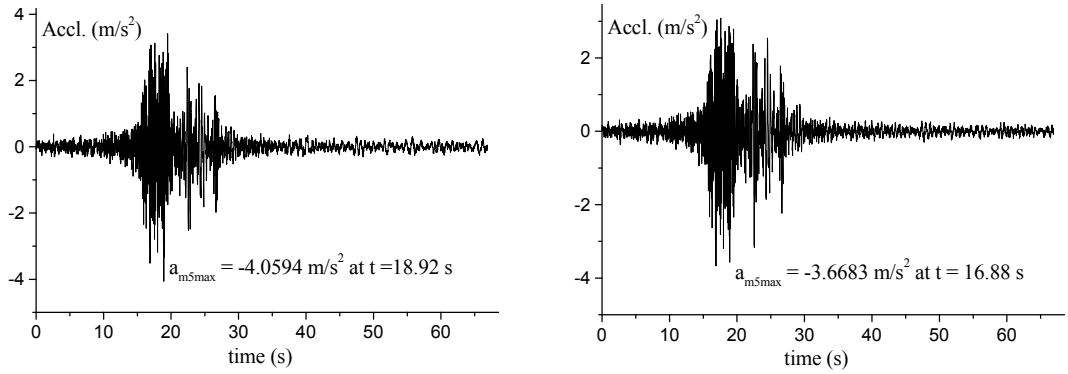

(a) Soft soil, a_s (b) Medium soil, a_m

Figure 3.4 Bedrock acceleration histories at supports with soft and medium soils

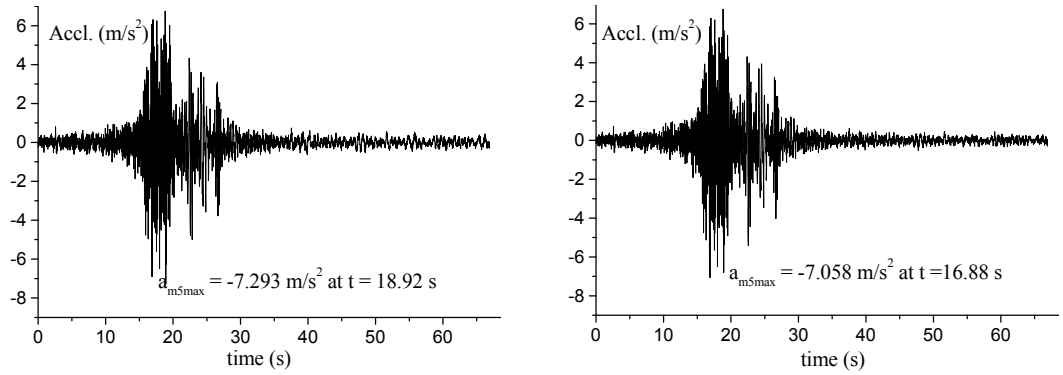

a) a_{s5} b) a_{m5}

Figure 3.5 Structure input acceleration histories

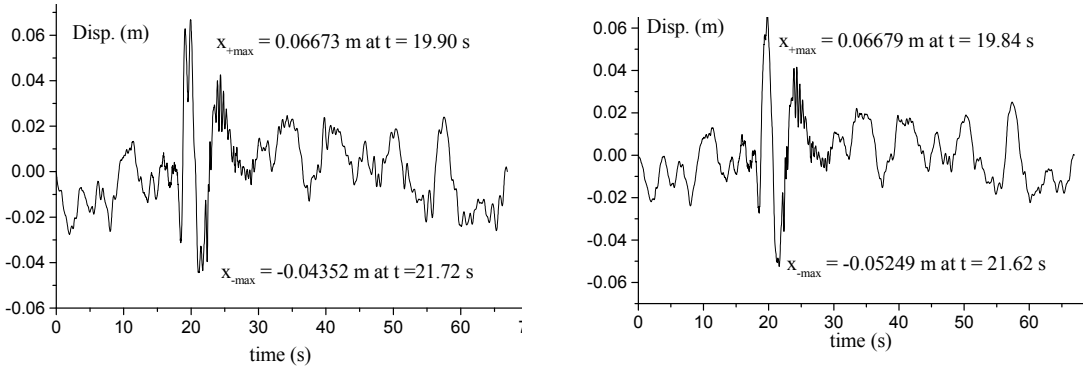

a) D_{s5} b) D_{m5}

Figure 3.6 Structure input displacement histories

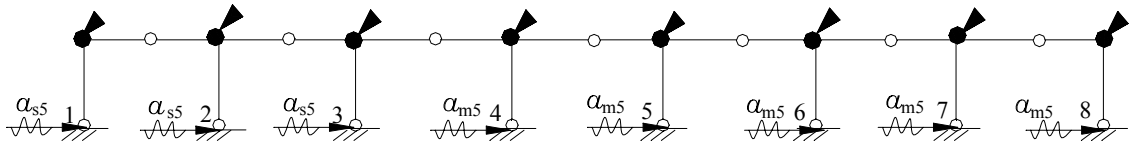

Figure 3.7 Earthquake input for Case 3

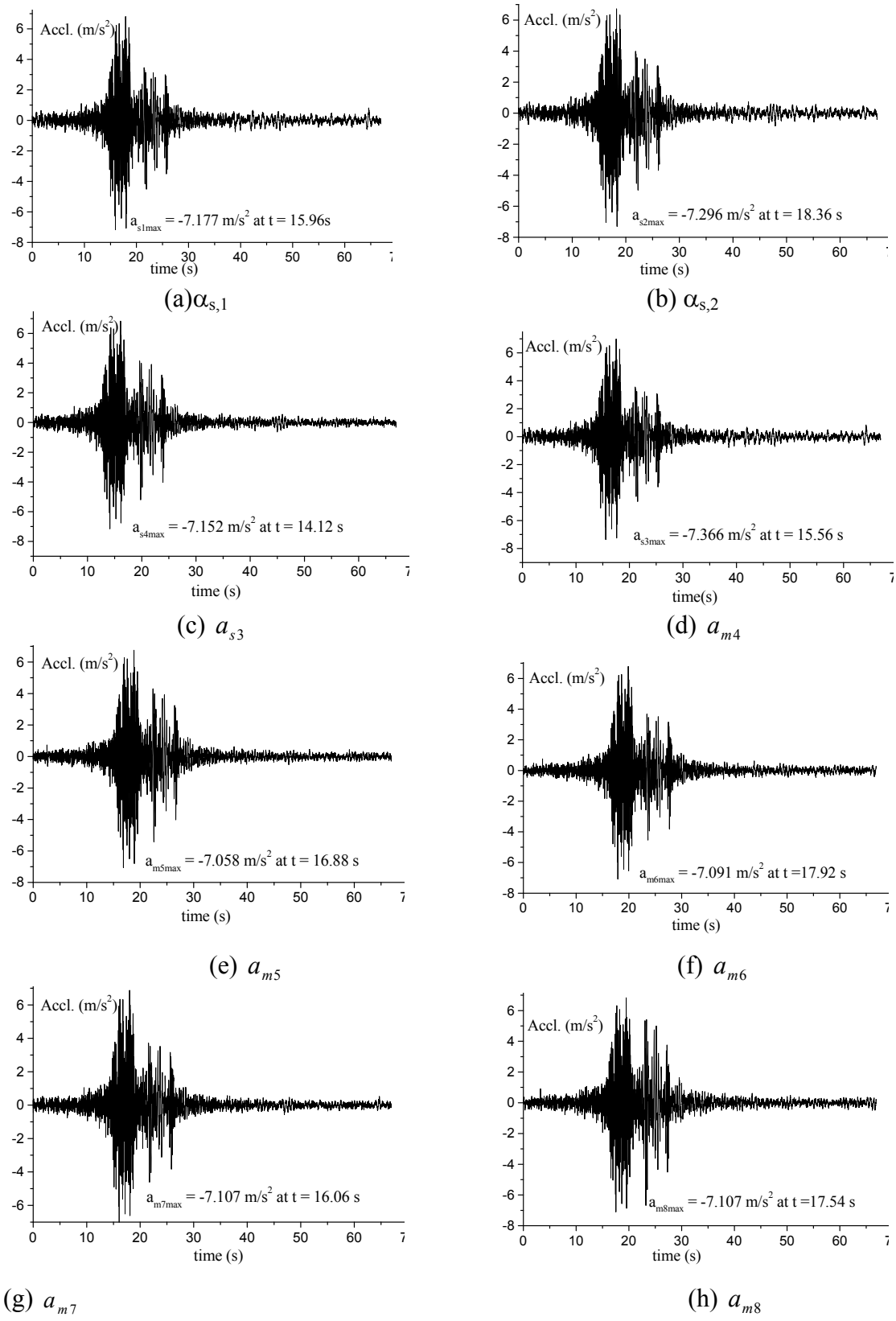

Figure 3.8 Acceleration Histories at Column Bases

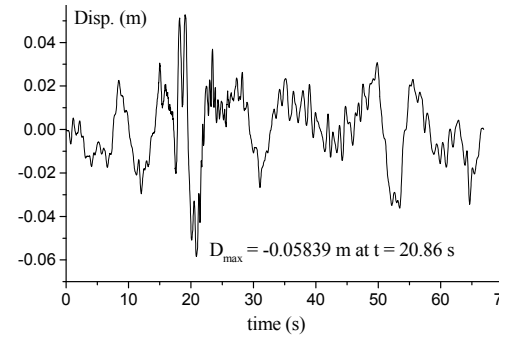

(a) d_{s1}

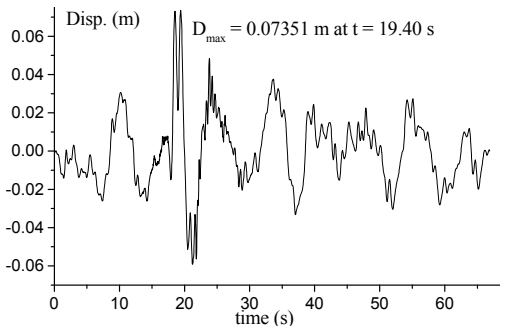

(b) d_{s2}

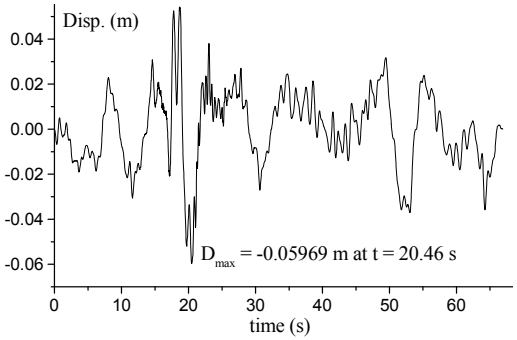

(c) d_{s3}

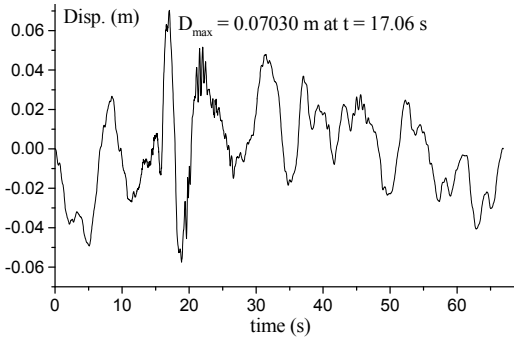

(d) d_{m4}

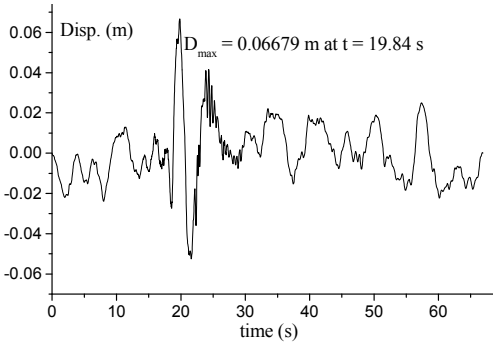

(e) d_{m5}

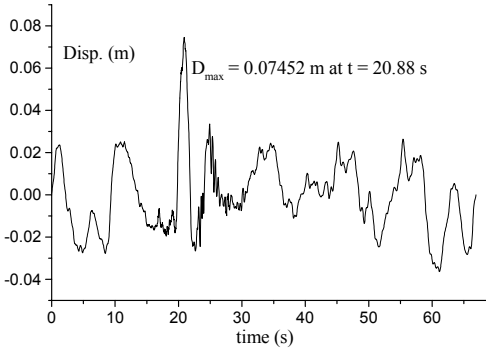

(f) d_{m6}

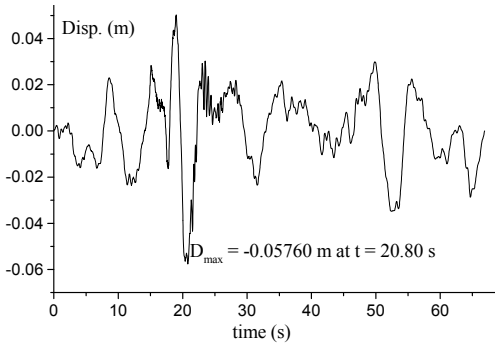

(g) d_{m7}

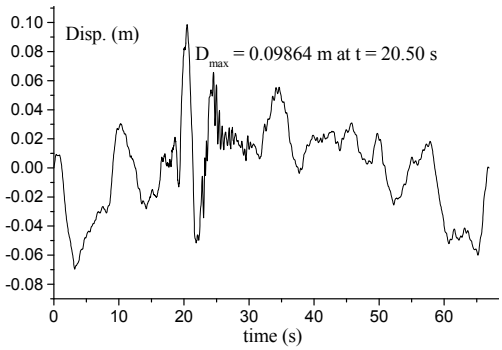

(h) d_{m8}

Figure 3.9 Displacement histories of the column bases

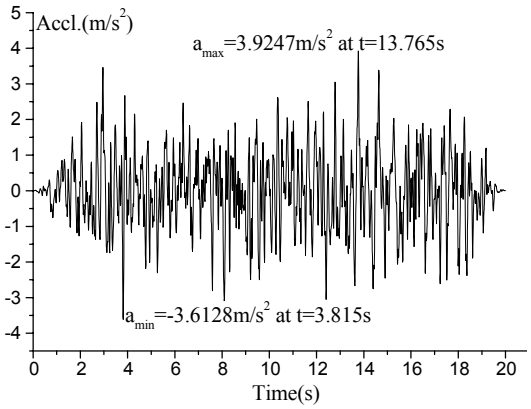

Figure 3.10 Time history of the bedrock

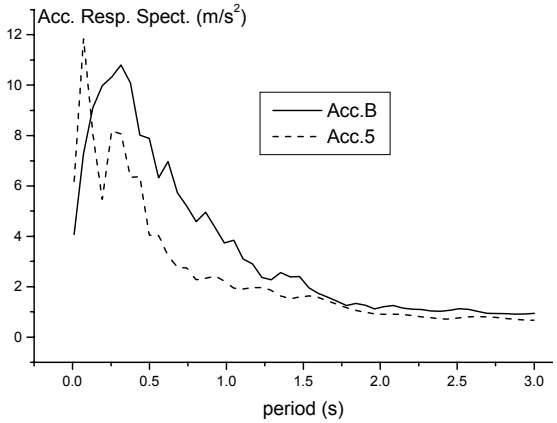

Figure 3.11 Response spectra

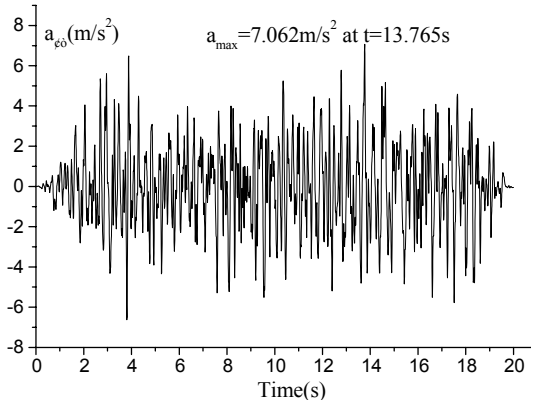

a) Type II

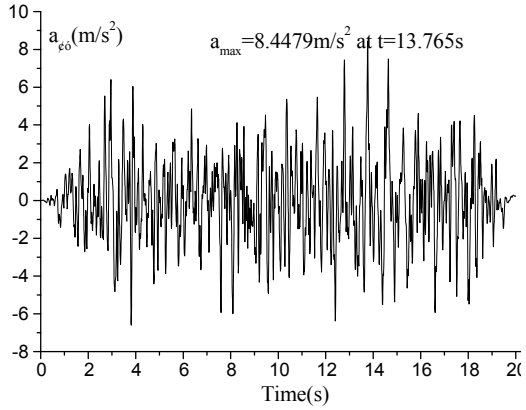

b) Type III

Figure 3.12 Absolute output acceleration of topsoil

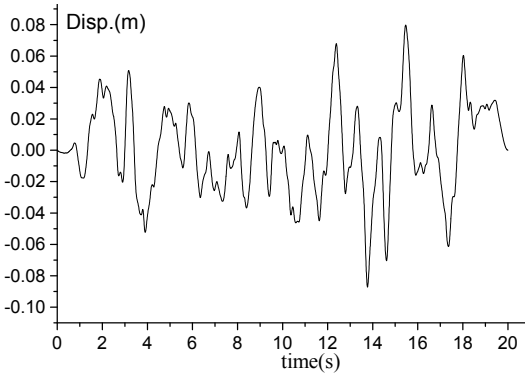

a) Type II

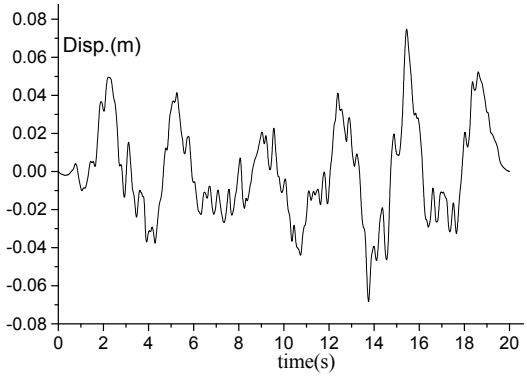

b) Type III

Figure 3.13 Absolute output displacement of topsoil

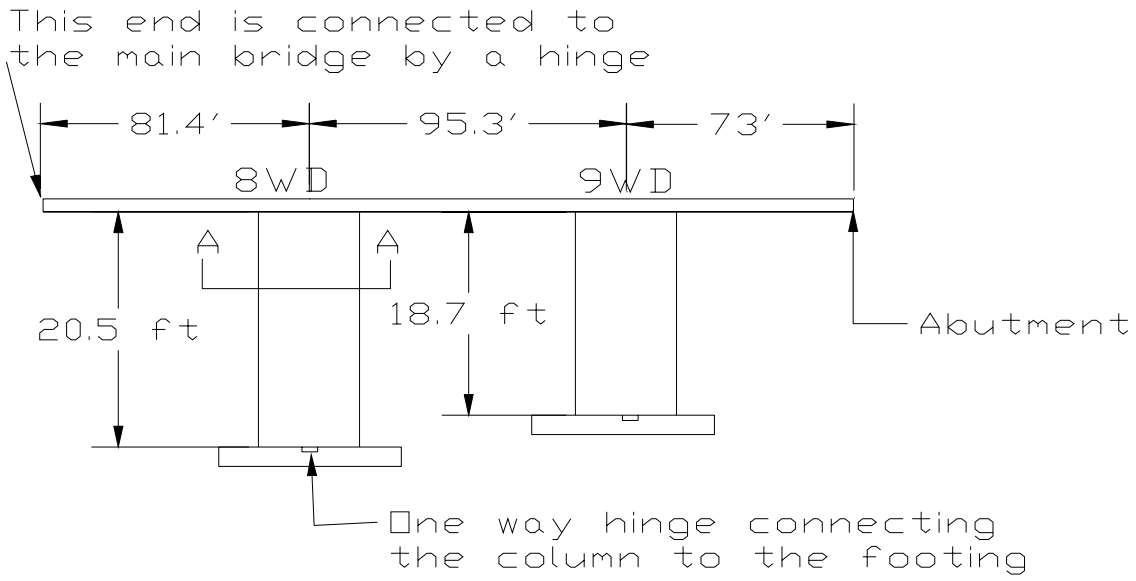

Figure 4.1 Elevation view of 1RWD off-ramp (not to scale)

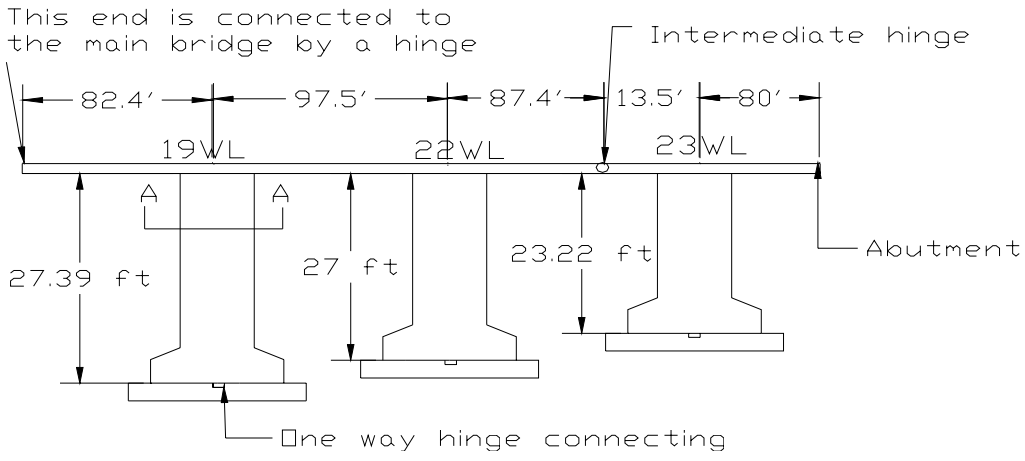

Figure 4.2: The Elevation view of 1RWL-2RWL Off-Ramp (not to scale)

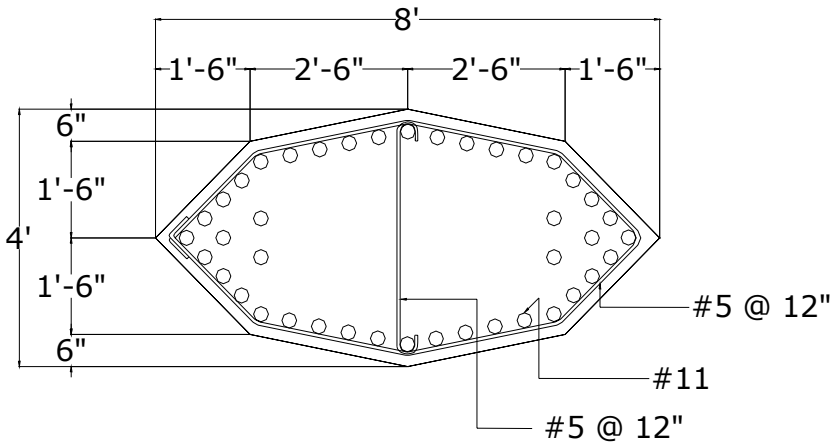

Figure 4.3 : Cross Section of 8WD and 9WD Columns of 1RWD Off-Ramp (drawing not to scale)

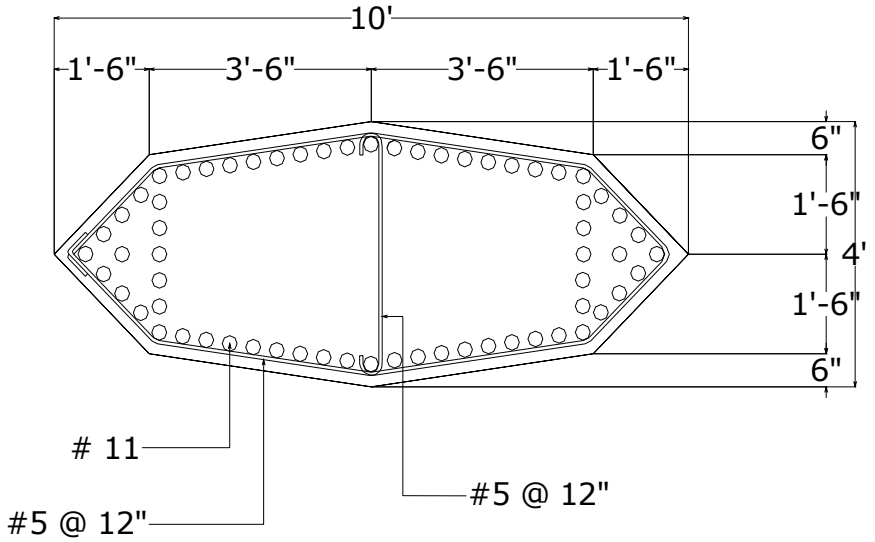

Figure 4.4: Cross section of 19WL,22WL and 23WL Columns of 1RWL-2RWL Off-Ramp (drawing not to scale)

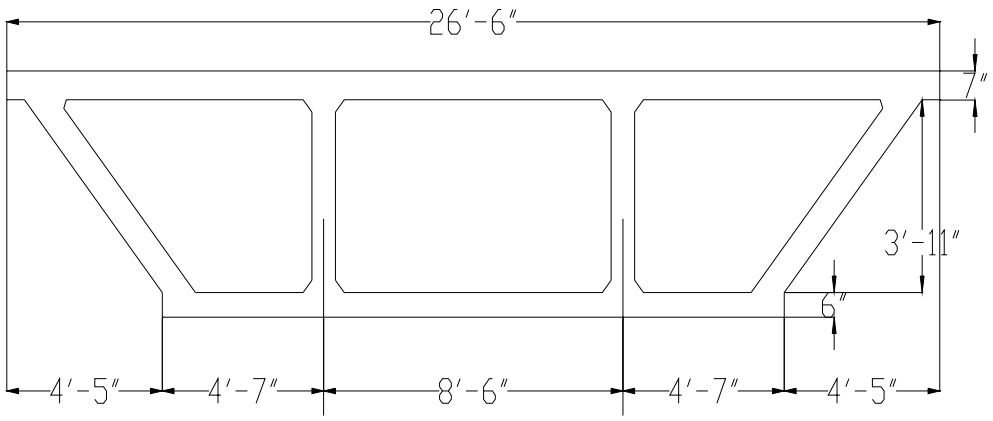

Figure 4.5: Cross Section of 1RWD Off-Ramp Bridge Deck (reinforcement not shown, drawing not to scale)

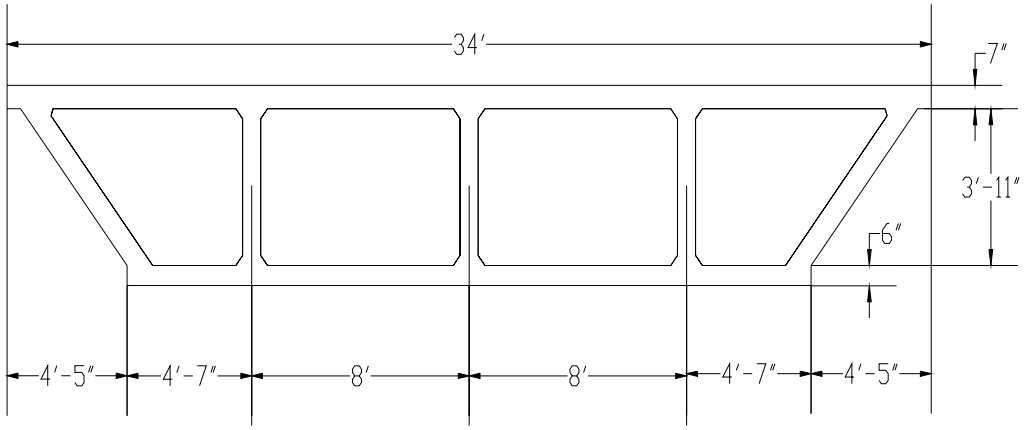

Figure 4.6: Cross Section of 1RWL-2RWL Off-Ramp Bridge Deck (reinforcement not shown, drawing not to scale)

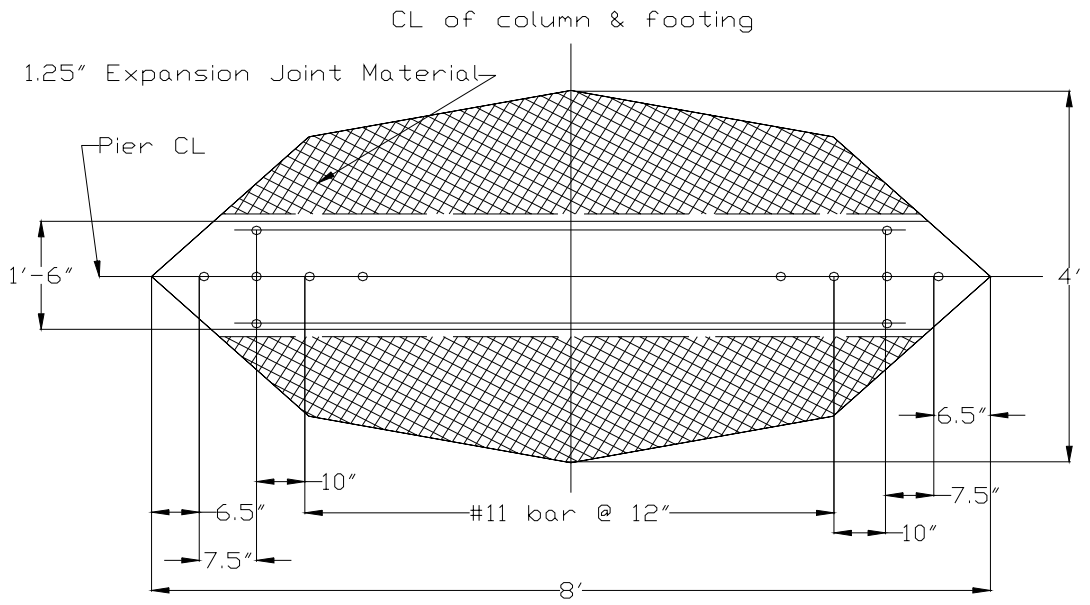

Figure 4.7: Detail of hinges on top of the footings of 1RWD off-ramp

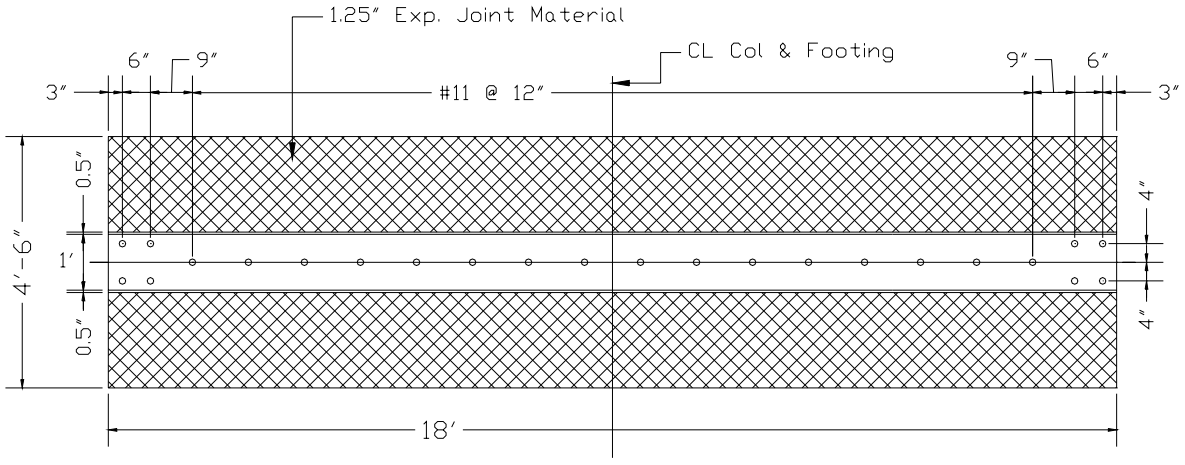

Figure 4.8: Detail of hinges on top of the footings of 1RWL-2RWL off-ramp

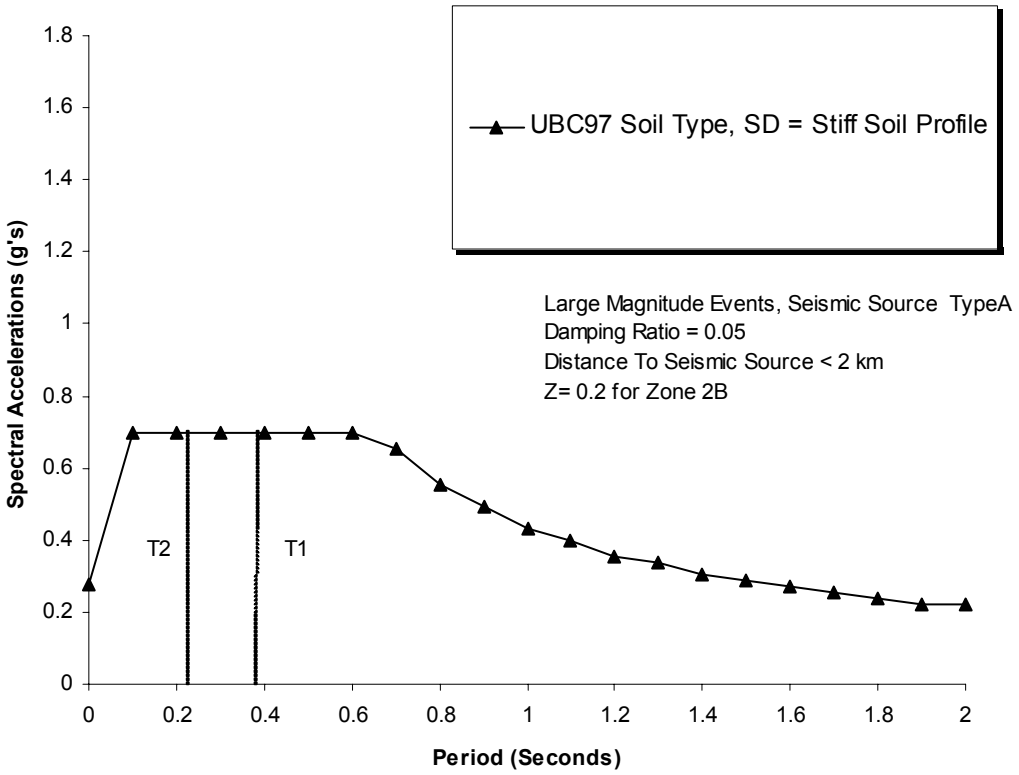

Figure4.9: UBC 97 design response spectra for stiff soil profile (SD) in seismic zone-2B

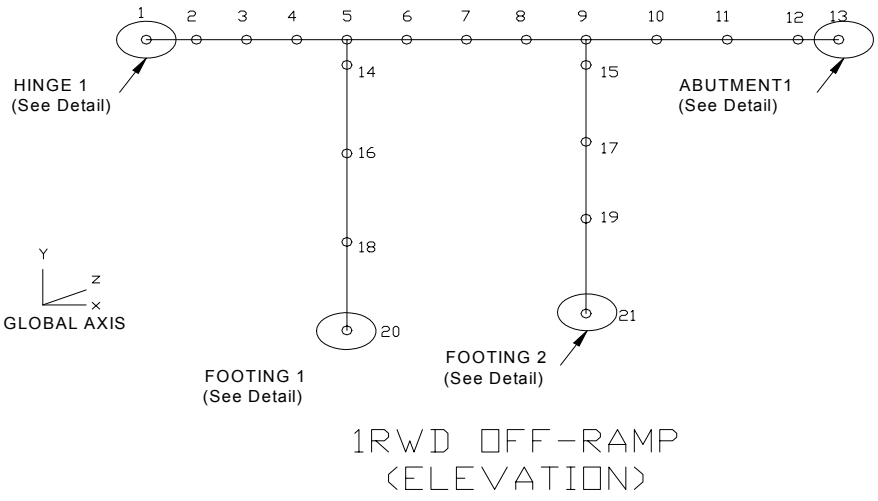

Figure 4.10: Elevation View of DRAIN-3DX Node Distribution on 1RWD Off-Ramp

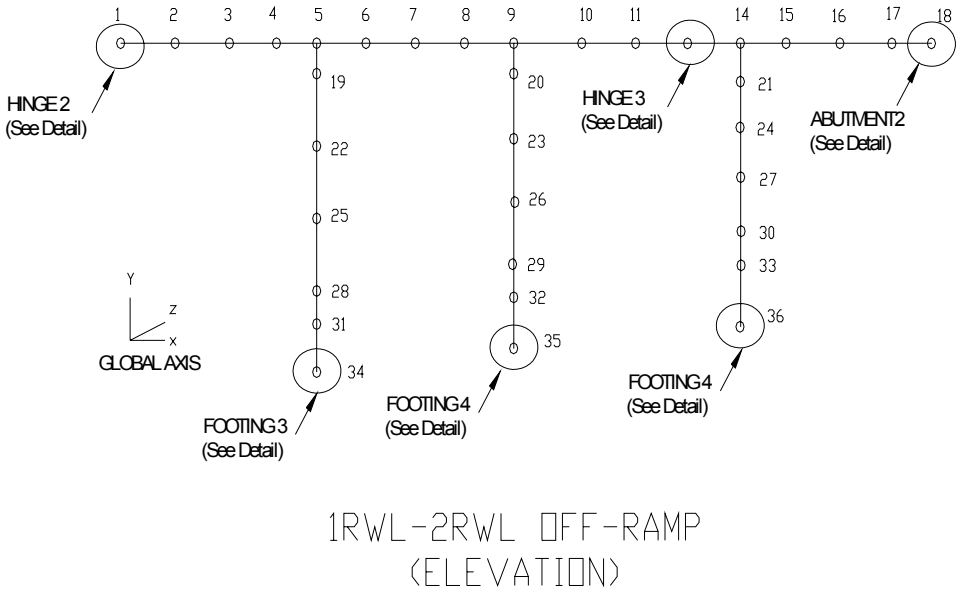

Figure 4.11: Elevation View of DRAIN-3DX Node Distribution on 1RWL-2RWL Off-Ramp

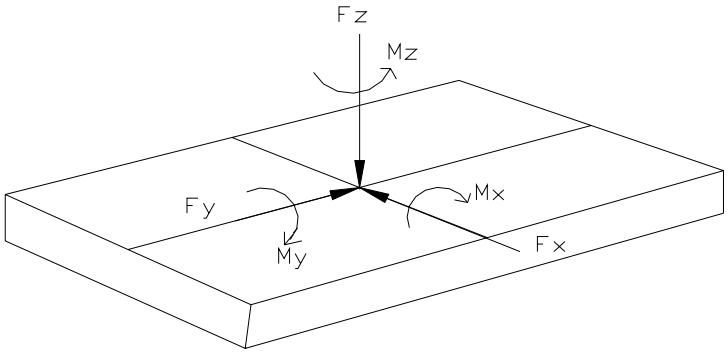

Figure 4.12: Rigid Footing with Six-Degrees of Freedom

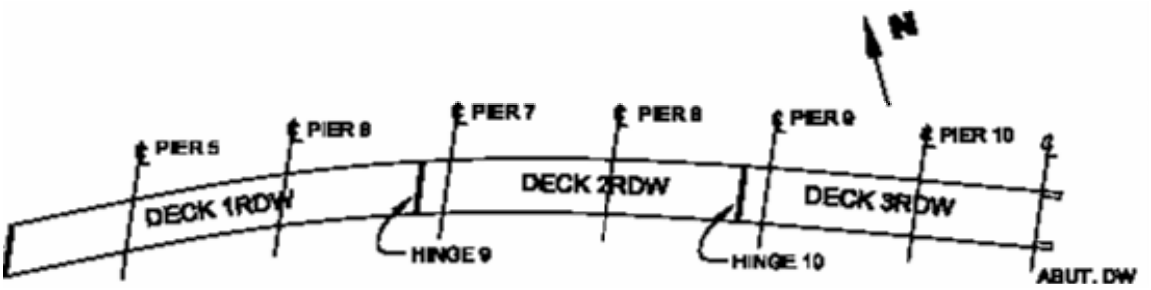

Figure 5-1 Plan View of Ramp DW

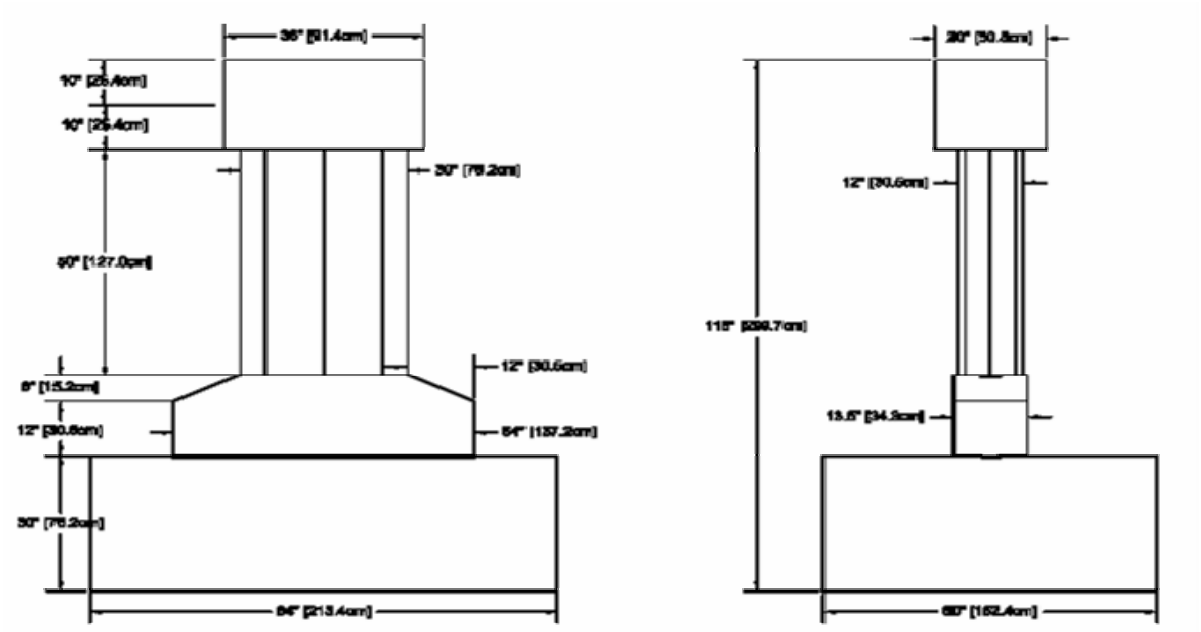

Figure 5-2 Elevation View if Quarter Scale Specimens

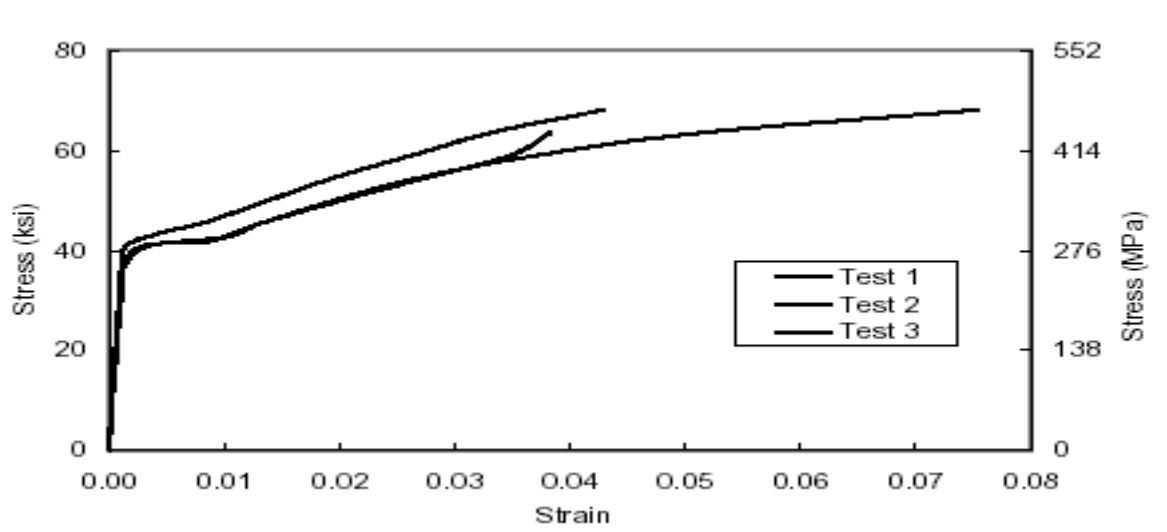

Figure 5-3 Stress-Strain curve for #3 rebar in specimens

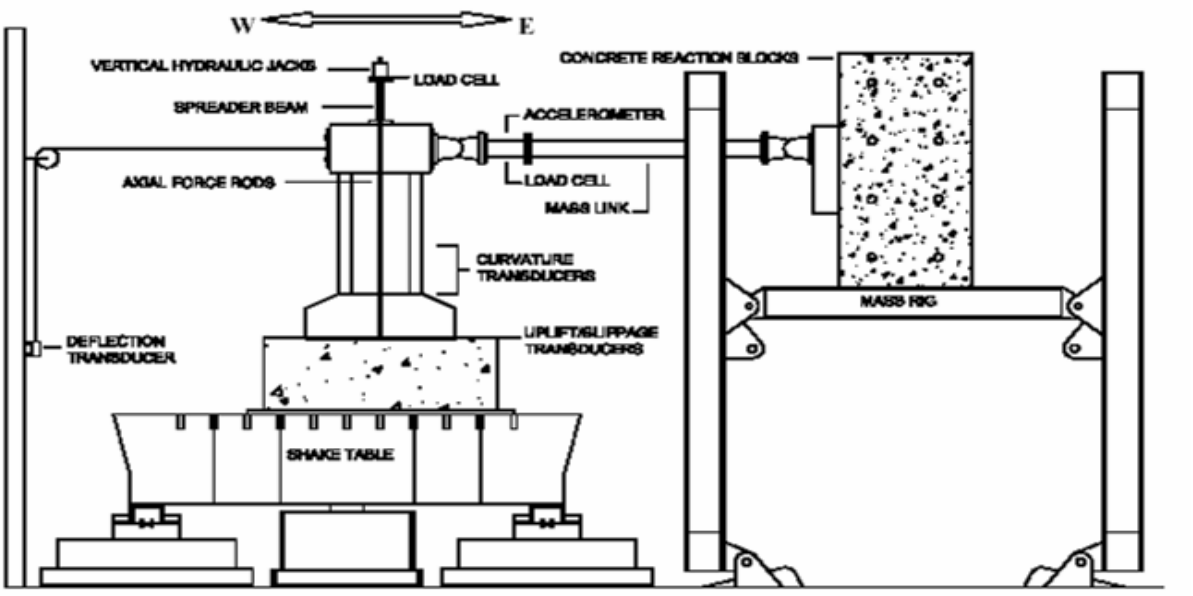

Figure 5-4 Shake Table Setup for OLVA

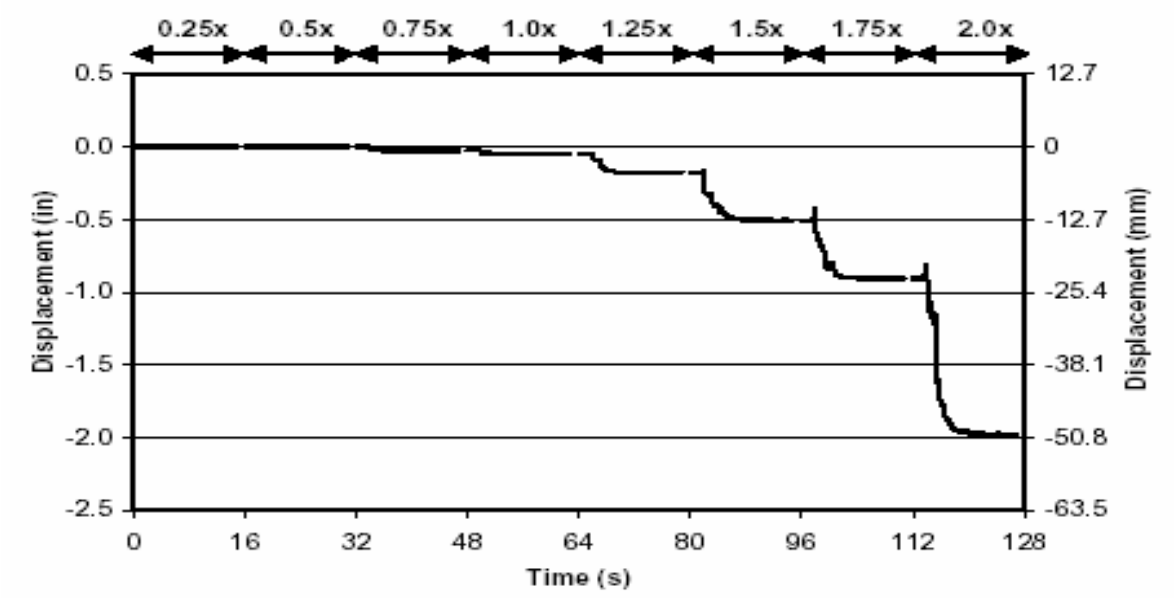

Figure 5-5 Transverse Displacement History of OLVA

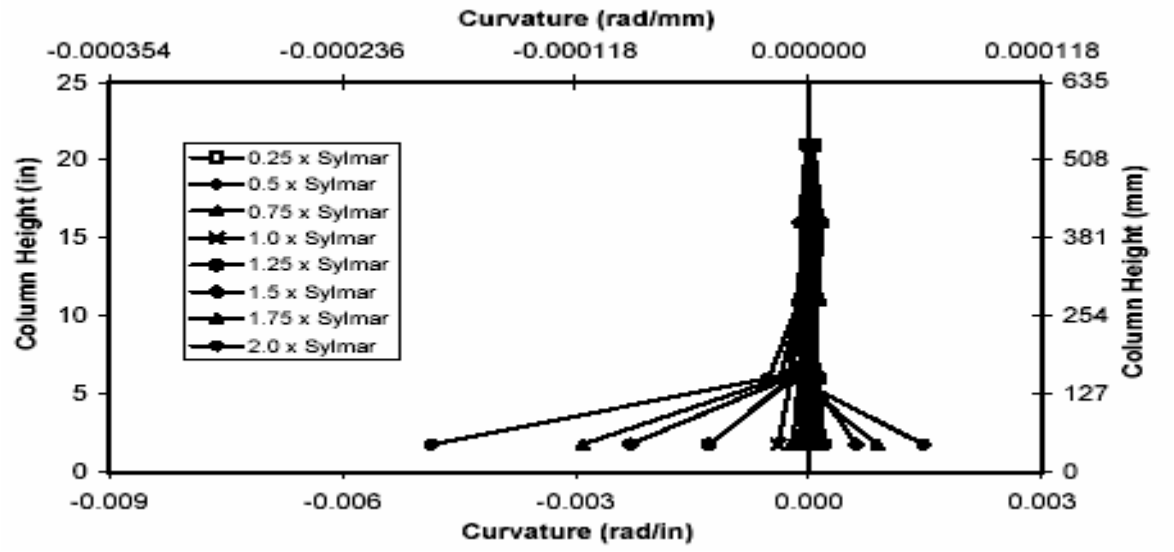

Figure 5-6 Column Curvature Profile from Top of Pedestal OLVA

Figure 5-7 OLVR-1 Bar Exposure after 2.75xSylmar

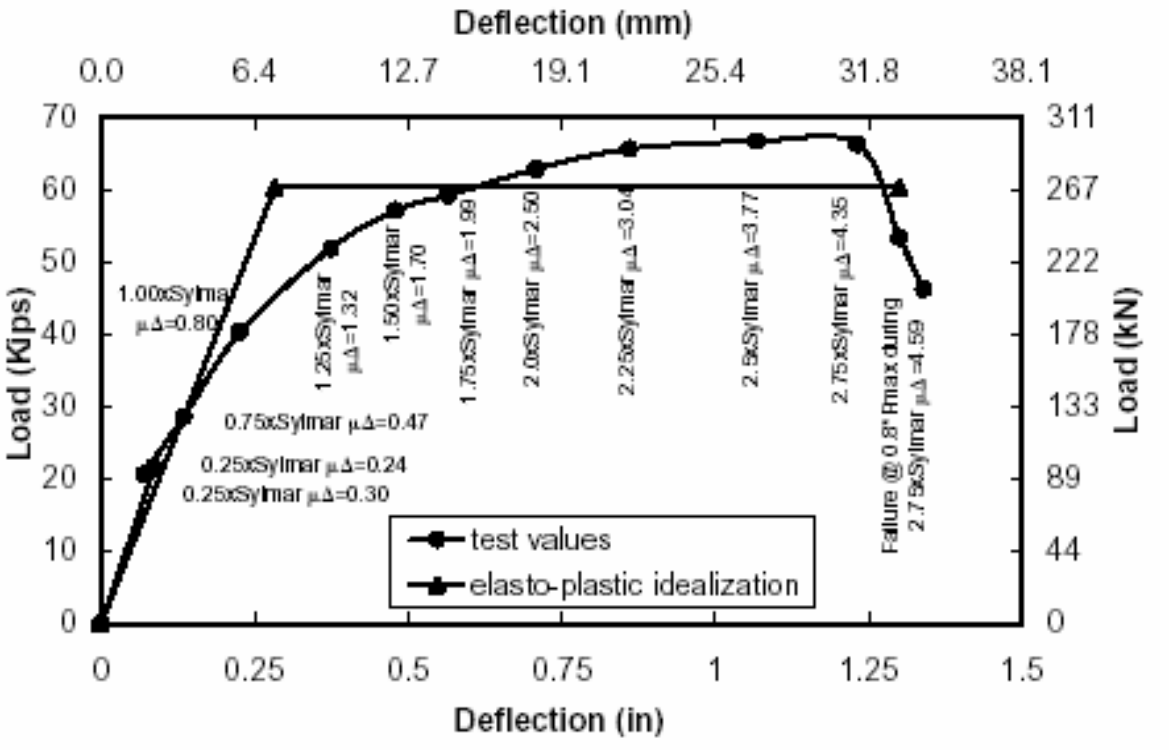

Figure 5-8 Load-Deflection Plot for OLVR-1

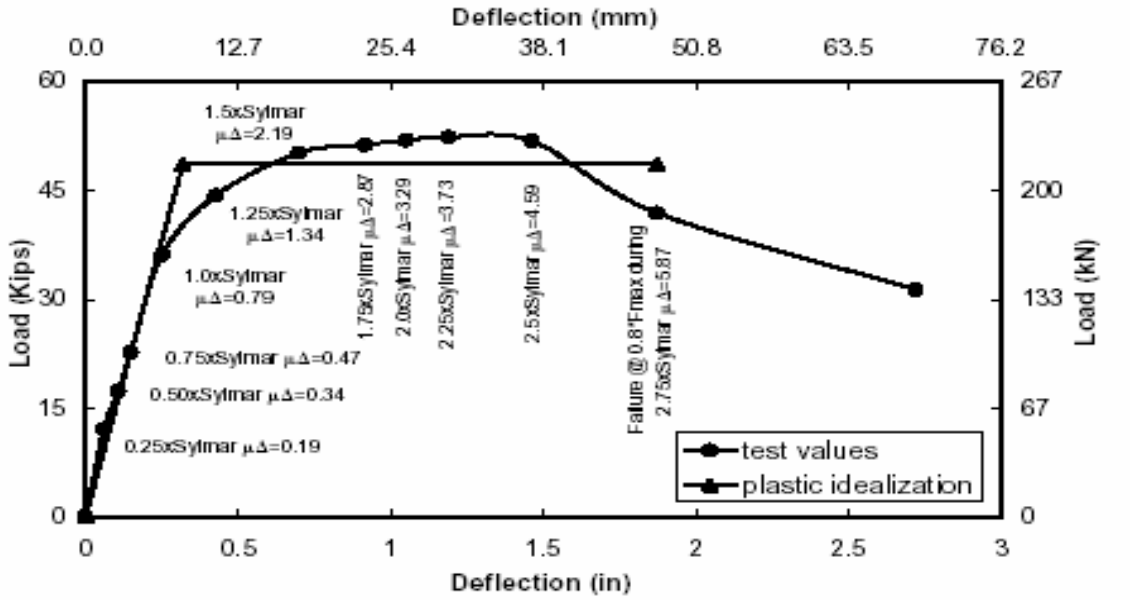

Figure 5-9 Load-Deflection Plot for OLVR-2

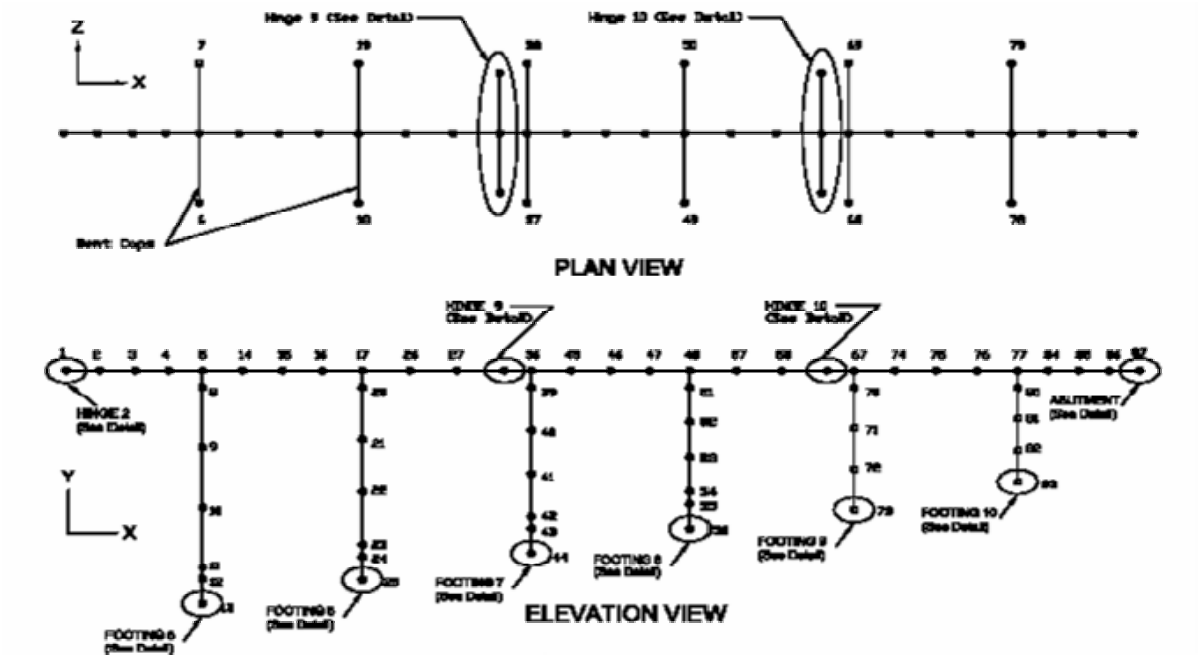

Figure 5-10 Nodal Layout of Drain 3DX Model of Ramp DW

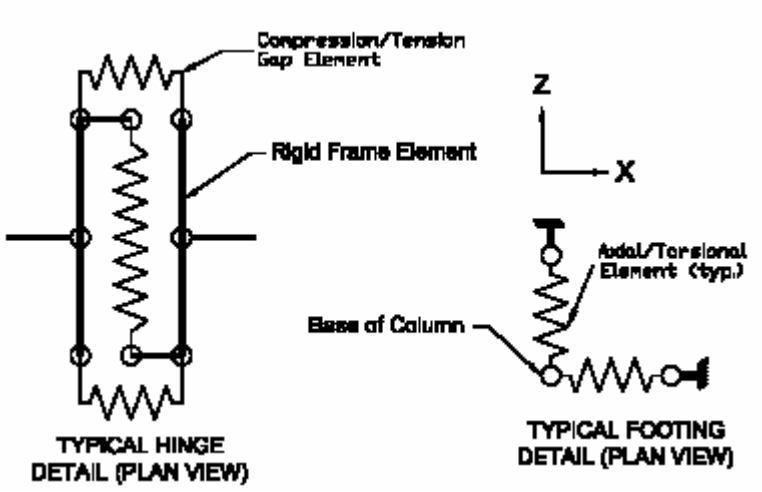

Figure 5-11 Hinge and Footing Details of Ramp DW Drain 3DX Model

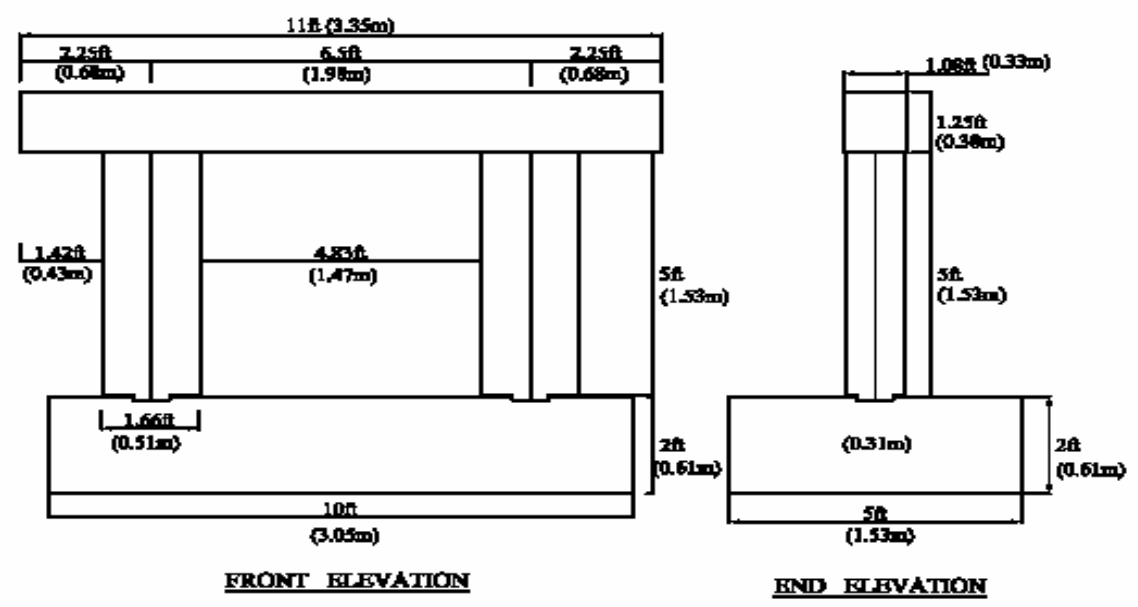

Figure 6-1 General Dimensions of the Specimen

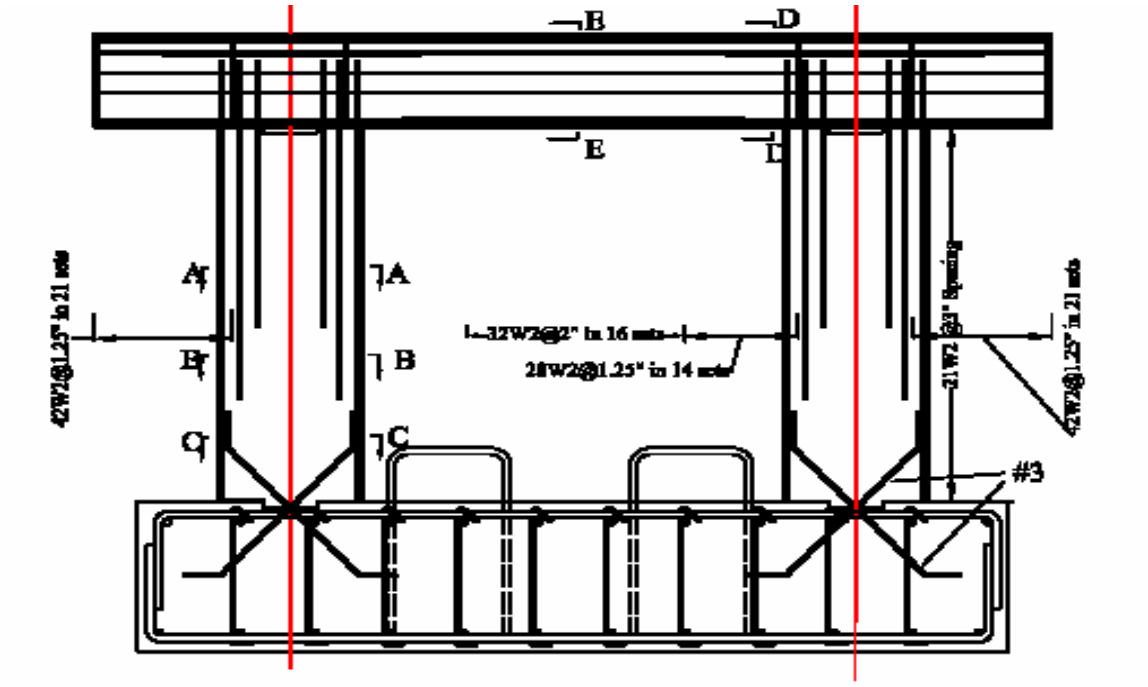

Figure 6-2 General Layout of the Reinforcement in the Specimen

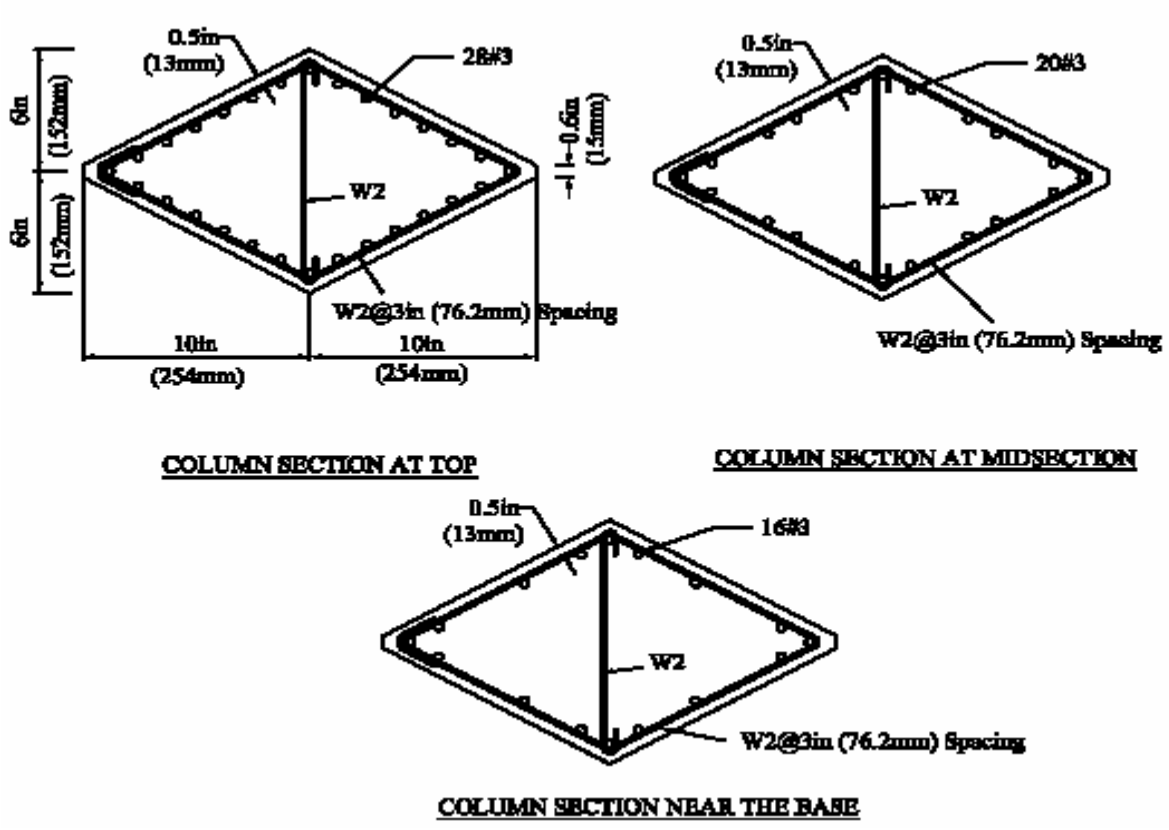

Figure 6-3 Column Cross Section

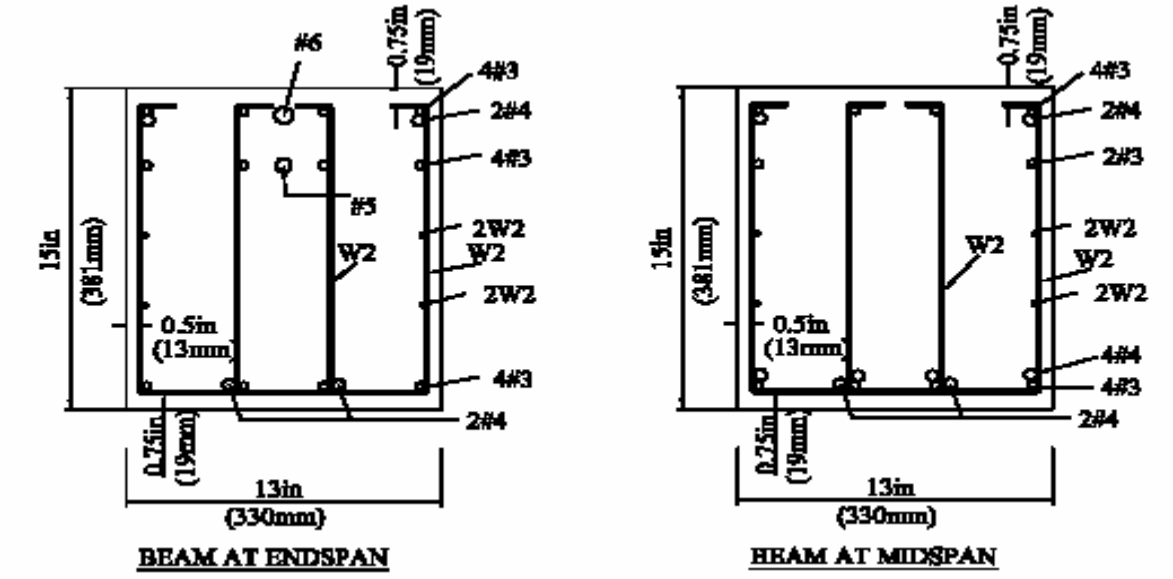

Figure 6-4 Beam Cross Sections

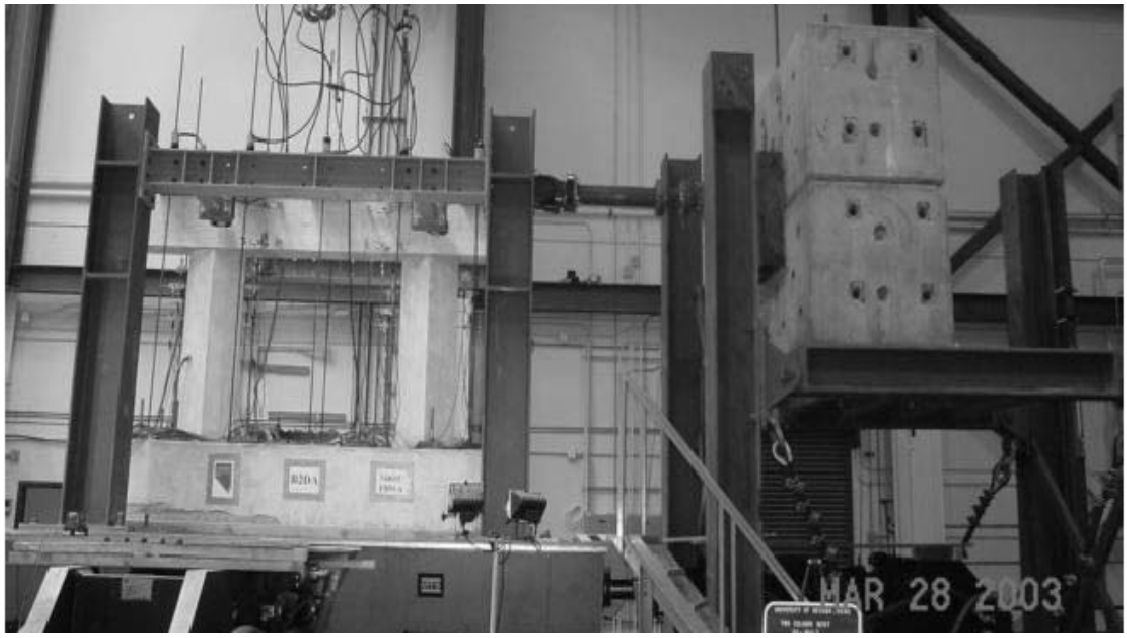

Figure 6-5 Test Setup

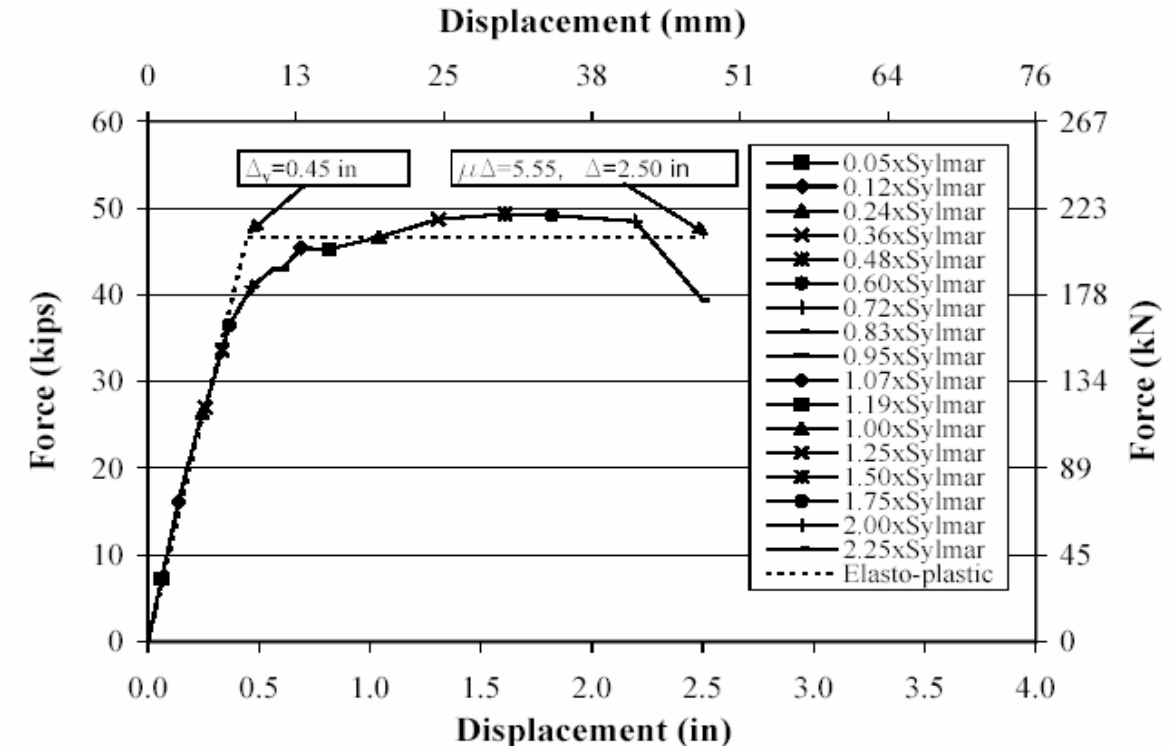

Figure 6-6 Measured and Idealized Force-Displacement Envelope for B2DA

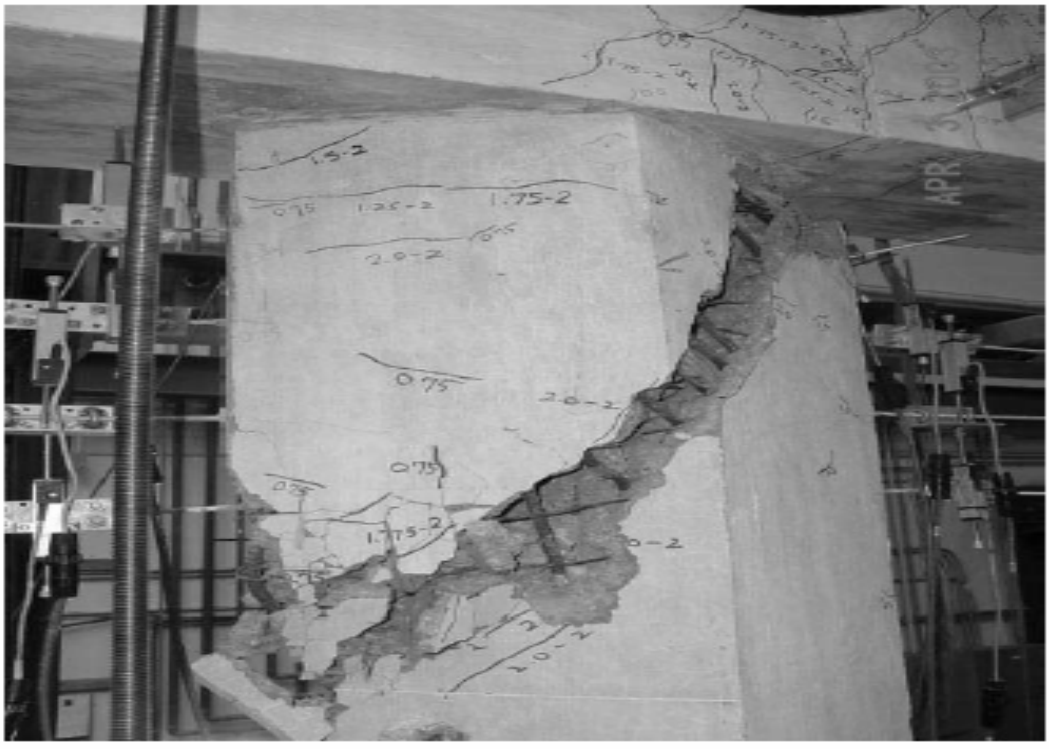

Figure 6-7 Shear Failure of the South Column during Run 23

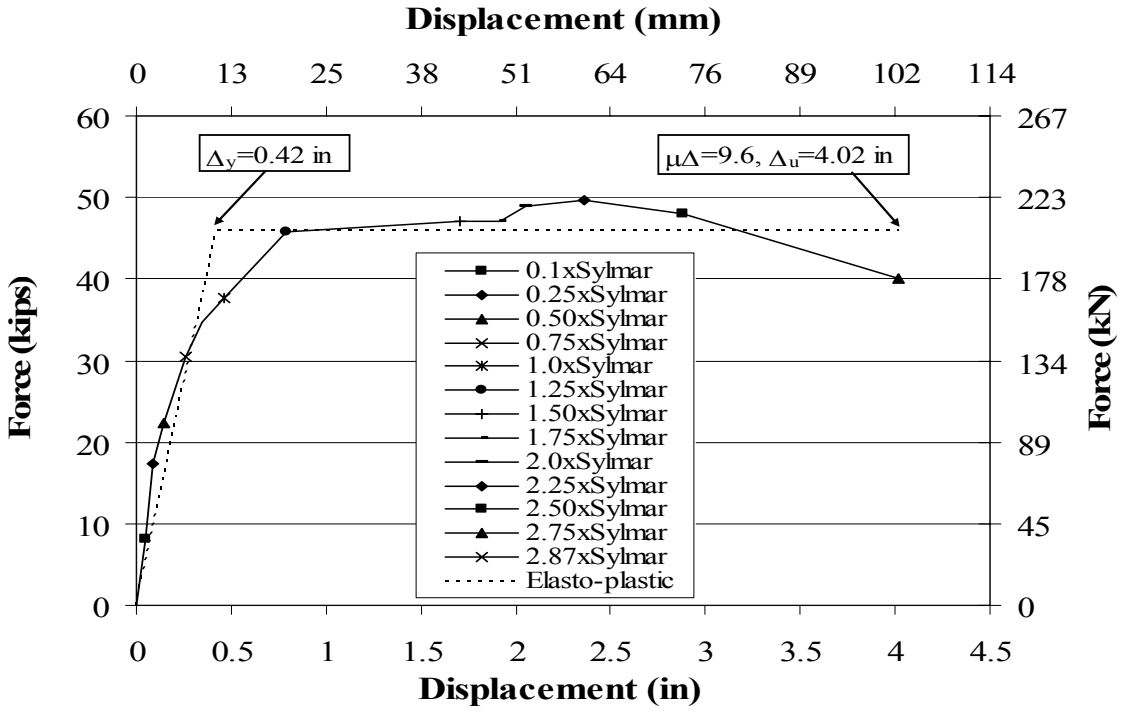

Figure 6-8 Force-Displacement Relationship of B2DC

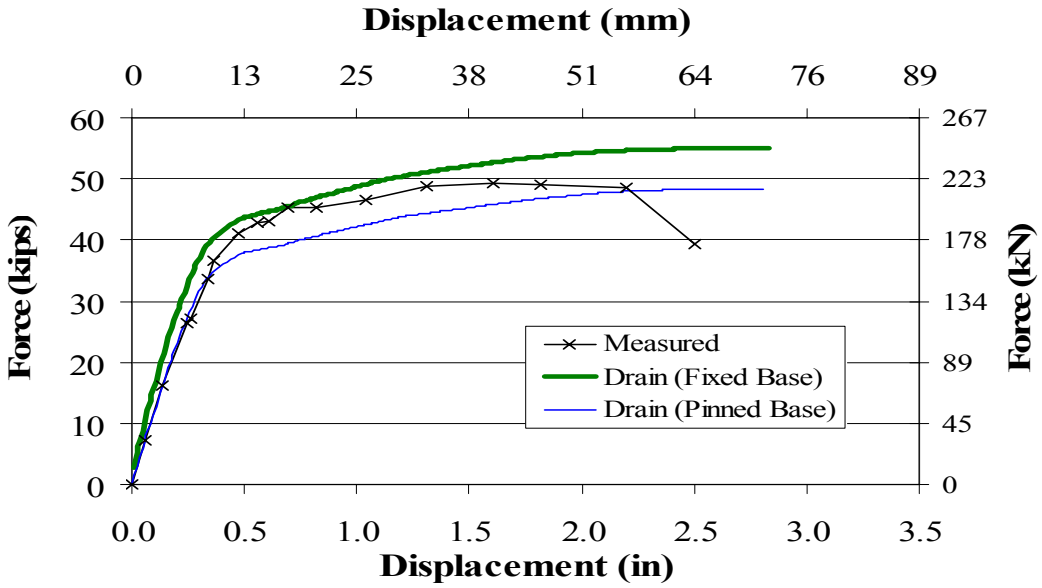

Figure 6-9 Comparison of Load-Displacement Curves for B2DA

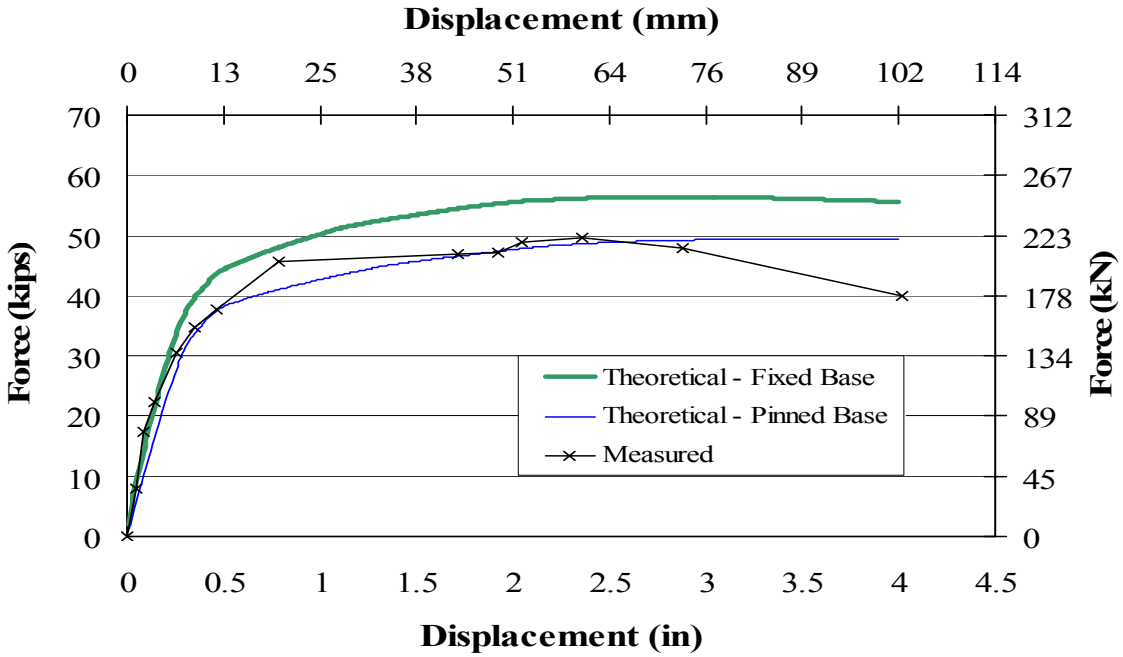

Figure 6-10 Comparison of Load-Displacement Curves for B2DC

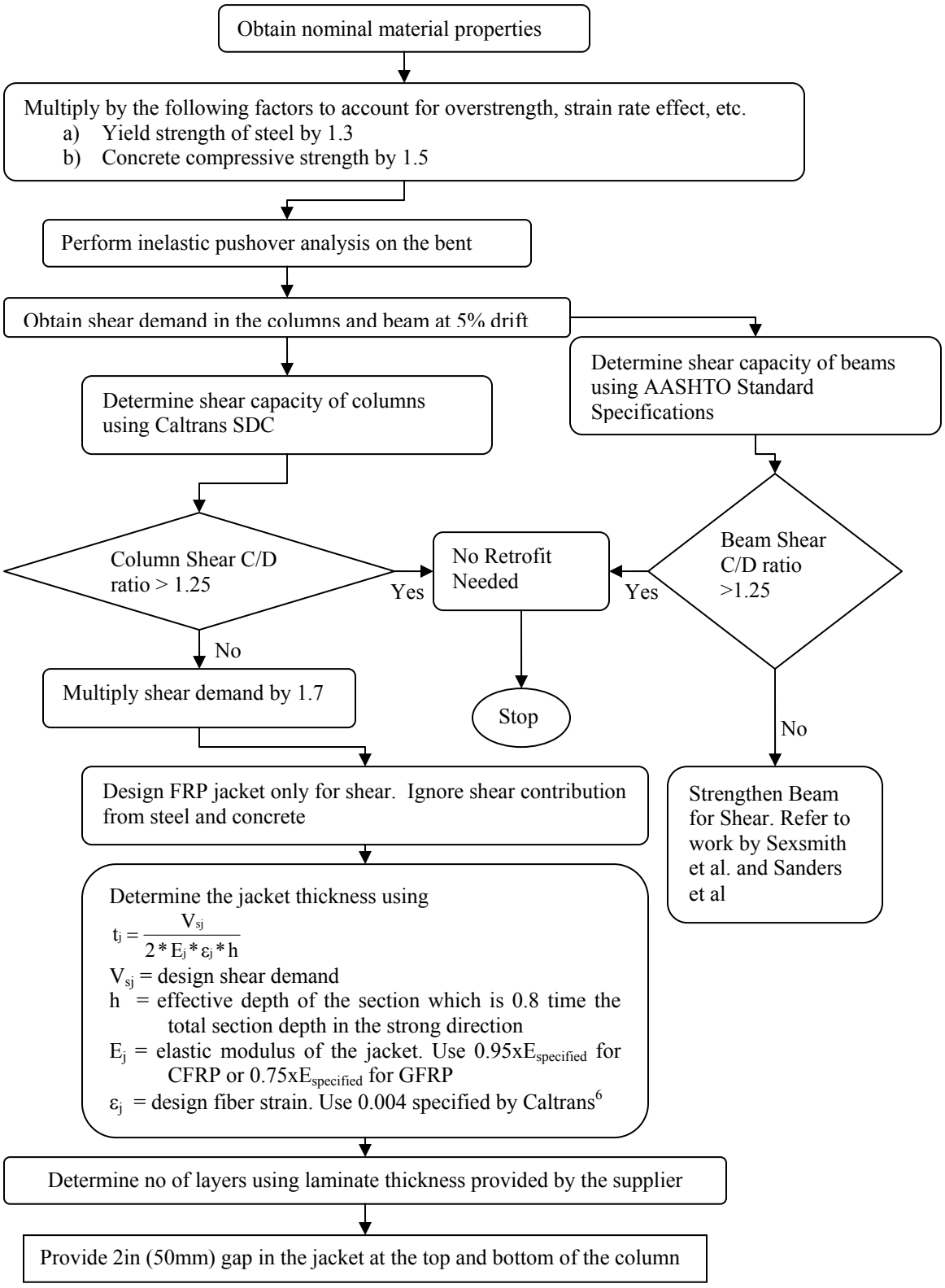

Figure 6-11 Flow Chart for Retrofit Design of Multi-Column Bent with Diamond Shape Columns

APPENDIX A

Retrofit Design Guidelines for Columns of On-Ramp Bridge Structure

A.1 Retrofit Guidelines for Columns with Pedestal

1) Determine the probable material properties for column analysis. Use the measured material properties from construction samples. Apply a factor of 1.2 to the concrete compressive strength and a factor of 1.25 to the steel yield strength to account for strain hardening.

2) Determine the plastic shear demand of the column by moment curvature analysis of the column section and pedestal base.

3) Calculate the pedestal retrofit design force at the pedestal-extension interface by multiplying the column plastic shear demand by 1.25 to provide margin against shear failure.

4) Calculate required reinforcement for the pedestal overlay to level the top of the pedestal. Use the shear friction design method and apply one half of the pedestal retrofit design force. Reinforcement strength at the overlay-pedestal interface must be checked for anchorage into existing pedestal and hook development into overlay and adjusted accordingly.

5) Design required steel for hinge throat pedestal extension. The edge of extension on each side is semicircular with a diameter equal to the pedestal width. Increase the design moment by 1.35 to insure that a plastic hinge will not form at the pedestal-footing interface

6) Design required development lengths of the reinforcement calculated in Step 5 for embedment into the pedestal extension and for anchorage into the existing footing.

7) Design connection of the pedestal extension at the pedestal-extension interface. Use the shear friction design method to find the lateral reinforcement required to fully develop the longitudinal reinforcement calculated in Step 5.

8) Design the pedestal FRP retrofit using either carbon or glass fiber reinforced plastics. Use the pedestal retrofit design force calculated in step 3 to design for tension in the long direction of the pedestal. Determine number of wraps using material properties of 75 percent of the specified modulus elasticity and 0.4 percent strain.

9) Detail section at the base of the column above the pedestal to have a 2 in (50 mm) high cut on either side of the column strong direction. The cut is to sever the first three layers of rebar on each side.

10) Design a FRP jacket for the column of the same material as in Step 8. Use the maximum plastic shear demand as the design force including the over strength discussed in Step 1. Ignore capacity of existing concrete, and transverse reinforcement to be conservative.

A.2 Retrofit Guidelines for Columns without a Pedestal

1) Determine the probable material properties for column analysis. Use the measured material properties from construction samples. Apply a factor of 1.2 to

the concrete compressive strength and a factor of 1.25 to the steel yield strength to account for strain hardening.

2) Using moment curvature analysis, determine the plastic moment capacity of the full column section above the one-way hinge.

3) Design a pedestal to envelop the base of the column and to extend the column one-way hinge section so that it has a plastic moment capacity of 1.35 times that of the column section. The height of the pedestal is governed by that needed to develop the flexural steel of the extension and the column. Lateral pedestal reinforcement is to be sufficient to resist 1.25 times the plastic shear demand at the vertical interface between the existing column and added pedestal.

3) Detail section at the base of the column above the pedestal to have a 2 in (50 mm) high cut on either side of the column strong direction. The cut is to sever the first two layers of rebar on each side.

4) Design a FRP jacket for the column using either carbon or glass fabric. Use the maximum plastic shear demand as the design force including the over strength discussed in Step 1. Ignore capacity of existing concrete, and transverse reinforcement to be conservative.

APPENDIX B

Retrofit Design Guidelines for Viaduct Main Structure with Diamond Shape Columns

B. 1 Design Guidelines

1) Obtain the nominal material properties for bent analysis. Apply a factor of 1.3 to the yield strength of steel and a factor of 1.5 to the compressive strength of concrete to account for overstrength, strain rate effect etc.
2) Determine the plastic shear demand on the columns and the cap beam at the required drift ratio from an inelastic pushover analysis using a nonlinear finite element programs such as Drain 3-DX or SAP 2000. It is suggested to use a 5% drift in this step.
3) Obtain the shear capacity of the columns using design guidelines from Caltrans SDC[53] and the shear capacity at the beam ends using AASHTO Standard Specifications[54].
4) Calculate the shear capacity-demand (C/D) ratio for columns and beam. If the ratio is above 1.25 no retrofit is needed. If C/D ratio is below 1.25 for beam then follow the retrofit techniques recommended by Sexsmith et al[55]. If C/D ratio is below 1.25 for columns then follow steps 5 to 8 presented below.
5) Calculate the maximum design shear demand on the columns and beam by multiplying the plastic shear demand from Step 2 by 1.7.
6) Determine the required FRP Jacket thickness for either carbon or glass fiber reinforced plastics using equation B.1

$$t_j = \frac{V_{sj}}{2 * E_j * \varepsilon_j * h * \cot\theta} \qquad \text{(B.1)}$$

Where

V_{sj} = design shear demand

h = effective depth of the section

E_j = elastic modulus of the jacket

ε_j = design fiber strain

θ = angle of principal compression strut, to be taken as 45^o

Use the design shear force calculated in Step 5 to design for shear. Ignore the contribution of concrete and transverse steel to the total shear capacity to have a conservative design. Use the following values to calculate the required layers of FRP jacket

a. Design fiber strain of 0.4 percent (recommended by Caltrans[39])
b. 95 percent of the specified elastic modulus for CFRP or 75 percent of the specified elastic modulus for GFRP
c. 80 percent of the effective depth of section. The effective depth of section is distance from the extreme compression fiber to the centroid of the steel area.

7) Determine the required number of layers using the laminate thickness provided the supplier. Round up to the nearest whole number.
8) Provide 2 in (51 mm) gap in the jacket at the top and bottom of the column.

B. 2 Design Example

This section discusses a design example for the design recommendation presented in Chapter 5 of this report. This is the retrofit design for the columns in Pier 16 West of the Las Vegas Viaduct.

Step 1

Material properties of the prototype from Construction Sample

Concrete compressive strength $f_c := 4$ ksi (27.6 MPa)

Average yield strength of steel $f_y := 40$ ksi (276 MPa)

Concrete compressive strength including strain rate effect, overstrength and aging effect $f_c := 4 \times 1.5$

$f_c = 6$ ksi (41.4 MPa)

Yield strength of steel including strain rate effect, overstrength and strain hardening $f_y := 40 \times 1.3$

$f_y = 52$ ksi (359 MPa)

If results from moment-curvature analysis are used for pushover analysis then multiply the yield strength of steel by factor of 1.2 because strain hardening is taken into accou

Step 2

Plastic Moment at Top of the Column from RCMC $M_{p1} := 74314$ kip-in (8391 kNm)

Plastic Moment at Base of the Column from RCMC $M_{p2} := 9907$ kip-in (1118 kNm)

Clear height of the Column $h := 240$ in (6096 mm)

Plastic Shear Demand on the Column $V_p := \frac{(M_{p1} + M_{p2})}{h}$

$V_p = 350.9$ kips (1562 kN)

The shear demand from Drain 3-DX, a finite element program $V := 429$ kips (1909 kN)

In this example the retrofit is done based on the shear demand from the Drain 3-DX and this shear demand on the column is at a 5% lateral drift of the specimen

Step 3

Factor of saftey against shear failure $\alpha := 1.7$ (Ref 56)

Maximum shear demand on the column including a safety factor $V_{max} := \alpha \times V$

$V_{max} = 729.3$ kips (3245 kN)

Step 4

Retrofit design shear force is the maximum shear demand less the shear contribution from concrete and steel

Shear contribution from concrete $V_c := 0$ due to extensive plastic hinging at the top of the column

Shear contribution from steel $V_s := 0$ Because of the excessive spacing betwee ties in the column

The above would result in a conservative design of CFRP

Therefore Retrofit shear force $V_{sj} := V_{max} - V_c - V_s$

$V_{sj} = 729.3$ kips (3245 kN)

Step 5

In this example Carbon fiber reinforced plastic (CFRP) is used as retrofit material.

CFRP was SCH-41 supplied by Fyfe Co LLC

The material properties specified by the supplier is given below

Tensile Modulus $E_j := 10500$ ksi (72450 MPa)

Ultimate Elongation of fiber $\varepsilon_j := 0.012$ ie 1.2%

Laminate thickness (one layer) $t_{1j} := 0.04$ in (1 mm)

The material properties used for design is as follows

Tensile modulus $E_j := 10500 \times 0.95$

$E_j = 9975$ ksi (68827 MPa)

Design strain of fiber $\varepsilon_j := 0.004$

The design values used above are based on Caltrans Memo to designers (Ref.3

Depth of section in the strong direction of the column $D := 80$ in (2032 mm)

80% of the effective depth of section $d := 0.8 \times (80 - 2.7)$

$d = 61.84$ in (1571 mm)

Angle of principle compression strut $\theta := 45$

Shear strength capacity of the jacket, $V_{sj} = 2 \times t_j \times E_j \times \varepsilon_j \times d \times \cot\theta$

Thickness of jacket $t_j := \dfrac{V_{sj}}{2 \times E_j \times \varepsilon_j \times d}$

$t_j = 0.15$

The required number of layers $n := \dfrac{t_j}{t_{1j}}$

$n = 3.69$

Therefore the columns need to be wrapped with 4 layers of CFRP

Step 6

Provide a 2 in (51 mm) gap at the top and the bottom of the column

LIST OF CCEER PUBLICATIONS

Report No.	Publication
CCEER-84-1	Saiidi, M., and R. Lawver, "User's Manual for LZAK-C64, A Computer Program to Implement the Q-Model on Commodore 64," Civil Engineering Department, Report No. CCEER-84-1, University of Nevada, Reno, January 1984.
CCEER-84-2	Douglas, B. and T. Iwasaki, "Proceedings of the First USA-Japan Bridge Engineering Workshop," held at the Public Works Research Institute, Tsukuba, Japan, Civil Engineering Department, Report No. CCEER-84-2, University of Nevada, Reno, April 1984.
CCEER-84-3	Saiidi, M., J. Hart, and B. Douglas, "Inelastic Static and Dynamic Analysis of Short R/C Bridges Subjected to Lateral Loads," Civil Engineering Department, Report No. CCEER-84-3, University of Nevada, Reno, July 1984.
CCEER-84-4	Douglas, B., "A Proposed Plan for a National Bridge Engineering Laboratory," Civil Engineering Department, Report No. CCEER-84-4, University of Nevada, Reno, December 1984.
CCEER-85-1	Norris, G. and P. Abdollaholiaee, "Laterally Loaded Pile Response: Studies with the Strain Wedge Model," Civil Engineering Department, Report No. CCEER-85-1, University of Nevada, Reno, April 1985.
CCEER-86-1	Ghusn, G. and M. Saiidi, "A Simple Hysteretic Element for Biaxial Bending of R/C in NEABS-86," Civil Engineering Department, Report No. CCEER-86-1, University of Nevada, Reno, July 1986.
CCEER-86-2	Saiidi, M., R. Lawver, and J. Hart, "User's Manual of ISADAB and SIBA, Computer Programs for Nonlinear Transverse Analysis of Highway Bridges Subjected to Static and Dynamic Lateral Loads," Civil Engineering Department, Report No. CCEER-86-2, University of Nevada, Reno, September 1986.
CCEER-87-1	Siddharthan, R., "Dynamic Effective Stress Response of Surface and Embedded Footings in Sand," Civil engineering Department, Report No. CCEER-86-2, University of Nevada, Reno, June 1987.
CCEER-87-2	Norris, G. and R. Sack, "Lateral and Rotational Stiffness of Pile Groups for Seismic Analysis of Highway Bridges," Civil Engineering Department, Report No. CCEER-87-2, University of Nevada, Reno, June 1987.
CCEER-88-1	Orie, J. and M. Saiidi, "A Preliminary Study of One-Way Reinforced Concrete Pier Hinges Subjected to Shear and Flexure," Civil Engineering Department, Report No. CCEER-88-1, University of Nevada, Reno, January 1988.
CCEER-88-2	Orie, D., M. Saiidi, and B. Douglas, "A Micro-CAD System for Seismic Design of Regular Highway Bridges," Civil Engineering Department, Report No. CCEER-88-2, University of Nevada, Reno, June 1988.
CCEER-88-3	Orie, D. and M. Saiidi, "User's Manual for Micro-SARB, a Microcomputer Program for Seismic Analysis of Regular Highway Bridges," Civil Engineering Department, Report No. CCEER-88-3, University of Nevada, Reno, October 1988.

CCEER-89-1 Douglas, B., M. Saiidi, R. Hayes, and G. Holcomb, "A Comprehensive Study of the Loads and Pressures Exerted on Wall Forms by the Placement of Concrete," Civil Engineering Department, Report No. CCEER-89-1, University of Nevada, Reno, February 1989.

CCEER-89-2 Richardson, J. and B. Douglas, "Dynamic Response Analysis of the Dominion Road Bridge Test Data," Civil Engineering Department, Report No. CCEER-89-2, University of Nevada, Reno, March 1989.

CCEER-89-2 Vrontinos, S., M. Saiidi, and B. Douglas, "A Simple Model to Predict the Ultimate Response of R/C Beams with Concrete Overlays," Civil Engineering Department, Report NO. CCEER-89-2, University of Nevada, Reno, June 1989.

CCEER-89-3 Ebrahimpour, A. and P. Jagadish, "Statistical Modeling of Bridge Traffic Loads - A Case Study," Civil Engineering Department, Report No. CCEER-89-3, University of Nevada, Reno, December 1989.

CCEER-89-4 Shields, J. and M. Saiidi, "Direct Field Measurement of Prestress Losses in Box Girder Bridges," Civil Engineering Department, Report No. CCEER-89-4, University of Nevada, Reno, December 1989.

CCEER-90-1 Saiidi, M., E. Maragakis, G. Ghusn, Y. Jiang, and D. Schwartz, "Survey and Evaluation of Nevada's Transportation Infrastructure, Task 7.2 - Highway Bridges, Final Report," Civil Engineering Department, Report No. CCEER 90-1, University of Nevada, Reno, October 1990.

CCEER-90-2 Abdel-Ghaffar, S., E. Maragakis, and M. Saiidi, "Analysis of the Response of Reinforced Concrete Structures During the Whittier Earthquake 1987," Civil Engineering Department, Report No. CCEER 90-2, University of Nevada, Reno, October 1990.

CCEER-91-1 Saiidi, M., E. Hwang, E. Maragakis, and B. Douglas, "Dynamic Testing and the Analysis of the Flamingo Road Interchange," Civil Engineering Department, Report No. CCEER-91-1, University of Nevada, Reno, February 1991.

CCEER-91-2 Norris, G., R. Siddharthan, Z. Zafir, S. Abdel-Ghaffar, and P. Gowda, "Soil-Foundation-Structure Behavior at the Oakland Outer Harbor Wharf," Civil Engineering Department, Report No. CCEER-91-2, University of Nevada, Reno, July 1991.

CCEER-91-3 Norris, G., "Seismic Lateral and Rotational Pile Foundation Stiffnesses at Cypress," Civil Engineering Department, Report No. CCEER-91-3, University of Nevada, Reno, August 1991.

CCEER-91-4 O'Connor, D. and M. Saiidi, "A Study of Protective Overlays for Highway Bridge Decks in Nevada, with Emphasis on Polyester-Styrene Polymer Concrete," Civil Engineering Department, Report No. CCEER-91-4, University of Nevada, Reno, October 1991.

CCEER-91-5 O'Connor, D.N. and M. Saiidi, "Laboratory Studies of Polyester-Styrene Polymer Concrete Engineering Properties," Civil Engineering Department, Report No. CCEER-91-5, University of Nevada, Reno, November 1991.

CCEER-92-1 Straw, D.L. and M. Saiidi, "Scale Model Testing of One-Way Reinforced Concrete Pier Hinges Subject to Combined Axial Force, Shear and Flexure," edited by D.N. O'Connor, Civil Engineering Department, Report No. CCEER-92-1, University of Nevada, Reno, March 1992.

CCEER-92-2 Wehbe, N., M. Saiidi, and F. Gordaninejad, "Basic Behavior of Composite Sections Made of Concrete Slabs and Graphite Epoxy Beams," Civil Engineering Department, Report No. CCEER-92-2, University of Nevada, Reno, August 1992.

CCEER-92-3 Saiidi, M. and E. Hutchens, "A Study of Prestress Changes in A Post-Tensioned Bridge During the First 30 Months," Civil Engineering Department, Report No. CCEER-92-3, University of Nevada, Reno, April 1992.

CCEER-92-4 Saiidi, M., B. Douglas, S. Feng, E. Hwang, and E. Maragakis, "Effects of Axial Force on Frequency of Prestressed Concrete Bridges," Civil Engineering Department, Report No. CCEER-92-4, University of Nevada, Reno, August 1992.

CCEER-92-5 Siddharthan, R., and Z. Zafir, "Response of Layered Deposits to Traveling Surface Pressure Waves," Civil Engineering Department, Report No. CCEER-92-5, University of Nevada, Reno, September 1992.

CCEER-92-6 Norris, G., and Z. Zafir, "Liquefaction and Residual Strength of Loose Sands from Drained Triaxial Tests," Civil Engineering Department, Report No. CCEER-92-6, University of Nevada, Reno, September 1992.

CCEER-92-7 Douglas, B., "Some Thoughts Regarding the Improvement of the University of Nevada, Reno's National Academic Standing," Civil Engineering Department, Report No. CCEER-92-7, University of Nevada, Reno, September 1992.

CCEER-92-8 Saiidi, M., E. Maragakis, and S. Feng, "An Evaluation of the Current Caltrans Seismic Restrainer Design Method," Civil Engineering Department, Report No. CCEER-92-8, University of Nevada, Reno, October 1992.

CCEER-92-9 O'Connor, D., M. Saiidi, and E. Maragakis, "Effect of Hinge Restrainers on the Response of the Madrone Drive Undercrossing During the Loma Prieta Earthquake," Civil Engineering Department, Report No. CCEER-92-9, University of Nevada, Reno, February 1993.

CCEER-92-10 O'Connor, D., and M. Saiidi, "Laboratory Studies of Polyester Concrete: Compressive Strength at Elevated Temperatures and Following Temperature Cycling, Bond Strength to Portland Cement Concrete, and Modulus of Elasticity," Civil Engineering Department, Report No. CCEER-92-10, University of Nevada, Reno, February 1993.

CCEER-92-11 Wehbe, N., M. Saiidi, and D. O'Connor, "Economic Impact of Passage of Spent Fuel Traffic on Two Bridges in Northeast Nevada," Civil Engineering Department, Report No. CCEER-92-11, University of Nevada, Reno, December 1992.

CCEER-93-1 Jiang, Y., and M. Saiidi, "Behavior, Design, and Retrofit of Reinforced Concrete One-way Bridge Column Hinges," edited by D. O'Connor, Civil Engineering Department, Report No. CCEER-93-1, University of Nevada, Reno, March 1993.

CCEER-93-2 Abdel-Ghaffar, S., E. Maragakis, and M. Saiidi, "Evaluation of the Response of the Aptos Creek Bridge During the 1989 Loma Prieta Earthquake," Civil Engineering Department, Report No. CCEER-93-2, University of Nevada, Reno, June 1993.

CCEER-93-3 Sanders, D.H., B.M. Douglas, and T.L. Martin, "Seismic Retrofit Prioritization of Nevada Bridges," Civil Engineering Department, Report No. CCEER-93-3, University of Nevada, Reno, July 1993.

CCEER-93-4 Abdel-Ghaffar, S., E. Maragakis, and M. Saiidi, "Performance of Hinge Restrainers in the Huntington Avenue Overhead During the 1989 Loma Prieta Earthquake," Civil Engineering Department, Report No. CCEER-93-4, University of Nevada, Reno, June 1993 (in final preparation).

CCEER-93-5 Maragakis, E., M. Saiidi, S. Feng, and L. Flournoy, "Effects of Hinge Restrainers on the Response of the San Gregorio Bridge During the Loma Prieta Earthquake," (in final preparation) Civil Engineering Department, Report No. CCEER-93-5, University of Nevada, Reno.

CCEER-93-6 Saiidi, M., E. Maragakis, S. Abdel-Ghaffar, S. Feng, and D. O'Connor, "Response of Bridge Hinge Restrainers During Earthquakes -Field Performance, Analysis, and Design," Civil Engineering Department, Report No. CCEER-93-6, University of Nevada, Reno, May 1993.

CCEER-93-7 Wehbe, N., Saiidi, M., Maragakis, E., and Sanders, D., "Adequacy of Three Highway Structures in Southern Nevada for Spent Fuel Transportion, Civil Engineering Department, Report No. CCEER-93-7, University of Nevada, Reno, August 1993.

CCEER-93-8 Roybal, J., Sanders, D.H., and Maragakis, E., "Vulnerability Assessment of Masonry in the Reno-Carson City Urban Corridor," Civil Engineering Department, Report No. CCEER-93-8, University of Nevada, Reno, May 1993.

CCEER-93-9 Zafir, Z. and Siddharthan, R., "MOVLOAD: A Program to Determine the Behavior of Nonlinear Horizontally Layered Medium Under Moving Load," Civil Engineering Department, Report No. CCEER-93-9, University of Nevada, Reno, August 1993.

CCEER-93-10 O'Connor, D.N., Saiidi, M., and Maragakis, E.A., "A Study of Bridge Column Seismic Damage Susceptibility at the Interstate 80/U.S. 395 Interchange in Reno, Nevada," Civil Engineering Department, Report No. CCEER-93-10, University of Nevada, Reno, October 1993.

CCEER-94-1 Maragakis, E., B. Douglas, and E. Abdelwahed, "Preliminary Dynamic Analysis of a Railroad Bridge," Report CCEER-94-1, January 1994.

CCEER-94-2 Douglas, B.M., Maragakis, E.A., and Feng, S., "Stiffness Evaluation of Pile Foundation of Cazenovia Creek Overpass," Civil Engineering Department, Report No. CCEER-94-2, University of Nevada, Reno, March 1994.

CCEER-94-3 Douglas, B.M., Maragakis, E.A., and Feng, S., "Summary of Pretest Analysis of Cazenovia Creek Bridge," Civil Engineering Department, Report No. CCEER-94-3, University of Nevada, Reno, April 1994.

CCEER-94-4 Norris, G.M. and Madhu, R., "Liquefaction and Residual Strength of Sands from Drained Triaxial Tests, Report 2," Civil Engineering Department, CCEER-94-4, University of Nevada, Reno, August 1994.

CCEER-94-5 Saiidi, M., Hutchens, E., and Gardella, D., "Prestress Losses in a Post-Tensioned R/C Box Girder Bridge in Southern Nevada," Civil Engineering Department, CCEER-94-5, University of Nevada, Reno, August 1994.

CCEER-95-1 Siddharthan, R., El-Gamal, M., and Maragakis, E.A., "Nonlinear Bridge Abutment , Verification, and Design Curves," Civil Engineering Department, CCEER-95-1, University of Nevada, Reno, January 1995.

CCEER-95-2 Norris, G.M., Madhu, R., Valceschini, R., and Ashour, M., "Liquefaction and Residual Strength of Loose Sands from Drained Triaxial Tests," Report 2, Civil Engineering Department, Report No. CCEER-95-2, University of Nevada, Reno, February 1995.

CCEER-95-3 Wehbe, N., Saiidi, M., Sanders, D., and Douglas, B., "Ductility of Rectangular Reinforced Concrete Bridge Columns with Moderate Confinement,"Civil Engineering Department, Report No. CCEER-95-3, University of Nevada, Reno, July 1995.

CCEER-95-4 Martin, T., Saiidi, M., and Sanders, D., "Seismic Retrofit of Column-Pier Cap Connections in Bridges in Northern Nevada," Civil Engineering Department, Report No. CCEER-95-4, University of Nevada, Reno, August 1995.

CCEER-95-5 Darwish, I., Saiidi, M., and Sanders, D., "Experimental Study of Seismic Susceptibility Column-Footing Connections," Civil Engineering Department, Report No. CCEER-95-5, University of Nevada, Reno, September 1995.

CCEER-95-6 Griffin, G., Saiidi, M., and Maragakis, E., "Nonlinear Seismic Response of Isolated Bridges and Effects of Pier Ductility Demand," Civil Engineering Department, Report No. CCEER-95-6, University of Nevada, Reno, November 1995.

CCEER-95-7 Acharya, S., Saiidi, M., and Sanders, D., "Seismic Retrofit of Bridge Footings and Column-Footing Connections," Report for the Nevada Department of Transportation, Civil Engineering Department, Report No. CCEER-95-7, University of Nevada, Reno, November 1995.

CCEER-95-8 Maragakis, E., Douglas, B., and Sandirasegaram, U., "Full-Scale Field Resonance Tests of a Railway Bridge," A Report to the Association of American Railroads, Civil Engineering Department, Report No. CCEER-95-8, University of Nevada, Reno, December 1995.

CCEER-95-9 Douglas, B., Maragakis, E., and Feng, S., "System Identification Studies on Cazenovia Creek Overpass," Report for the National Center for Earthquake Engineering Research, Civil Engineering Department, Report No. CCEER-95-9, University of Nevada, Reno, October 1995.

CCEER-96-1 El-Gamal, M.E. and Siddharthan, R.V., "Programs to Computer Translational Stiffness of Seat-Type Bridge Abutment," Civil Engineering Department, Report No. CCEER-96-1, University of Nevada, Reno, March 1996.

CCEER-96-2 Labia, Y., Saiidi, M., and Douglas, B., "Evaluation and Repair of Full-Scale Prestressed Concrete Box Girders," A Report to the National Science Foundation, Research Grant CMS-9201908, Civil Engineering Department, Report No. CCEER-96-2, University of Nevada, Reno, May 1996.

CCEER-96-3 Darwish, I., Saiidi, M., and Sanders, D., "Seismic Retrofit of R/C Oblong Tapered Bridge Columns with Inadequate Bar Anchorage in Columns and Footings," A Report to the Nevada Department of Transportation, Civil Engineering Department, Report No. CCEER-96-3, University of Nevada, Reno, May 1996.

CCEER-96-4 Ashour, M., Pilling, P., Norris, G., and Perez, H., "The Prediction of Lateral Load Behavior of Single Piles and Pile Groups Using the Strain Wedge Model," A Report to the California Department of Transportation, Civil Engineering Department, Report No. CCEER-96-4, University of Nevada, Reno, June, 1996.

CCEER-97-1-A Rimal, P. and Itani, A. "Sensitivity Analysis of Fatigue Evaluations of Steel Bridges", Center for Earthquake Research, Department of Civil Engineering, University of Nevada,

Reno, Nevada Report No. CCEER-97-1-A, September, 1997.

CCEER-97-1-B Maragakis, E., Douglas, B., and Sandirasegaram, U. "Full-Scale Field Resonance Tests of a Railway Bridge," A Report to the Association of American Railroads, Civil Engineering Department, University of Nevada, Reno, May, 1996.

CCEER-97-2 Wehbe, N., Saiidi, M., and D. Sanders, "Effect of Confinement and Flares on the Seismic Performance of Reinforced Concrete Bridge Columns," Civil Engineering Department, Report No. CCEER-97-2, University of Nevada, Reno, September 1997.

CCEER-97-3 Darwish, I., M. Saiidi, G. Norris, and E. Maragakis, "Determination of In-Situ Footing Stiffness Using Full-Scale Dynamic Field Testing," A Report to the Nevada Department of Transportation, Structural Design Division, Carson City, Nevada, Report No. CCEER-97-3, University of Nevada, Reno, October 1997.

CCEER-97-4 Wehbe, N., and M. Saiidi, "User's manual for RCMC v. 1.2 : A Computer Program for Moment-Curvature Analysis of Confined and Unconfined Reinforced Concrete Sections," Center for Civil Engineering Earthquake Research, Department of Civil Engineering, University of Nevada, Reno, Nevada, Report No. CCEER-97-4, November, 1997.

CCEER-97-5 Isakovic, T., M. Saiidi, and A. Itani, "Influence of new Bridge Configurations on Seismic Performance," Department of Civil Engineering, University of Nevada, Reno, Report No. CCEER-97-5, September, 1997.

CCEER-98-1 Itani, A., Vesco, T. and Dietrich, A., "Cyclic Behavior of "as Built" Laced Members With End Gusset Plates on the San Francisco Bay Bridge" Center for Civil Engineering Earthquake Research, Department of Civil Engineering, University of Nevada, Reno, Nevada Report No. CCEER-98-1, March, 1998.

CCEER-98-2 G. Norris and M. Ashour, "Liqueficiation and Undraned response evaluation of Sands from Drained Formulation." Center for Civil Engineering Earthquake Research, Department of Civil Engineering, University of Nevada, Reno, Nevada, Report No. CCEER-98-2, May, 1998.

CCEER-98-3 Qingbin, Chen, B. M. Douglas, E. Maragakis, and I. G. Buckle, "Extraction of Nonlinear Hysteretic Properties of Seismically Isolated Bridges from Quick-Release Field Tests", Center for Civil Engineering Earthquake Research, Department of Civil Engineering, University of Nevada, Reno, Nevada, Report No. CCEER-98-3, June, 1998.

CCEER-98-4 Maragakis, E., B. M. Douglas, and C. Qingbin, "Full-Scale Field Capacity Tests of a Railway Bridge", Center for Civil Engineering Earthquake Research, Department of Civil Engineering, University of Nevada, Reno, Nevada, Report No. CCEER-98-4, June, 1998.

CCEER-98-5 Itani, A., Douglas, B., and Woodgate, J., "Cyclic Behavior of Richmond-San Rafael Retrofitted Tower Leg". Center for Civil Engineering Earthquake Research, Department of Civil Engineering, University of Nevada, Reno. Report No. CCEER-98-5, June 1998

CCEER-98-6 Moore, R., Saiidi, M., and Itani, A., "Seismic Behavior of New Bridges with Skew and Curvature". Center for Civil Engineering Earthquake Research, Department of Civil Engineering, University of Nevada, Reno. Report No. CCEER-98-6, October, 1998.

CCEER-98-7 Itani, A and Dietrich, A, "Cyclic Behavior of Double Gusset Plate Connections", Center for Civil Engineering Earthquake Research, Department of Civil Engineering, University of Nevada, Reno, Nevada, Report No. CCEER-98-5, December, 1998.

CCEER-99-1 Caywood, C., M. Saiidi, and D. Sanders, " Seismic Retrofit of Flared Bridge Columns With Steel Jackets," Civil Engineering Department, University of Nevada, Reno, Report No. CCEER-99-1, February 1999.

CCEER-99-2 Mangoba, N., M. Mayberry, and M. Saiidi, "Prestress Loss in Four Box Girder Bridges in Northern Nevada," Civil Engineering Department, University of Nevada, Reno, Report No. CCEER-99-2, March 1999.

CCEER-99-3 Abo-Shadi, N., M. Saiidi, and D. Sanders, "Seismic Response of Bridge Pier Walls in the Weak Direction", Civil Engineering Department, University of Nevada, Reno, Report No. CCEER-99-3, April 1999.

CCEER-99-4 Buzick, A., and M. Saiidi, "Shear Strength and Shear Fatigue Behavior of Full-Scale Prestressed Concrete Box Girders", Civil Engineering Department, University of Nevada, Reno, Report No. CCEER-99-4, April 1999.

CCEER-99-5 Randall, M., M. Saiidi, E. Maragakis and T. Isakovic, "Restrainer Design Procedures For Multi-Span Simply-Supported Bridges", Civil Engineering Department, University of Nevada, Reno, Report No. CCEER-99-5, April 1999.

CCEER-99-6 Wehbe, N. and M. Saiidi, "User's Manual for RCMC v. 1.2, A Computer Program for Moment-Curvature Analysis of Confined and Unconfined Reinforced Concrete Sections", Civil Engineering Department, University of Nevada, Reno, Report No. CCEER-99-6, May 1999.

CCEER-99-7 Burda, J. and A. Itani, "Studies of Seismic Behavior of Steel Base Plates," Civil Engineering Department, University of Nevada, Reno, Report No. CCEER-99-7, May 1999.

CCEER-99-8 Ashour, M., and G. Norris, "Refinement of the Strain Wedge Model Program," Civil Engineering Department, University of Nevada, Reno, Report No. CCEER-99-8, March 1999.

CCEER-99-9 Dietrich, A., and A. Itani, "Cyclic Behavior of Laced and Perforated Steel Members on the San Francisco-Oakland Bay Bridge," Civil Engineering Department, University, Reno, Report No. CCEER-99-9, December 1999.

CCEER 99-10 Itani, A., A. Dietrich, "Cyclic Behavior of Built Up Steel Members and their Connections," Civil Engineering Department, University of Nevada, Reno, Report No. CCEER-99-10, December 1999.

CCEER 99-11 Itani, A., J. Woodgate, "Axial and Rotational Ductility of BuiltUp Structural Steel Members," Civil Engineering Department, University of Nevada, Reno, Report No. CCEER-99-11, December 1999.

CCEER-99-12 Sgambelluri, M., Sanders, D.H., and Saiidi, M.S., Behavior of One-Way Reinforced Concrete Bridge Column Hinges in the Weak Direction, Department of Civil Engineering, University of Nevada, Reno, Report No. CCEER-99-12, December 1999.

CCEER-99-13 Laplace, P., Sanders, D.H., Douglas, B, and Saiidi, M, Shake Table Testing of Flexure Dominated Reinforced Concrete Bridge Columns, Report No. Department of Civil Engineering, University of Nevada, Reno, December 1999.

CCEER-99-14 Ahmad M. Itani, Jose A. Zepeda, and Elizabeth A. Ware "Cyclic Behavior of Steel Moment Frame Connections for the Moscone Center Expansion," December 1999.

CCEER 00-1 Ashour, M., and Norris, G. "Undrained Lateral Pile and Pile Group Response in Saturated Sand", Civil Engineering Department, University of Nevada, Reno, Report No. CCEER-00-1, May 1999. January 2000.

CCEER 00-2 Saiidi, M. and Wehbe, N., "A Comparison of Confinement Requirements in Different Codes for Rectangular, Circular, and Double-Spiral RC Bridge Columns," Civil Engineering Department, University of Nevada, Reno, Report No. CCEER-00-2, January 2000.

CCEER 00-3 McElhaney, B., M. Saiidi, and D. Sanders, "Shake Table Testing of Flared Bridge Columns With Steel Jacket Retrofit," Civil Engineering Department, University of Nevada, Reno, Report No. CCEER-00-3, January 2000.

CCEER 00-4 Martinovic, F., M. Saiidi, D. Sanders, and F. Gordaninejad, "Dynamic Testing of Non-Prismatic Reinforced Concrete Bridge Columns Retrofitted with FRP Jackets," Civil Engineering Department, University of Nevada, Reno, Report No. CCEER-00-4, January 2000.

CCEER 00-5 Itani, A., and M. Saiidi, "Seismic Evaluation of Steel Joints for UCLA Center for Health Science Westwood Replacement Hospital," Civil Engineering Department, University of Nevada, Reno, Report No. CCEER-00-5, February 2000.

CCEER 00-6 Will, J. and D. Sanders, "High Performance Concrete Using Nevada Aggregates," Civil Engineering Department, University of Nevada, Reno, Report No. CCEER-00-6, May 2000.

CCEER 00-7 French, C., and M. Saiidi, "A Comparison of Static and Dynamic Performance of Models of Flared Bridge Columns ," Civil Engineering Department, University of Nevada, Reno, Report No. CCEER-00-7, October 2000.

CCEER 00-8 Itani, A., H. Sedarat, "Seismic Analysis of the AISI LRFD Design Example of Steel Highway Bridges," Civil Engineering Department, University of Nevada, Reno, Report No. CCEER 00-08, November 2000.

CCEER 00-9 Moore, J., D. Sanders, and M. Saiidi, "Shake Table Testing of 1960's Two Column Bent with Hinges Bases," Civil Engineering Department, University of Nevada, Reno, Report No. CCEER 00-09, December 2000.

CCEER 00-10 Asthana, M., D. Sanders, and M. Saiidi, "One-Way Reinforced Concrete Bridge Column Hinges in the Weak Direction," Civil Engineering Department, University of Nevada, Reno, Report No. CCEER 00-10, April 2001.

CCEER 01-1 Ah Sha, H., D. Sanders, M. Saiidi, "Early Age Shrinkage and Cracking of Nevada Concrete Bridge Decks, "Civil Engineering Department, University of Nevada, Reno, Report No. CCEER 01-01, May 2001.

CCEER 01-2 Ashour, M. and G. Norris, "Pile Group program for Full Material Modeling an Progressive Failure." Civil Engineering Department, University of Nevada, Reno, Report No. CCEER 01-02, July 2001.

CCEER 01-3 Itani, A., C. Lanaud, and P. Dusicka, "Non-Linear Finite Element Analysis of Built-Up Shear Links." Civil Engineering Department, University of Nevada, Reno, Report No. CCEER 01-03, July 2001.

CCEER 01-4 Saiidi, M., J. Mortensen, and F. Martinovic, "Analysis and Retrofit of Fixed Flared Columns with Glass Fiber-Reinforced Plastic Jacketing," Civil Engineering Department, University of Nevada, Reno, Report No. CCEER 01-4, August 2001

CCEER 01-5 Saiidi, M., A. Itani, I. Buckle, and Z. Cheng," Performance of A Full-Scale Two-Story Wood Frame Structure Supported on Ever-Level Isolators," Civil Engineering Department, University of Nevada, Reno, Report No. CCEER 01-5, October 2001.

CCEER 01-6 Laplace, P., D. Sanders, and M. Saiidi, "Experimental Study and Analysis of Retrofitted Flexure and Shear Dominated Circular Reinforced Concrete Bridge Columns Subjected to Shake Table Excitation, "Civil Engineering Department, University of Nevada, Reno, Report No. CCEER 01-6, June 2001.

CCEER 01-7 Reppi, F., and D. Sanders, "Removal and Replacement of Cast-in-Place, Post-tensioned, Box Girder Bridge," Civil Engineering Department, University of Nevada, Reno, Report No. CCEER 01-7, December 2001.

CCEER 02-1 Pulido, C., M. Saiidi, D. Sanders, and A. Itani, "Seismic Performance and Retrofitting of Reinforced Concrete Bridge Bents," Civil Engineering Department, University of Nevada, Reno, Report No. CCEER 02-1, January 2002.

CCEER 02-2 Yang, Q., M. Saiidi, H. Wang, and A. Itani, "Influence of Ground Motion Incoherency on Earthquake Response of Multi-Support Structures," Civil Engineering Department, University of Nevada, Reno, Report No. CCEER 02-2, May 2002.

CCEER 02-3 M. Saiidi, B. Gopalakrishnan, E. Reinhardt, and R. Siddharthan, A Preliminary Study of Shake Table Response of A Two-Column Bridge Bent on Flexible Footings Civil Engineering Department, University of Nevada, Reno, Report No. CCEER 02-03, June 2002.

CCEER 02-4 Not Published

CCEER 02-5 Banghart, A., Sanders, D., Saiidi, M., "Evaluation of Concrete Mixes for Filling the Steel Arches in the Galena Creek Bridge," Civil Engineering Department, University of Nevada, Reno, Report No. CCEER 02-05, June 2002.

CCEER 02-6 Dusicka, P., Itani, A., Buckle, I. G., "Cyclic Behavior of Shear Links and Tower Shaft Assembley of San Francisco – Oakland Bay Bridge Tower" Civil Engineering Department, University of Nevada, Reno, Report No. CCEER 02-06, July 2002.

CCEER 02-7 Mortensen, J., and M. Saiidi, " A Performance-Based Design Method for Confinement in Circular Columns," Civil Engineering Department, University of Nevada, Reno, Report No. CCEER 02-07, November 2002.

CCEER 03-1 Wehbe, N., and M. Saiidi, "User's manual for SPMC v. 1.0 : A Computer Program for Moment-Curvature Analysis of Reinforced Concrete Sections with Interlocking Spirals," Center for Civil Engineering Earthquake Research, Department of Civil Engineering, University of Nevada, Reno, Nevada, Report No. CCEER-03-1, May, 2003.

CCEER 03-2 Wehbe, N., and M. Saiidi, "User's manual for RCMC v. 2.0 : A Computer Program for Moment-Curvature Analysis of Confined and Unconfined Reinforced Concrete Sections," Center for Civil Engineering Earthquake Research, Department of Civil Engineering, University of Nevada, Reno, Nevada, Report No. CCEER-03-2, June, 2003.

CCEER 03-3 Nada, H., D. Sanders, and M. Saiidi, " Seismic Performance of RC Bridge Frames with Architectural-Flared Columns," Civil Engineering Department, University of Nevada, Reno, Report No. CCEER 03-3, January 2003.

CCEER 03-4 Reinhardt, E., M. Saiidi, and R. Siddharthan, " Seismic Performance of a CFRP/ Concrete Bridge Bent on Flexible Footings." Civil Engineering Department, University of Nevada, Reno. Report No. CCEER 03-4, August 2003.

CCEER 03-5 Johnson, N., M. Saiidi, A. Itani, and S. Ladkany, "Seismic Retrofit of Octagonal Columns with Pedestal and One-Way Hinge at the Base," Center for Civil Engineering Earthquake Research, Department of Civil Engineering, University of Nevada, Reno, Nevada, Report No. CCEER-03-5, August 2003.

CCEER 03-6 Mortensen, C., M. Saiidi, and S. Ladkany, "Creep and Shrinkage Losses in Highly Variable Climates," Center for Civil Engineering Earthquake Research, Department of Civil Engineering, University of Nevada, Reno, Nevada, Report No. CCEER-03-6, September 2003.

CCEER 03- 7 Ayoub, C., M. Saiidi, and A. Itani, "A Study of Shape-Memory-Alloy-Reinforced Beams and Cubes," Center for Civil Engineering Earthquake Research, Department of Civil Engineering, University of Nevada, Reno, Nevada, Report No. CCEER-03-7, October 2003.

CCEER 03-8 Chandane, S., D. Sanders, and M. Saiidi, "Static and Dynamic Performance of RC Bridge Bents with Architectural-Flared Columns," Center for Civil Engineering Earthquake Research, Department of Civil Engineering, University of Nevada, Reno, Nevada, Report No. CCEER-03-8, November 2003.

CCEER 04-1 Olaegbe, C., and Saiidi, M., "Effect of Loading History on Shake Table Performance of A Two-Column Bent with Infill Wall," Center for Civil Engineering Earthquake Research, Department of Civil Engineering, University of Nevada, Reno, Nevada, Report No. CCEER-04-1, January 2004.

CCEER 04-2 Johnson, R., Maragakis, E., Saiidi, M., and DesRoches, R., "Experimental Evaluation of Seismic Performance of SMA Bridge Restrainers," Center for Civil Engineering Earthquake Research, Department of Civil Engineering, University of Nevada, Reno, Nevada, Report No. CCEER-04-2, February 2004.

CCEER 04-3 Moustafa, K., Sanders, D., and Saiidi, M., "Impact of Aspect Ratio on Two-Column Bent Seismic Performance," Center for Civil Engineering Earthquake Research, Department of Civil Engineering, University of Nevada, Reno, Nevada, Report No. CCEER-04-3, February 2004.

CCEER 04-4 Maragakis, E., Saiidi, M., Sanchez-Camargo, F., and Elfass, S., "Seismic Performance of Bridge Restrainers At In-Span Hinges," Center for Civil Engineering Earthquake Research, Department of Civil Engineering, University of Nevada, Reno, Nevada, Report No. CCEER-04-4, March 2004.

CCEER 04-5 Ashour, M., Norris, G. and Elfass, S., "Analysis of Laterally Loaded Long or Intermediate Drilled Shafts of Small or Large Diameter in Layered Soil," Center for Civil Engineering Earthquake Research, Department of Civil Engineering, University of Nevada, Reno, Nevada, Report No. CCEER-04-5, June 2004.

CCEER 04-6 Correal, J., Saiidi, M. and Sanders, D., "Seismic Performance of RC Bridge Columns Reinforced with Two Interlocking Spirals," Center for Civil Engineering Earthquake

Research, Department of Civil Engineering, University of Nevada, Reno, Nevada, Report No. CCEER-04-6, August 2004.

CCEER 04-7 Dusicka, P., Itani, A. and Buckle, I., "Cyclic Response and Low Cycle Fatigue Characteristics of Plate Steels," Center for Civil Engineering Earthquake Research, Department of Civil Engineering, University of Nevada, Reno, Nevada, Report No. CCEER-04-7, November 2004.

CCEER 04-8 Dusicka, P., Itani, A. and Buckle, I., " Built-up Shear Links as Energy Dissipaters for Seismic Protection of Bridges," Center for Civil Engineering Earthquake Research, Department of Civil Engineering, University of Nevada, Reno, Nevada, Report No. CCEER-04-8, November 2004.

CCEER 04-9 Sureshkumar, K., Saiidi, S., Itani, A. and Ladkany, S., "Seismic Retrofit of Two-Column Bents with Diamond Shape Columns," Center for Civil Engineering Earthquake Research, Department of Civil Engineering, University of Nevada, Reno, Nevada, Report No. CCEER-04-9, November 2004.

CCEER 05-1 Wang, H. and Saiidi, S., "A Study of RC Columns with Shape Memory Alloy and Engineered Cementitious Composites," Center for Civil Engineering Earthquake Research, Department of Civil Engineering, University of Nevada, Reno, Nevada, Report No. CCEER-05-1, January 2005.

CCEER 05-2 Johnson, R., Saiidi, S. and Maragakis, E., "A Study of Fiber Reinforced Plastics for Seismic Bridge Restrainers," Center for Civil Engineering Earthquake Research, Department of Civil Engineering, University of Nevada, Reno, Nevada, Report No. CCEER-05-2, January 2005.

CCEER 05-3 Carden, L.P., Itani, A.M., Buckle, I.G, "Seismic Load Path in Steel Girder Bridge Superstructures," Center for Civil Engineering Earthquake Research, Department of Civil Engineering, University of Nevada, Reno, Nevada, Report No. CCEER-05-3, January 2005.

CCEER 05-4 Carden, L.P., Itani, A.M., Buckle, I.G, "Seismic Performance of Steel Girder Bridge Superstructures with Ductile End Cross Frames and Seismic Isolation," Center for Civil Engineering Earthquake Research, Department of Civil Engineering, University of Nevada, Reno, Nevada, Report No. CCEER-05-4, January 2005.

CCEER 05-5 Goodwin, E., Maragakis, M., Itani, A. and Luo, S., "Experimental Evaluation of the Seismic Performance of Hospital Piping Subassemblies," Center for Civil Engineering Earthquake Research, Department of Civil Engineering, University of Nevada, Reno, Nevada, Report No. CCEER-05-5, February 2005.

Kenny C. Guinn, Governor

Jeff Fontaine, P.E. Director
Prepared by Research Division
Tie He, Research Division Chief
(775) 888-7803
the@dot.state.nv.us
1263 South Stewart Street
Carson City, Nevada 89712